Post polymerization of polyester for fiber formation

Citation for published version (APA):
Ma, Y. (2005). *Post polymerization of polyester for fiber formation*. [Phd Thesis 1 (Research TU/e / Graduation TU/e), Chemical Engineering and Chemistry]. Technische Universiteit Eindhoven. https://doi.org/10.6100/IR590790

DOI:
10.6100/IR590790

Document status and date:
Published: 01/01/2005

Document Version:
Publisher's PDF, also known as Version of Record (includes final page, issue and volume numbers)

Please check the document version of this publication:

• A submitted manuscript is the version of the article upon submission and before peer-review. There can be important differences between the submitted version and the official published version of record. People interested in the research are advised to contact the author for the final version of the publication, or visit the DOI to the publisher's website.
• The final author version and the galley proof are versions of the publication after peer review.
• The final published version features the final layout of the paper including the volume, issue and page numbers.

Link to publication

General rights
Copyright and moral rights for the publications made accessible in the public portal are retained by the authors and/or other copyright owners and it is a condition of accessing publications that users recognise and abide by the legal requirements associated with these rights.

- Users may download and print one copy of any publication from the public portal for the purpose of private study or research.
- You may not further distribute the material or use it for any profit-making activity or commercial gain
- You may freely distribute the URL identifying the publication in the public portal.

If the publication is distributed under the terms of Article 25fa of the Dutch Copyright Act, indicated by the "Taverne" license above, please follow below link for the End User Agreement:

www.tue.nl/taverne

Take down policy
If you believe that this document breaches copyright please contact us at:

openaccess@tue.nl

providing details and we will investigate your claim.

Download date: 16. Nov. 2023

Post Polymerization of Polyester for Fiber Formation

CIP DATA LIBRARY TECHNISCHE UNIVERSITEIT EINDHOVEN

Ma, Yunqian

Post polymerization of polyester for fiber formation / by Yunqian Ma. –
Eindhoven : Technische Universiteit Eindhoven, 2005.
Proefschrift. – ISBN 90-386-2557-X
NUR 913

Trefwoorden: polymerisatie / polyestervezels / molecuulgewicht /
polymeren ; mechanische eigenschappen / treksterkte / Young's Modulus
Subject headings: polymerization / polyester fibers / molecular weights /
polymers ; mechanical properties / tensile strength / Young's Modulus

© 2005, Yunqian Ma
Printed by the Eindhoven University Press, Eindhoven, the Netherlands

Post Polymerization of Polyester for Fiber Formation

PROEFSCHRIFT

ter verkrijging van de graad van doctor aan de
Technische Universiteit Eindhoven, op gezag van de
Rector Magnificus, prof.dr.ir. C.J. van Duijn, voor een
commissie aangewezen door het College voor
Promoties in het openbaar te verdedigen
op donderdag 26 mei 2005 om 16.00 uur

door

Yunqian Ma

geboren te Hebei, China

Dit proefschrift is goedgekeurd door de promotor:

prof.dr. P.J. Lemstra

Copromotor:

dr. U.S. Agarwal

Acknowledgements

This work and this thesis would not have been realised without the support of many persons who have guided my Ph.D. studies. I would like to thank those who contributed in one way or another to the research and those who assisted in the preparation of the thesis. I would like to name especially:

- Dr Uday S. Agarwal, my supervisor, not only for his willing to share his rich academic knowledge and experience, but also for his consistent encouragement for me to achieve the goal. Without his great character of perseverance and rich experience, I would not be able to go through this work.
- Prof. Piet J. Lemstra, for his hard work for arranging my PhD defense, especially at the latter stage of the thesis preparation.
- Prof. Yimin Wang from Donghua University in Shanghai, China, for allowing me to use their equipment to carry out the fiber spinning trial and the generous help in writing the thesis.
- The management of Dutch Polymer Institute, for the financial support, and for allowing publication of this thesis and articles.
- Prof. Doetze J. Sikkema, for his valuable discussion in polymer chemistry.
- Dr J. Vekemans for his kind instruction in organic chemistry.
- Many members of the Faculty of Chemistry. Especially Dr Yang Xiaoniu and Dr Zheng Xuejing for their kind help and discussions in SEM, TEM, and X-ray methods and its application in polymer characterization. Lijing Xue, Cees Weijers, Merina Rajan and Irina Cotiugă for their help in preparing the thesis. And many more colleagues and teachers in SKT groups in TU/e.
- Special thanks to Edgar Karssenberg who helped me to prepare my thesis from Shanghai.
- Akzo Nobel company in Arnhem for allowing to use their equipment to carry out the GPC measurement and solid state polymerization.

Last but not least, I would like to thank my parents for their continuous support and encouragement.

Table of Contents

Chapter 1 General Introduction 1

1.1 Poly (ethylene terephthalate) (PET) as an important polymer 1

1.1.1 PET fibers 1

1.1.2 PET films 2

1.1.3 PET Bottles 2

1.1.4 Engineering plastics 2

1.2 PET production by melt-polymerization 2

1.3 High molecular weight PET by solid state polymerization (SSP) 5

1.4 (Ultra)-high molecular weight (UHMW) PET 5

1.4.1 Swollen State Polymerization 8

1.5 High modulus / high strength fibers from UHMW PET 9

1.6 Integration of solvent assisted post-polymerization and spinning 10

1.7 Aim of the thesis 11

References 12

Chapter 2 NMR based determination of minute acid functionality: end-groups in PET 15

2.1 Introduction 15

2.2 Experimental 16

2.2.1 Materials 16

2.2.2 NMR Analysis 17

2.2.3 Esterification of benzoic acid with HFIP in $CDCl_3$ 17

2.2.4 Esterification of highly diluted benzoic acid with large excess of HFIP in $CDCl_3$ 17

2.2.5 Esterification of acid end-groups of PET with HFIP 17

2.2.6 Fluoroderivatization of the hydroxyl end-groups of PET with TFA 18

2.2.7 Fluoroderivatization of hydroxyl and acid end-groups of PET with TFAA and HFIP 18

2.3 Results and discussion 18

2.3.1 Carbodiimide mediated esterification of benzoic acid with HFIP 18

2.3.2 Determination of the acid end-groups of PET by 'fluoroesterification' 19

2.3.3 Determination of the hydroxyl end-groups of PET by fluoroderivatization 22

2.3.4 Simultaneous determination of the hydroxyl and acid end-groups of PET 23

2.4 Conclusions 24

References 25

Chapter 3 Solid-state polymerization of PET: influence of nitrogen sweep and high vacuum 27

3.1 Introduction 27

3.1.1 The Chemistry behind solid state polymerization 27

3.1.2 Depletion of end groups during SSP 30

3.1.3 Effect of nature and flow rate of carrier gas 31

3.2 Experimental 32

3.2.1 Materials 32

3.2.2 NMR Analysis 33

3.2.3 Intrinsic Viscosity (IV) of PET 33

3.2.4 Liquid Chromatography – Mass Spectrometry (LC-MS) 34

3.2.5 Solid-state polymerization in N_2 (SSP-N_2) 34

3.2.6 Sublimate collection during SSP-N_2 34

3.2.7 Solid-state polymerization in vacuum (SSP-vacuum) 35

3.2.8 Sublimate collection during SSP-vacuum 35

3.2.9 Determination of acid end-groups in PET 35

3.2.10 Determination of hydroxyl end-groups in PET 36

3.2.11 Preparation of TA and MHET mixture 36

3.2.12 Fluoroesterification of acid mixture or sublimate 36

3.3 Results and Discussion 37

3.3.1 SSP-N_2 kinetics and crystallization induced chain-end immobility 40

3.3.2 SSP-Vacuum 43

3.4 Conclusions 50

References 51

Chapter 4 Solvent assisted post-polymerization of PET 55

4.1 Introduction 55

4.1.1 Role of crystallization during SSP 55

4.1.2 Solvent assisted polymerization of PET 56

4.2 Experimental 57

4.2.1 Materials 57

4.2.2 NMR Analysis 58

4.2.3 Intrinsic Viscosity (IV) of PET 58

4.2.4 Differential Scanning Calorimetry (DSC) 58

4.2.5 WAXD 58

4.2.6 Swollen state polymerization (SwSP) 59

4.2.7 Solution polymerization (SolP) 59

4.2.8 Solid state polymerization in vacuum (SSP-vacuum) 60

4.2.9 Determination of acid end-groups in PET 60

4.2.10 Determination of hydroxyl end-groups in PET 60

4.2.11 Size exclusion chromatography (SEC) 61

4.3 Results and Discussion 61

4.3.1 SwSP kinetics and crystallization limited chain-end mobility 61

4.3.2 SolP 67

4.4 Conclusions 69

References 70

Chapter 5 Crystallization of PET from dilute solutions 73

5.1 Introduction 73

5.2 Experimental 74

5.2.1 Materials 74

5.2.2 Detection of phase transition by light scattering 74

5.2.3 Isothermal crystallization from solution 75

5.2.4 Film formation and drawing from solution-crystallized PET 75

5.2.5 DSC 76

5.2.6 WAXD 76

5.2.7 FTIR 76

5.2.8 Scanning electron microscopy 76

5.2.9 Transmission electron microscopy (TEM) 76

5.2.10 Preparation of solid-state crystallized PET 77

5.2.11 Fiber formation from concentrated PET solution 77

5.3 Results and Discussion 77

5.3.1 Detection of phase transition 77

5.3.2 Crystallization characteristics of PET from solution in DPE-BP 79

5.3.3 Morphology of PET crystallized from solution in DPE-BP 81

5.3.4 Mechanical properties of PET crystallized from dilute solution 87

5.4 Conclusions 89

References 90

Chapter 6 Spinning trial of high molecular weight PET 93

6.1 Introduction 93

6.2 Experimental 94

6.3 Results and discussion 96

6.4 Conclusions 101

References 102

Conclusions 105

Technology Assessment 109

Summary 113

Samenvatting 115

Curriculum vitae 117

Chapter 1 General Introduction

1.1 Poly (ethylene terephthalate) (PET) as an important polymer

Poly(ethylene terephthalate) (PET) was invented in the 1940s by Winfield and Dickson [1,2,3], and commercialized in the 1950s as Dacron^{TM} (EI DuPont de Nemours) and Terylene^{TM} (ICI) [4] fibers. Since then, PET has been one of the most important polymers, widely used in fiber, film, bottles, packaging materials, etc. Recent developments even allow it to be used in bottles for applications such as for beer packaging that demands superior barrier properties.

1.1.1 PET fibers

Of all man-made fibers, PET has become the most dominant, with worldwide usage exceeding 20 million tons in 2002 [5], thus replacing cotton fiber as the number one in terms of output. The growing production of polyester fibers is projected to reach 33 million tons by 2010 [6]. The emergence of PET as the most successful of the man-made fibers is due to its mechanical properties combined with high temperature resistance, cheap and easy availability of the raw materials, economical processing without much environmental pollution, and the possibility of recycling.

PET fibers are produced in a variety of forms such as staple fibers, textile filaments and industrial filaments. Textile filaments yarns are continuous, used for producing woven or knitted fabric with aesthetics akin to natural silk. Staple PET fibers are those with cut lengths and diameters similar to their blend partners (such as cotton or wool) 30-100 mm long and 10-20 μm in diameter. Staple fibers are typically spun into yarns and then formed into fabrics by weaving or knitting. The world's current production of polyester fibers for textiles is split evenly between staple and filament yarns. Industrial yarns constitute another major market for polyester fibers, e.g. for reinforcement of rubber and for high-strength technical fabrics. Most passenger car tires produced in the USA are reinforced with yarns made from high molecular weight PET, so processed as to yield high strength and low shrinkage.

1.1.2 PET films

PET is widely processed as films, for applications such as packaging material, carrier (for photographic, video and audio tapes, etc.) and engineering material (capacitors and insulators). While the market for magnetic tapes has been saturated, the demand for thin industrial and packaging films is still growing.

1.1.3 PET Bottles

The demand of PET for bottle applications is growing fast. This fact is based on the outstanding and versatile properties of PET, such as tensile strength, toughness, dimensional stability, transparency, and chemical resistance. Nowadays, nearly all the beverage bottles or mineral water bottles are made from PET.

1.1.4 Engineering plastics

PET may be considered as a low cost raw material for engineering plastics. Its abundant availability and good processibility make it an excellent choice for the production of toughened compounds that can in many cases compete directly with toughened and glass-filled nylons at a considerable cost advantage. For example, glass-filled, toughened PET resins can be readily moulded into highly impact-resistant structural parts for appliances and automotive components. The PET based compounds are also suitable for construction (e.g. as structural members), equipment housings (e.g. printer and copier parts), agricultural applications (e.g. mower and tractor engine covers), materials handling (e.g. pallets and trays), furniture (e.g. office chair bases), as well as electrical and electronics applications.

1.2 PET production by melt-polymerization

PET mainly is produced by two routes named after the monomers being used: the dimethyl terephthalate (DMT) route and purified terephthalic acid (PTA) route [7]. Since the polymer production by condensation mechanism demands high purity of the monomer, and since PTA of sufficient purity was not available in the early days, the DMT route was the only process used in commercial production of PET. Later on, PTA route has become increasingly popular.

The PTA route to PET is made up of two steps. The first is the esterification of terephthalic acid with ethylene glycol (EG) to convert to prepolymer that contains bis-hydroxyethyl terephthalate (BHET) and short chain oligomers.

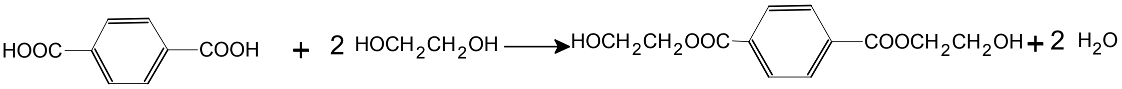

PTA EG BHET Water (1.1)

The esterification is not complete, and some acid end-groups remain in the prepolymer. The esterification by-product water is removed via a column system. The second reaction step is polycondensation, in which mainly the following transesterification reaction

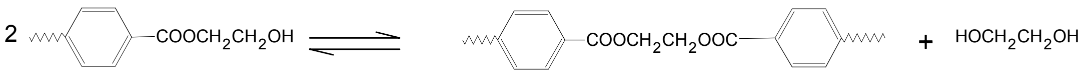

(1.2)

as well as the following esterification reaction

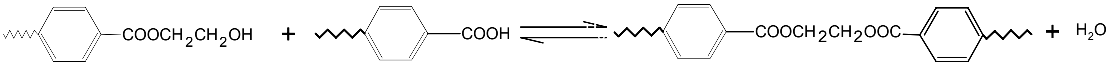

(1.3)

lead to step-growth polymerization in the melt phase. The reversible nature of the reactions demands that the condensates ethylene glycol (EG) and water are removed from the melt efficiently by using high vacuum. Fig. 1.1 is a typical continuous process scheme of the melt phase polycondensation of PET [8]. The first esterification reactor and the second esterification reactors are a series of stirred tank reactors to convert TPA to BHET and oligomeric PET at temperatures of about 280 ^{o}C. Because the melt viscosity remains relatively low, the EG and water condensation products formed during the process can evaporate efficiently. When the molecular weight increases further, the melt viscosity of PET becomes so high that bubble formation is hindered even under the applied vacuum, and EG and water have to diffuse out. Hence it is critical to reduce the diffusion path at the following reaction stage in order to improve removal of EG and water. This is accomplished by feeding the melt into a disk ring reactor, that creates thin and renewable film of the polymer melt, thus significantly increasing the available surface area, and decreasing the diffusion path for condensate removal. Several reviews have looked at the physical and engineering aspects of the melt polymerization of PET [9-12]. At the end of the reaction, the melt is either directly spun into fibers, or extruded into 2-4 mm thick strands that solidify due to the cooling and are cut into somewhat cylindrical chips for future processing.

The DMT route is very similar to PTA route, except that methanol is condensed in the first step:

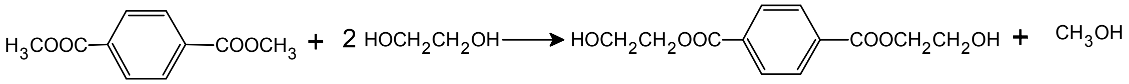
H3COOC
COOCH3
+
2 HOCH2CH2OH
HOCH2CH2OOC
COOCH2CH2OH
+
CH3OH

DMT EG BHET Methanol

(1.4)

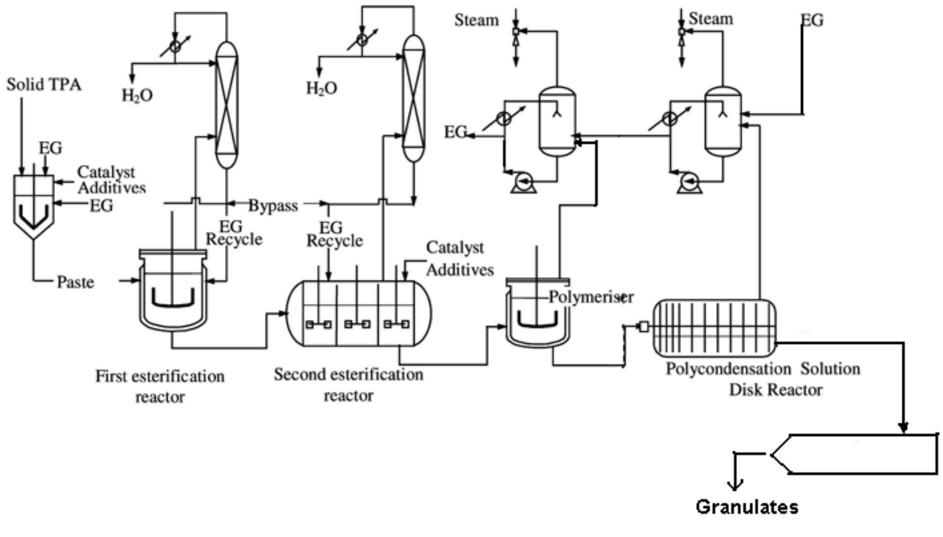
Steam
Steam
EG
Solid TPA
H2O
H2O
EG
EG
Catalyst
Additives
EG
Bypass
EG
Recycle
EG
Recycle
Catalyst
Additives
Paste
Polymeriser
First esterification reactor
Second esterification reactor
Polycondensation Solution Disk Reactor
Granulates

Figure 1.1: A typical industrial process for PET production [8]

The DMT route is economically unfavorable because of the involvement of methanol and the additional step needed to produce DMT from terephthalic acid and methanol.

1.3 High molecular weight PET by solid state polymerization (SSP)

Even with the disk reactors, it is difficult to obtain PET of number average molar mass $\overline{M_n}$ greater than 20,000 g/mole (intrinsic viscosity, IV ~ 0.6 dL/g). This is because of the relatively high viscosity of the melt which reduces the mass transfer rates for removal of EG and water, and the chemical degradation accompanying the higher temperature needed to reduce the viscosity and the long residence time needed to obtain the high molecular weight. The PET produced from melt polymerization is directly used primarily as textile material for clothing etc. where higher molecular weight is not necessary. Applications such as bottles and industrial fibers demand higher molecular weight PET, which is generally achieved by post-polymerization of the PET chips produced by melt polymerization.

The current industrial practice for post polymerization of PET is the solid state polymerization (SSP). The chemical reactions taking place during SSP are the same as those in the melt polymerization, i.e. Eqs. 3.2 and 3.3, except that the SSP takes place in the solid state. The amorphous PET chips obtained during SSP are first subjected to crystallization at 100 to 170 ^{o}C to avoid sticking during subsequent processing at higher temperature, and then charged into the SSP reactor at 200-230 ^{o}C, i.e. about 50 ^{o}C lower than the melt polymerization temperature. EG and water are removed either by nitrogen sweeping or applying vacuum during the solid state polymerization [13]. Kinetics calculation have been used to show that the reaction temperature drop from 285 to 230 ^{o}C reduces the polycondensation rate by a factor of 6, whereas the chemical degradation reaction rate drops by a factor of over 40 [14]. Problems associated with the stirring of the viscous melt are eliminated in the solid state. PET with number average molar mass up to 27000 g/mole (IV ~ 0.9 dL/g) for bottles, and as high as 38000 g/mole (IV ~ 1.20 dL/g) for industrial yarns can be obtained.

1.4 (Ultra)-high molecular weight (UHMW) PET

Since the invention of gel spinning of UHMW polyethylene (PE) to achieve high strength and modulus polyethylene fibers [15], it is anticipated that such high performance fibers can also be similarly achieved from PET, with improved temperature resistance as compared to PE. Therefore, polymerization of PET to ultra-high molecular weight (IV ≥ 2 dL/g) and its solution spinning has been a quite active research area.

Table 1.1 summarizes the reports describing SSP of PET to IV higher than 1.5 dL/g or $\overline{M_n}$ higher than 70,000 g/mole. We notice that this requires sub mm particle size as well as reaction temperature close to the PET melting point (~ 250 °C). The small particle size is required for reducing the diffusion path length (l) and hence the time (t) required for the condensates (with diffusion coefficient D) to diffuse to the particle surface [16]:

$$t \sim \frac{l^2}{2D} \tag{1.5}$$

IV can be related to $\overline{M_n}$ using the IV-$\overline{M_n}$ relationship:

$$IV = K\overline{M}_n{}^a \tag{1.6}$$

Several workers have reported the coefficients K and a, and these are summarized in Table 3.2 in chapter 3. Fig 1.2 shows the relationship between IV and number average molar mass $\overline{M_n}$ according to the results of Koepp and Werner.

Table 1.1: SSP of PET to (ultra)high molecular weight.

No.	**Authors**	**Characteristics of initial PET**	**SSP conditions**	**Final $\overline{M_n}$ or IV (dL/g)**
1	Hsu [17]	0.18-0.25 mm particle $\overline{M_n}$ =16,500 g/mol	250 °C 40 hr N_2 ~ 2 cm/s	$\overline{M_n}$ =120,000 g/mol IV = 2.27
2	Kurita et al. [18]	Standard chips IV = 0.6	237 °C 12 hr N_2	IV = 3.42
3	Cohn [19, 20]	Porous fibrous pellet IV = 1.9 $\overline{M_w}$ = 100,800 g/mol	220-240 °C 10 hr N_2	$\overline{M_n}$ =191,000 g/mol IV = 5.3
4	Rinehart [21]	Porous pills made by compacting 0.84 mm particles IV = 0.5	250 °C 5 hr N_2	IV = 2.39
5	Ito et al. [22]	Solution grown crystals, 2-10μ IV = 0.67	253 °C 24 hr vacuum	IV = 2.41
6	Ito et al. [23, 24]	Porous and fibrous aggregates IV = 0.61	240 °C 12 hr 10 mtorr	IV = 3.2 Up to 4.9 in multi-steps
7	Sasaki et al. [25]	Film, 0.01 mm IV = 0.15	320 °C (melt) 1.5 min 0.5 torr	IV = 2.31
8	Boiko and Marikhin [26]	100 μ film $\overline{M_n}$ =15,000 g/mol	250 °C 20 hr 0.05 mtorr	$\overline{M_n}$ = 151680 g/mol

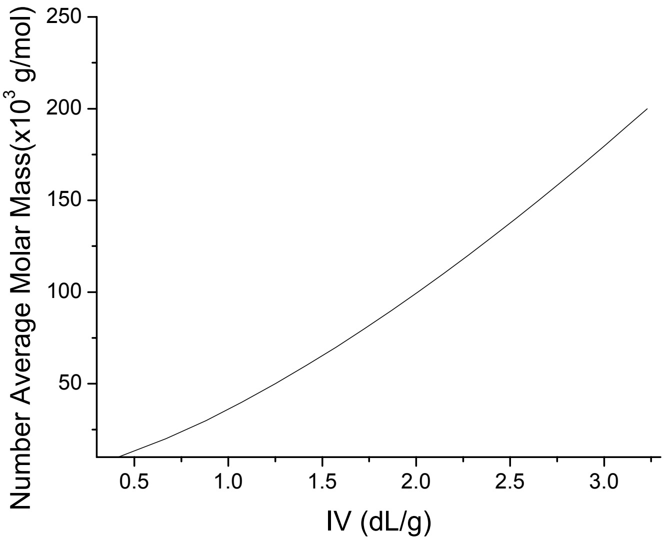

Fig. 1.2 Relationship of IV vs $\overline{M_n}$ *according to the measurement of Koepp and Werner.*

Obtaining small particle size (e.g. by cryogenic grinding) is a slow and expensive process. Further, the ground particles at temperatures close to the melting point tend to sinter, thus resulting in solids handling problems as well as reduced mass transfer. Therefore it appears difficult to employ SSP to produce large quantities of UHMW PET.

1.4.1 Swollen State Polymerization

Considering the reversible nature of the polycondensation reactions (2) and (3) between the hydroxyl and the acid end-groups attached to polymeric chains, one can visualize the following four steps that determine the overall reaction rate:

- Diffusion of the end-groups to each other;
- The chemical reaction between the end-groups, with Arrhenius type temperature dependence;
- Diffusion of the condensates EG and water through the PET to polymer surface;
- Mass transfer of the condensates EG and water away from the polymer surface.

When the diffusion length for condensate removal in PET is small ($l << \sqrt{D/(kC)}$, where C is the condensate concentration, and k is the corresponding rate constant, the diffusion of the condensates EG and water through the polymer is no more limiting [27]. Mass transfer of the condensate from the polymer surface is efficiently achieved through inert gas flow or high vacuum. Under such conditions, the overall reaction rate may become limited by the low mobility of end groups attached to long polymer chains. A recent innovation for obtaining UHMW PET is the swollen state polymerization (SwSP) [28, 29, 30, 31]. Here, the polymerization of PET chips is carried out by swelling in a suitable solvent that does not dissolve the chips. The rate of such SwSP is higher than SSP at the same temperature, and attributed to the increased mobility of the chain ends due to the presence of the solvent [32]. Suitable solvents for this process are heat stable molecules with high boiling point such as biphenyl, diphenyl ether, its eutectic mixture, or hydrogenated terphenyl.

1.5 High modulus / high strength fibers from UHMW PET

Many attempts have been made in the last decade to obtain high modulus/high strength PET fibers from UHMW-PET. While PET can be formed into fibers by melt spinning when IV is less than 1.2 dL/g, higher molecular weight PET is difficult to melt spin into fibers because of its high melt viscosity. For example, the PET polymer with an IV of 2.1 dL/g reaches a melt viscosity of 8×10^5 P under zero shearing at 300 ^{o}C [33]. Hence, in order to reduce the melt viscosity, the melt processing of high molecular weight PET has to be conducted at temperatures over 300 ^{o}C. Such high temperatures may cause serious thermal degradation of the polymer [33, 34, 35]. This is avoided by employing solution-spinning for processing UHMW PET into fibers. Several papers and patents describe attempts to obtain high modulus/high strength PET fibers by solution spinning (Table 1.2).

Table 1.2: Reports on solution spinning of UHMW PET.

Author	**IV (dL/g)**	**Solvent**	**Conc. of spinning dope**	**Overall draw ratio (DR)**	**Tenacity (σ) of the fiber or film**	**Modulus (E) of the fiber or film**
Tate et al. [36] (Toyobo)	1.82	1:1 (vol. ratio) TFA-CH_2Cl_2	23%	9.9	11.4 g/d (1.4GPa)	227 g/d (28.1GPa)
Tsukamoto et al. [37] (Teijin)	2.37	2,4-dichlorophenol	25 %	6	10.5 g/d (1.3 GPa)	130 g/d (16.1GPa)
Tate et al. [38] (Toyobo)	2.0	1-methyl-naphthalene	80%	8.4	16.3 g/d (2.0GPa)	238 g/d (29.5GPa)
Rogers [39] (ICI)	1.71	73.5:26.5 DPE-BP	25.1%	N/A	N/A	90 g/d (11.2GPa)
Ito et al. [40] (Goodyear)	3.77	50:50 (wt. ratio) TFA-CH_2Cl_2	13.1%	8.08	9.8 g/d (1.2 GPa)	235 g/d (29.2GPa)
Kumakawa [41] (Toyobo)	5.0	Dichloroacetic acid, nitro-benzene, or chlorophenol	6%(w/w)	20	28.9 g/d (3.6GPa)	N/A
			4%(w/w)	22.5	34.8 g/d (4.3GPa)	
Toshihiko [42] (Toyobo)	2.46	nitrobenzene	10% (w/w)	14	10.4 g/d (1.29GPa)	200 g/d (24.8GPa)
	1.2	nitrobenzene	20% (w/w)	10.5	8.1 g/d (1.0GPa)	136 g/d (15.6GPa)
Ito et al. [43, 44]	2.6 - 3.6	50/50(v/v) HFIP/DCM	8-9wt%	16.4	2.3 GPa (18.5g/d)	39 GPa (313 g/d)
Wu and Cuculo [45]	3.3	Nitrobenzene or m-Cresol	8wt%	11	12.9 g/d (1.6 GPa)	230 g/d (28.3 GPa)
Hagura [46]	1.45	solvents contg. 40% HFIP	15%	9	15 g/d (1.9GPa)	220 g/d (27.3GPa)

**HFIP is hexafluoro-2-propanol, TFA is trifluoroacetic acid, and DCM is dichloromethane*

1.6 Integration of solvent assisted post-polymerization and spinning

As seen from Table 1.2, the solvents used to spin PET fiber, such as trifluoroacetic acid, hexafluoroisopropanol, and nitrobenzene are often very toxic, aggressive and expensive or require high processing temperatures. The associated molecular weight degradation during spinning and drawing may be responsible for the limited success in achieving the mechanical properties. The theoretical maximum achievable modulus of PET is 140 GPa, and the maximum achievable strength is 13.5 GPa [47]. Even when a suitable solvent has been used for assisting the polymerization, a different solvent has been used for fiber spinning [38]. Thus, intermediate drying and re-dissolution processes are required, resulting in added energy and environmental costs.

1.7 Aim of the thesis

In the thesis the ultimate aim is to use the **same** solvents to assist the post polymerization and the subsequent solution spinning, thus eliminating the intermediate drying and re-dissolution steps and reducing hydrolytic/thermal degradation of the UHMW PET during spinning and drawing. The target is high drawing ratios of the spun fibers by manipulating the polymer concentration to achieve disentangled crystals (with potential to unfold during drawing, similar to UHMW PE) in spun fiber. Since Tate et al. [28, 29] demonstrated the use of the eutectic mixture of diphenyl ether and biphenyl (DPE-BP) for SwSP, and Rogers [39] described its use as spinning solvent, we choose DPE-BP as the solvent for integrating the post polymerization and the solution spinning processes. Easy availability of DPE-BP, which is widely used as heating medium (e.g. Dowtherm^{TM} from Dow Chemicals), is another factor that influenced this choice.

In the thesis, we start examining the kinetics of post polymerization. The associated need to follow depletion of the small concentration of the acid and hydroxyl end-groups necessitated the development of a new fluoroderivatization and ^{19}F-NMR based method, which is described in chapter 2. The influence of reaction medium on post polymerization is then examined, as we compare the SSP under inert gas flow and SSP under vacuum in chapter 3. Further in chapter 4 we compare solvent assisted post polymerization in the swollen and the solution states. In chapter 5, we study the crystallization behaviour of high molecular weight PET from dilute solution, and describe our attempt to obtain disentangled PET crystals with expected potential for high extent of drawing. Preliminary spinning experiments are described in chapter 6. The conclusions and technical feasibility are discussed in chapter 7.

References

[1] Whinfield JR, Dickson JT. Br Patent 578079; 1946, Calico Printers Association.
[2] Whinfield JR. Nature, 1946;158: 930.
[3] Scheirs J, Long T. Modern polyesters*,* Wiley, Chichester, UK, 2003:6-7.
[4] Mark HF, Bikales NM, Overberger CG, Menges G. Encyclopaedia of Polymer science and Engineering Vol 12, 2nd ed. New York, Wiley-Interscience 1990;1–250.
[5] Aizanshtein EM, Fiber Chemistry 2003;35(5).
[6] Julian I. Int Fiber J 2004;19(1).
[7] S. K. Gupta, A. Kumar, ‘‘Reaction Engineering of Step Growth Polymerization’’, Plenum Press, New York 1987.
[8] Mallon FK, Ph.D. thesis, 1996,University of Wisconsin at Madison.
[9] Ravindranath K, Mashelkar RA. Chem Eng Sci 1986; 41:2197.
[10] Ravindranath K, Mashelkar RA. Chem Eng Sci 1986;41:2969.
[11] Jacobsen LL, Ray WH. AIChE J 1992;38:911.
[12] Gantillon B, Spitz R, McKenna TF. Macromol Mater Eng 2004;289:88-105.
[13] Chang S, Sheu MF, Chen SM. J Appl Polym Sci 1983;28:3289.
[14] Ravindranath K, Mashelkar RA. J Appl Polym Sci 1990;39:1325.
[15] Paul S, Piet L. Journal of Materials Science 1980;15(2):505-14.
[16] Crank J, The mathematics of diffusion, oxford, Oxford University Press, 1975, 2ed, 36-37
[17] Hsu LC. J Macromol Sci—Phys B1 1967;4:801.
[18] Kurita K, Hayashi M, Ohta T, Ishihara H, Okada F, Yoshikawa W, Chiba A, Tate S. US patent 4851508, 1989.
[19] Cohn G. Polym Prepr 1989; 30: 160.
[20] Cohn G. US patent 4792573, 1988.
[21] Rinehart VR. US patent 4755587, 1988.
[22] Ito M, Takahashi K, Kanamoto T. J Appl Polym Sci 1990;40:1257.
[23] Ito M, Wakayama Y, Kanamoto T. Polymer 1992; 48: 569.
[24] Ito M, Wakayama Y, Kanamoto T. Sen-I-Gakkaishi, 1994; 35: 1210.
[25] Sasaki I, Hiroshi M, Masaharu F. EP0182352; 1985.
[26] Boiko YM, Marikhin VA. Polym Sci USSR Ser. A 2000;42:1169.
[27] Ravindranath K , Mashelkar RA. J Appl Polym Sci 1990;39:1325.
[28] Tate S, Watanabe Y, Chiba A. Polymer 1993; 34:4974.
[29] Tate S, Ishimaru F. Polymer 1995;36,353.
[30] Tate S, Watanabe Y. Polymer 1995;36:4991.
[31] Burke ALC, Marier G, DeSimone JM. Polym Mater Sci Eng 1996;74:248.
[32] Parashar MK, Gupta RP, Jain A, Agarwal US. J Appl Polym Sci 2002; 67:1589–95.
[33] Tate S, Narusawa H, Polymer 1996;37:1583.
[34] Tomita K, Polymer 1973; 14: 50.

[35] Ziabicki A., Textile Res J 1996; 66: 705.
[36] Hayashi M, Yoshikawa W, Okada F, Ota T, Tate S, Chiba A. JP 62223333;1987.
[37] Tsukamoto R, Hachiman K. JP 06313212; 1994.
[38] Tate S, Chiba C, Tani K. Polymer 1996; 37: 4421.
[39] Rogers V. EP 336556; 1989.
[40] Ito M, Tang M, Kim SL. USP 5061425;1989.
[41] Shiro K. JP 61-207616;1986.
[42] Toshihiko O, Fujio O, Masahiro H, JP62-030024; 1987.
[43] Ito M, Wakayama Y, Kanamoto T., Sen-I-Gakkaishi 1992;48: 569.
[44] Huang B, Ito M, Kanamoto T. Polymer 1994;35: 1329.
[45] Wu G, and Cucolo JA. J Appl Polym Sci 1995;56: 869.
[46] Hagura S. JP-040-73212;1992, to Mitsubishi rayon Co.
[47] He T. Polymer 1986; 27:253-255.

Chapter 2 NMR based determination of minute acid functionality: end-groups in PET

2.1 Introduction

Poly(ethylene terephthalate) (PET) is one of the most important commodity and engineering polymers with worldwide consumption second only to Polyolefins (PE + PP). One of its critical properties is its thermal and hydrolytic degradation resistance, which is significantly controlled by the acid and hydroxyl end-groups [1-2]. Hence, their regular determination at production facilities is the key both for quality control and for monitoring the progress of polymerization aiming to minimize the acid end-groups [2, 3]. Quantitative analysis of the end-groups in polymers is most often based on titration [4-8]. Some of the associated problems are: large sample size requirement, considerable amounts of toxic solvents, and difficulties with exact determination of the end-point when minute concentrations of acid functionality are involved. An infra-red based technique involving deuteration has been described for determination of hydroxyl end-groups [9-13]. Need for development of new techniques has recently been emphasized [2]. NMR based techniques can offer the advantage of small sample requirement and quick and reliable determination of the end-groups. A ^{1}H NMR based technique has been described in recent years for the determination of hydroxyl end-groups [14-16]. In this chapter, we describe a ^{19}F NMR based technique for acid end-group determination in PET. In addition, the hydroxyl end-group concentration may also be determined from NMR of the same sample, thus enabling estimation of the number average molar mass ($\overline{M_n}$). There are, however, some other end groups that could be present in PET, such as vinyl end-groups. Their amount, however, is usually very small and can not be detected in H-NMR directly, unless PET goes through thermal degradation at temperature as high as 290 ^{o}C [16]. In our case, vinyl end groups are normally negligible in calculating the number average molar mass.

This chapter is adapted from a pubished article: Ma Y, Agarwal US, Vekemans JAJM, Sikkema DJ. Polymer 2003; 44: 4429-4434.

The following issues are crucial in NMR based end-group determination of PET. First, the ester groups of PET are liable to undergo degradation, generating additional acid/hydroxyl groups in acidic/basic environment at elevated temperature. Hence, it is desirable that the high molecular weight PET has sufficient room temperature solubility in the solvent used. Second, since the resolution of the chemical shifts of the aromatic hydrogen (minute acid linked vs. dominantly ester linked) in PET is poor, an indirect method such as reaction with an alcohol to form an NMR identifiable ester is desired. Third, since the end-group concentration is very low for up to 5 wt% solution (needed for NMR) of high molecular weight PET, an intrinsically rapid esterification reaction is desirable. Finally, since the δ ~4.7 ppm region in ^{1}H NMR dominated by the large CH_2 peak of PET, it is essential that a new ester signal appears in an isolated δ region. Hexafluoroisopropanol (HFIP), applied both as solvent and as reactive alcohol, appears to satisfy these requirements as esterification is known to result in large shift of the CH peak [17,18]. Since a rapid room temperature esterification of the acid end-groups of PET is required to avoid generation of additional acid end-groups, we explore carbodiimide-mediated esterification [17, 19, 20] at room temperature.

2.2 Experimental

2.2.1 Materials

PET chips were obtained from Wilton Research Center (ICI, UK), and the following characteristics were determined at Twaron Research (Arnhem): intrinsic viscosity = 0.501 dL/g (in *m*-cresol at 30 ^oC), $\overline{M_n}$=20,500 g/mol, diethyleneglycol (DEG) = 0.69 wt. %. Element content coming from addtitives: Sb = 212 ppm, Ti = 14 ppm, P = 78 ppm. Average weight per chip= 0.045 g.

Deuterated chloroform ($CDCl_3$, 99.9 atom D %), hexafluoroisopropanol (HFIP, 99%), α,α,α-trifluorotoluene (TFT, 99%), 4-pyrrrolidino pyridine (98%), trifluoroacetic acid (TFA, 99%), benzoic acid (BA, 99%) and trifluoroacetic anhydride (TFAA, 99%) were obtained from Aldrich. Dicyclohexyl carbodiimide (DCC, 99%) was obtained from Merck. All chemicals were used as received.

2.2.2 NMR Analysis

A 400 MHz Varian Mercury Vx 400 was used to carry out the ^{1}H NMR and ^{19}F NMR measurements, using a $CDCl_3$ mixture with HFIP or TFA as the solvent.

2.2.3 Esterification of benzoic acid with HFIP in $CDCl_3$

Benzoic acid (0.0244 g, 0.2 mmol) was dissolved in $CDCl_3$ (1.03 g), and the catalyst 4-pyrrolidinopyridine (0.011 g, 0.074 mmol) and DCC (0.0422 g, 0.205 mmol) were added. Finally HFIP (0.065 g, 0.386 mmol) was added. Characterization of hexafluoro-isopropyl benzoate (**1**): ^{1}H NMR: δ 8.11 [d, 2H], 7.68 [t, 1H], 7.52 [t, 2H], 6.04 [septet, 1H]. ^{19}F NMR: δ -73.45 [d,6F]. Conversion (from ^{1}H NMR) of benzoic acid to **1** was complete. Caution: HFIP is extremely destructive to tissues of the mucous membranes and upper respiratory tract.

2.2.4 Esterification of highly diluted benzoic acid with large excess of HFIP in $CDCl_3$

Benzoic acid (0.0052 g, 0.042 mmol) was dissolved in a mixture of HFIP (0.102 g) and $CDCl_3$ (0.903 g). Part (0.106 g) of this solution was diluted with HFIP (0.101 g) and $CDCl_3$ (1.007 g). To the latter solution was added part (0.102 g) of a solution of a mixture of DCC (0.0096 g, 0.046 mmol) and 4-pyrrolidinopyridine (0.0012 g, 0.008 mmol) in $CDCl_3$ (1.03 g) to give the sample for NMR analysis. Characterization of **1**: as in section 2.2.3 . Conversion (from ^{1}H NMR) of benzoic acid to **1** was complete.

2.2.5 Esterification of acid end-groups of PET with HFIP

Two pellets of PET (0.095 g, ~ 0.0047 mmol) were dissolved in a mixture of HFIP (0.203 g) and $CDCl_3$ (1.007 g) at room temperature. Firstly, part (0.105 g) of a solution of 4-pyrrolidinopyridine (0.0011 g) in $CDCl_3$ (1.012 g) was added and subsequently, part (0.303 g) of a solution of DCC (0.0075 g) in $CDCl_3$ (1.504 g) was added. After waiting for 10 min, part (0.102 g) of a solution of TFT (0.0103) in $CDCl_3$ (2.078 g) was added to the above reaction mixture to give the sample for NMR analysis. Characterization of the hexafluroisopropylester of PET (**3**): ^{1}H NMR δ 6.04 [septet, 1H], ^{19}F NMR: δ -73.41 [d, 6F].

2.2.6 Fluoroderivatization of the hydroxyl end-groups of PET with TFA

Two pellets of PET (0.092 g) were dissolved in a mixture of TFA (0.206 g) and $CDCl_3$ (1.03 g). Part (0.107 g) of a solution of TFT (0.011 g) in $CDCl_3$ (2.03 g) was added to the above reaction mixture. ^{19}F NMR analysis was carried out repeatedly at various times. Integration of the δ -75.21 [s, 3F] peak for the trifluoroacetate of PET (**4**) relative to the δ -62.9 [s, 3F] peak of TFT allowed quantification of the acid end-groups. Caution: TFA may cause burns to skin or eyes. Inhalation or ingestion may cause burns to mucous membranes.

2.2.7 Fluoroderivatization of hydroxyl and acid end-groups of PET with TFAA and HFIP

Two pellets of PET (0.0976 g, ~ 0.0047 mmol) were dissolved in a mixture of TFA (0.531 g) and TFAA (0.203 g, 1 mmol) over 1 hr. The solvent removal was carried out by threefold washing with $CHCl_3$ (1.023 g), evaporation by blowing nitrogen, drying under vacuum (5×10^{-3} mbar). The dried PET was dissolved in a mixture of HFIP (0.183 g) and $CDCl_3$ (1.012 g) at room temperature. Part (0.106 g) of a solution of 4-pyrrolidinopyridine (0.001 g) in $CDCl_3$ (1.002 g) was added and subsequently, part (0.310 g) of a solution of DCC (0.078 g) in $CDCl_3$ (1.503 g) was added. After waiting for 10 min, part (0.0735 g) of a solution of TFT (0.0181) in $CDCl_3$ (2.080 g) was added to the above reaction mixture to give the sample for NMR analysis. ^{19}F NMR **4**: δ -75.21 [s, 3F], **3**: δ -73.41 [d, 6F]. Caution: TFAA may cause burns to skin or eyes, inhalation or ingestion may be fatal.

2.3 Results and discussion

2.3.1 Carbodiimide mediated esterification of benzoic acid with HFIP

We started by examining the DCC mediated esterification of benzoic acid with HFIP to form hexafluoroisopropyl benzoate (**1**).

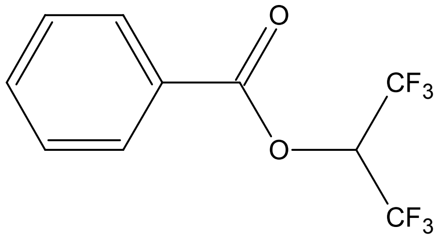

1

The ester **1** has been synthesized previously [18], albeit by reaction of benzaldehyde with hexafluoroacetone. The DCC mediated esterification is non-trivial due to the possibility of many side reactions [19, 20]. For example, we found that DCC undergoes reaction with HFIP, leading to formation of adduct **2**.

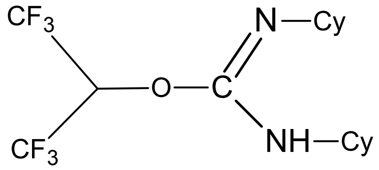

2

Thus, the sequence of addition of reactants can be critical, and seems to need optimization for individual reactions [20]. We found that it was essential to first add catalyst and DCC to benzoic acid before the addition of HFIP (section 2.2.3), for complete conversion of the acid to **1** (septet, $\delta = 6.04$ ppm).

For similar esterification of the acid end-groups of PET, we wished to utilize HFIP also as a reaction medium since it enables PET dissolution at room temperature. However, the corresponding high concentration of HFIP resulted in complete conversion of the added DCC to adduct **2**. This problem was circumvented by utilizing $CDCl_3$-HFIP (10:1 by wt.) as a mixed solvent for PET. We first established (section 2.2.4) that for this solvent system, a low concentration of benzoic acid (3.4 meq per kg reaction mixture) could be completely converted to **1**.

2.3.2 Determination of the acid end-groups of PET by 'fluoroesterification'

Having achieved quantitative 'fluoroesterification' of benzoic acid at very low concentration in $CDCl_3$-HFIP mixture, we applied (section 2.2.5) this method to esterify the acid end-groups of PET with HFIP to afford the hexafluoroisopropyl ester **3** (Eq. 2.1):

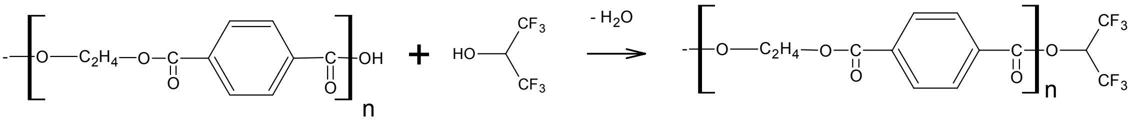

3 (2.1)

A ^{1}H NMR signal (septet, δ = 6.04 ppm, -CH $(CF_3)_2$) was observed, corresponding to the formation of **3**. The ^{19}F NMR (Figure 2.1) features sharp peaks for the ester **3** (d, δ = -73.41 ppm, J=5.6 Hz) and the adduct **2** (d, δ = -73.55 ppm, J=5.6 Hz), in addition to the HFIP doublet (δ = -75.98 ppm).

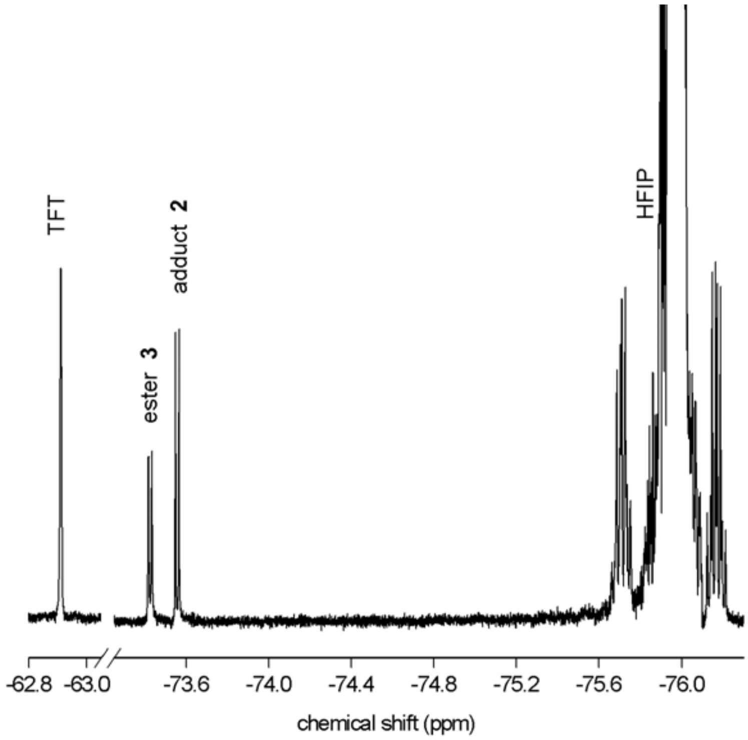

Figure 2.1: ^{19}F NMR spectrum of the reaction product (section 2.2.5) of PET with HFIP and DCC.

Quantification with respect to the PET was facilitated by addition (section 2.2.5) of a ^{19}F NMR detectable secondary standard α,α,α-trifluorotoluene (TFT) (s, δ = -62.90 ppm), allowing calculation (Fig. 2.1) of the acid end-group concentration as 20.1 meq/kg PET. In this experiment, DCC was 6 times in excess of the measured acid end-groups. When the amount of DCC was only 1.5 times the stoichiometric requirement, the acid value was measured to be only 14 meq/kg, due to the competing conversion of DCC to the adduct **2**. Repeating this experiment four times with PET of same grade and quantity, but with varying amount of DCC (4-8 times the stoichiometric requirement) resulted in measured acid end-group concentrations of 20.5, 19.4, 19.1 and 21.2 meq/kg. This shows good reproducibility of this method, and the ± 5% variations between measurements can be attributed to the limited accuracy of NMR peak integration, and some chip-to-chip variation arising during the polymerization process itself. This value also compares well with the acid end-group concentration of 23 meq/kg determined by titration method (at Twaron Research, Arnhem), since the expected accuracy of a single titration method measurement is ± 3 meq/kg. We also carried out the esterification experiments with reduced concentration of acid end-groups, by using the same grade but smaller quantities of the PET, and maintaining HFIP: PET =2:1 (w:w). Results in Fig. 2.2 show the expected linear variation of the measured hexafluoroisopropyl ester concentration with PET concentration. This suggests that acid concentrations as low as 6 meq/kg PET can be reliably measured by using a 5 wt% polymer concentration in reaction mixture (i.e., 0.3 meq acid / kg reaction mixture).

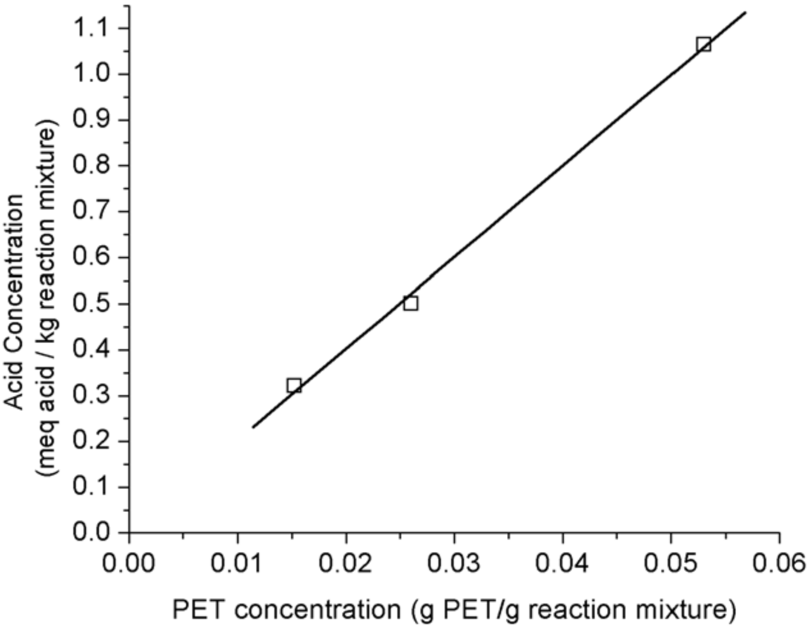

Figure 2.2: Effect of the PET concentration (during reaction) on the measured acid concentration.

It is straightforward to extend this method to simultaneous determination of the hydroxyl end-groups, using the known [16] peak assignments of the CH_2CH_2OH ends (δ = 4.01 ppm). The masking of this peak by the large HFIP peaks ($\delta_{-CH=}$ = 4.40 ppm, δ_{-OH}: ranging from 4 to7 ppm, depending on DCC concentration) in that spectral region is eliminated by use of deuterated HFIP instead of of HFIP. In addition, the ester peak in the ^{19}F NMR now appears as a singlet, thereby improving the peak integration for the acid determination. Furthermore, adding tetrachloroethane (s, δ = 6.0 ppm) as internal standard for ^{1}H NMR has permitted easy quantification by integration, and the hydroxyl end-group concentration is determined as 82 meq/kg PET. The concentration of acid and hydroxyl end-groups leads us to estimate $\overline{M_n} = 2([\mathrm{COOH}]+[\mathrm{OH}])^{-1} = 1.96\mathrm{x}10^4$ g/mole, consistent with the value determined from the measured intrinsic viscosity (section 2.2.1).

2.3.3 Determination of the hydroxyl end-groups of PET by fluoroderivatization

The hydroxyl end-groups could also be determined by the slow fluoroderivatization (section 2.2.6) with TFA (Eq. 2.2).

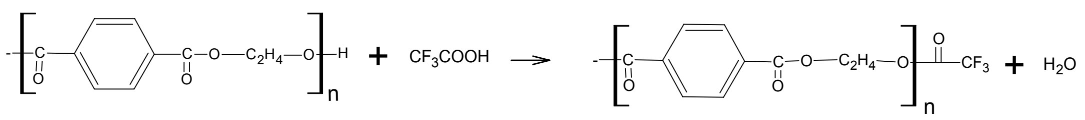

4 (2.2)

At (δ = -75.2 ppm), a singlet appeared in the ^{19}F NMR corresponding to the trifluoroacetate of PET (**4**). Comparison of the peak area with respect to the added (section 2.2.6) secondary standard (TFT) (s, δ = -62.90 ppm) allowed quantification of y, the concentration of **4** (Fig. 2.3). The concentration y was found to increase with time t passed between the dissolution and the NMR analysis, and leveled off after about 48 h. This is similar to the observation of Kenwright et al. [15], but they had used ^{1}H NMR to monitor the concentration of unreacted hydroxyl end-groups. A first order kinetic fit

$$y = y_o\ (1 - e^{-kt}) \tag{2.3}$$

shown in Fig. 2.3 resulted in a rate constant $k = 0.103$/h and a final concentration of **4** $y_o = 82.9$ meq/kg-PET. This corresponds to the concentration of hydroxyl end-groups in the starting PET sample, and compares well with the value determined by the ^{1}H NMR of the starting sample (section 2.3.2).

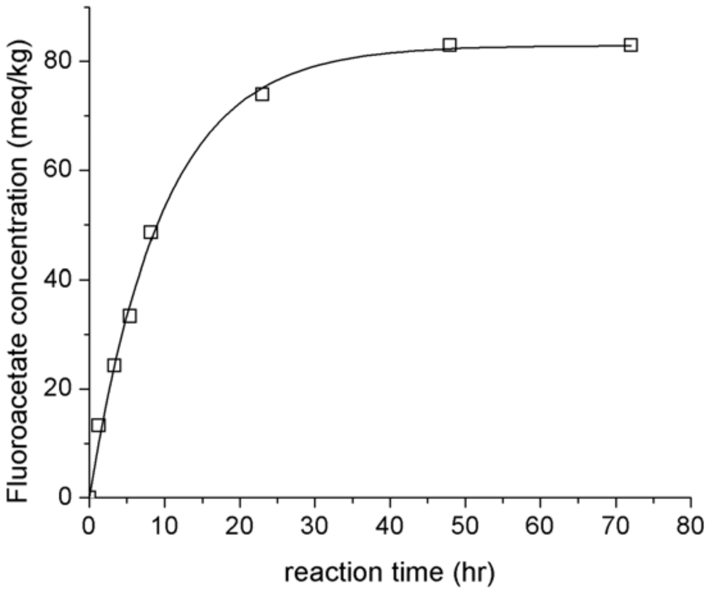

*Figure 2.3: Conversion of the hydroxyl end-groups of PET to the trifluoroacetate (**4**) (Eq. 2.2). Symbols are the experimental measurements (section 2.2.6) by ^{1}F NMR, and the continuous line represents the first order kinetics (Eq. 2.3).*

2.3.4 Simultaneous determination of the hydroxyl and acid end-groups of PET

We found that the fluoroderivatization of the hydroxyl end-groups can be carried out rapidly (section 2.2.7) with TFAA in TFA

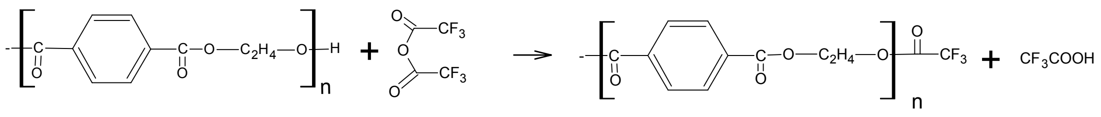

(2.4)

Removal of the TFAA and TFA, and subsequent carbodiimide mediated fluoroesterification (section 2.2.7) of the acid end-groups allows NMR detection of both the carboxylic acid and the hydroxyl end-groups in a single ^{19}F NMR measurement (Fig. 2.4). Comparing with Fig. 2.1, the doublet at (δ = -73.41 ppm) corresponds to **3**, while the singlet at (δ = -75.21 ppm) corresponds to **4**. In addition, the small singlet (δ = -74.53 ppm) and doublet (δ = -73.36 ppm) correspond to hexafluoroisopropyl trifluoroacetate (HFIP-TFA ester) [21] and the large singlets (δ =-69.8, -70.1 ppm) correspond to TFA-DCC adducts. This suggests that the removal of TFA was incomplete even after threefold washing with $CHCl_3$ and drying. Consumption of DCC in these reactions with the leftover TFA was responsible for the much higher amount of DCC needed (section 2.2.7) as compared to the reaction in absence of TFA (section 2.2.5). Using the integrations of the peaks corresponding to **4** and **3** relative to the TFT peak, the concentrations of the hydroxyl and the carboxylic acid end-groups are simultaneously determined as 76 meq/kg and 19 meq/kg, respectively. The marginally lower values of the acid and hydroxyl end-group concentrations measured here are within the accuracy of the NMR integrations, but could also be related to some loss of the smallest end-group carrying molecules during the repeated washings.

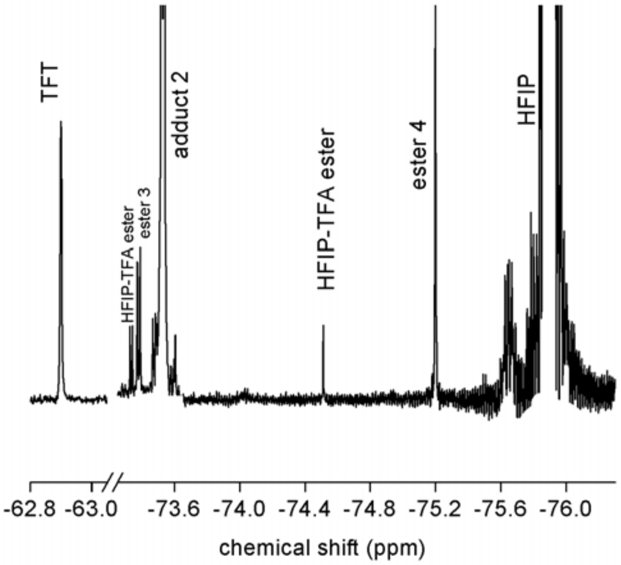

Figure 2.4: ^{19}F NMR spectrum after consecutive reactions (section 2.2.7) of PET with TFAA and with HFIP.

2.4 Conclusions

We have presented methods for determination of the acid and hydroxyl end-groups (and thus an estimation of $\overline{M_n}$) of PET from small specimen analyzed by a combination of ^{1}H NMR and ^{19}F NMR, or by ^{19}F NMR alone. In the following chapters, we report application of this technique for samples with a wide range of end-group concentrations obtained during solid-state polymerization of PET. The fluoroderivatization enables identification of some new post-polymerization characteristics of PET: the influence of reaction environment (vacuum, inert gas) on the kinetics, and identification of the sublimate (chapter 3). This technique has also been extended to carboxylic acid and hydroxyl content determinations in other polymers such as minutely functionalized polystyrenes [22]. Potential applications exist in determination of minute quantities of acids in animal (meat/milk) and plant based foods, food supplements and pharmaceutical formulations, where chromatographic techniques are presently used.

References

[1] Zimmerman H, Kim NT. Polym Engng Sci 1980; 20: 680.
[2] Xanthos M. Reactive modification/Compatibilization of Polyesters. In: Fakirov S. editor, Handbook of Thermoplastic Polyesters, New York, Wiley, 2002; Vol. 2.
[3] Ravindranath K, Mashelkar RA. Chem Engng Sci 1986; 41: 2197.
[4] Pohl HA. Anal Chem 1954; 26: 1614.
[5] Conix A. Makromoleculare Chem 1967; 103: 19.
[6] Lingen RLM van Z. Anal Chem 1969; 247: 232.
[7] Houwelingen GDB van. Analyst 1981; 106: 1057.
[8] Weisskopf K. J Polym Sci, Polym Chem 1988; 26: 1919.
[9] Ward IM. Nature 1957; 180: 141.
[10] Al-AbdulRazzak S, Lofgren EA, Jabarin SA. Polym Int 2002; 51: 174.
[11] Ward IM. Trans Faraday Soc 1957; 3: 1406.
[12] Ravens DAS, Ward IM. Trans Faraday Soc 1961; 57: 150.
[13] Ravens DAS, Ward IM. Trans Faraday Soc 1961; 57: 150.
[14] Zhang H, Rankin A, Ward IM. Polymer 1996; 37: 1079 .
[15] Kenwright AM, Peace SK, Richards RW, Bunn A, MacDonald WA. Polymer 1999; 40:2035-2040.
[16] Amari T, Nishimura K, Minou K, Kawabata A, Ozaki Y. J Polym Sci, Polym Chem 2001; 39: 665.
[17] Barton P, Laws AP, Page MI. J Chem Soc, Perkin Trans 2 1994; 2021.
[18] Urry WH, Nishihara A, Niu JHY. J Org Chem 1967; 32: 347.
[19] Boden EP, Keck GE. J Org Chem 1985; 50: 2394.
[20] Araki, J, Kuga S, Magoshi J. J Appl Polym Sci 2002; 85: 1349.
[21] Majid A, Shreeve JM. J Org Chem 1973; 38: 4028.
[22] Rajan M, Cotiuga I, Ma Y., Picchioni F, Agarwal US. e-polymer 2003;046

Chapter 3 Solid-state polymerization of PET: influence of nitrogen sweep and high vacuum

3.1 Introduction

3.1.1 The Chemistry behind solid state polymerization

Post polymerization of poly (ethylene terephthalate) (PET) in the solid-state is often utilized to enhance its number average molar mass $\overline{M_n}$ beyond 20,000 g/mol desired for applications such as soft drink bottles, tire cord filaments and industrial fibers. The following reactions are generally considered to take place [1-5] when the solid PET pellets are heated to T=200-250 °C:

Transesterification / polycondensation

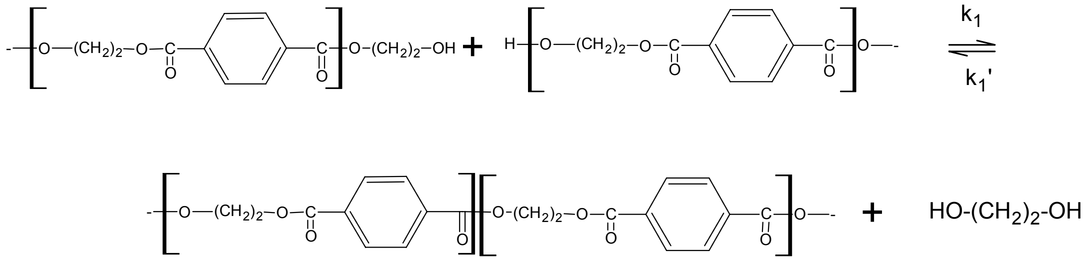

(3.1)

Esterification

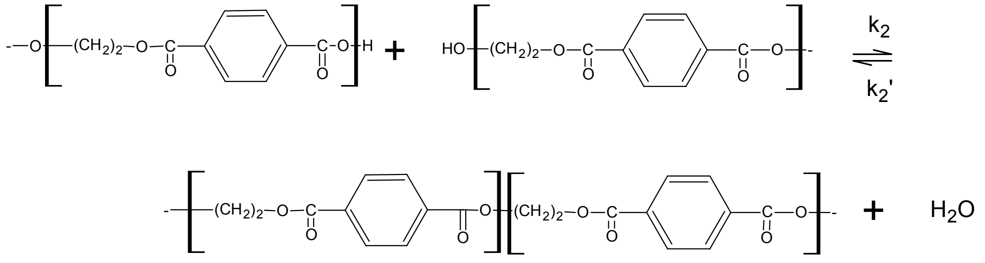

(3.2)

Here, water and ethylene glycol (EG) are the by-products of the reversible reactions.

This chapter is adapted from published work: Ma Y, Agarwal US, Sikkema DJ, and Lemstra PJ. Polymer 2003; 44: 4085-4096.

The forward reactions are facilitated by the by-product removal either by flow of inert gas or by maintaining reduced pressure, or a combination of the two [6, 7]. During PET polymerization process, there are side reactions that will lead to additional acid and vinyl end group formation (Eq. 3.3 and 3.4), however, these reactions are much slower and do not play significant role in reaction kinetics. Vinyl end group can react further with hydroxyl end group by polycondensation (Eq. 3.5). The above-mentioned reactions are negligible and can be ignored especially in kinetics modeling.

Additional acid end group formation:

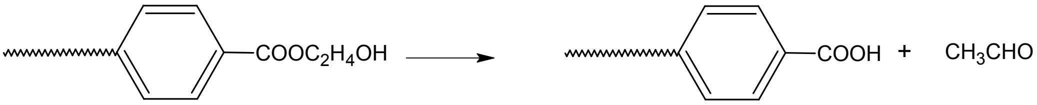
COOC2H4OH
COOH
+
CH3CHO

AA (3.3)

The vinyl end group formation:

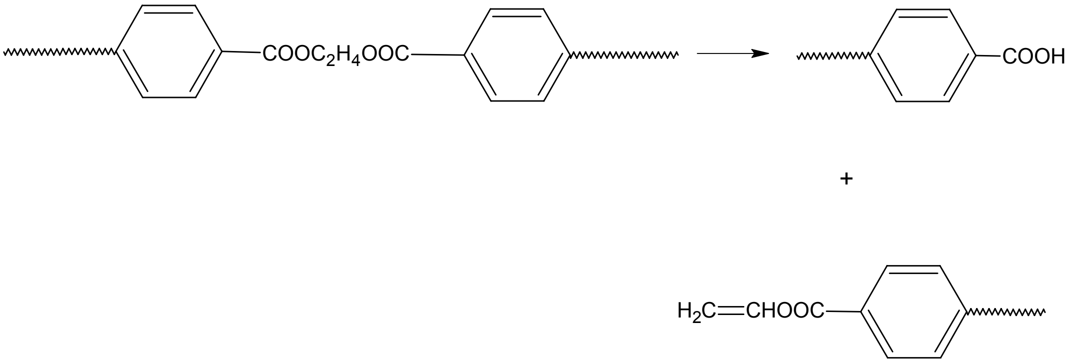
COOC2H4OOC
COOH
+
H2C=CHOOC

Vinyl (3.4)

Polycondensation of vinyl end group:

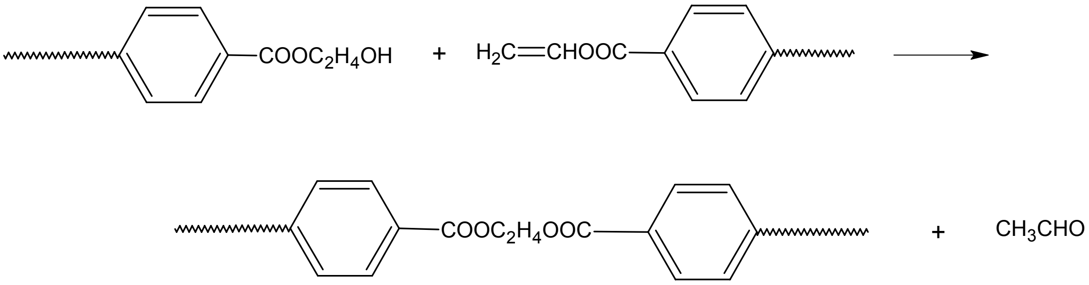
COOC2H4OH
+
H2C=CHOOC
COOC2H4OOC
+
CH3CHO

AA (3.5)

The overall reaction rate is influenced by a combination of the intrinsic reaction rate [3, 8-16], diffusion of the reactive end-groups [8, 13, 17-22] as limited by crystallization [23-25] or facilitated by interchange reactions [20], the diffusion of the by-products from the pellet interior to the pellet surface [3, 11, 14, 15, 22, 26] and their removal by the inert gas stream [8, 13-15, 22]. With the objective of obtaining high reaction rate, yet controlling the product quality as defined by the concentrations of the acid (COOH) and hydroxyl (OH) end-groups, diethylene glycol groups, and acetic aldehyde, studies have been conducted to examine the influence of reaction parameters such as temperature [1, 3, 8-10, 15, 27- 29], pellet size [3, 8, 9, 23, 27, 28], crystallinity level [13, 16, 25, 27, 28], nature and rate of carrier gas [1, 8, 13, 14, 15, 22], catalyst concentration [30, 31], etc. In the absence of condensate diffusion limitations, which results in the fast removal of condensates, backward reactions are eliminated, and the reaction kinetics is described by the following expressions [4, 13, 14, 21]:

$$\frac{d[OH]}{dt} = -2R_{EG} - R_{H_2O} \tag{3.6}$$

$$\frac{d[COOH]}{dt} = -R_{H_2O} \tag{3.7}$$

Since other end groups, for instance, vinyl end-groups, are negligible in number average molar mass calculation, the following equation is used in $\overline{M}_n$ calculation.

$$\overline{M}_n = \frac{2}{[OH]+[COOH]} \tag{3.8}$$

where

$$R_{EG} = 2k_1[OH]^2 \tag{3.9}$$

and

$$R_{H_2O} = k_2[COOH][OH] \tag{3.10}$$

are the rates of production (or rates of removal) of EG and water respectively. In Eq. 3.9, the additional factor of 2 is taken to account for the two pairs of reaction sites for a given pair of chain ends [32], the rate constants being taken as those corresponding to the reactive groups.

While PET of intrinsic viscosity (IV) of 0.6-1.0 dL/g is useful for applications such as fibers, films and molding, its SSP to IV as high as 3 dL/g is desired for its solution spinning leading to high modulus high strength fibers [33-35]. The Table 1.1 in chapter 1 summarizes the reports describing SSP of PET to IV higher than 1.5 dL/g or $\overline{M_n}$ higher than 70,000 g/mol.

Of the references in the Table 1.1, only Hsu [8], Ito et al. [23] and Boiko and Marikhin [24] have reported kinetics data, though limited to IV (t) profiles. Further, the SSP experiments summarized in Table 1.1 were conducted either only at atmospheric pressure (with nitrogen sweep) or only in vacuum. Thus, SSP under otherwise identical conditions, but differing in vacuum or carrier gas atmosphere, were not compared.

3.1.2 Depletion of end groups during SSP

Several authors have followed the reduction in the OH and the COOH end group concentrations with progress of SSP to moderate molecular weights, and their results are summarized in Table 3.1. These studies are all limited to $\overline{M_n}$ not exceeding 52000 g/mol, and it is only recently that Zhi-Lian et al. [14], Wu et al. [23] and Kang [21] have analyzed such end-group data in terms of the two simultaneous reactions (Eqs. 3.1 and 3.2). Even these workers did not consider the role of crystallization in limiting the accessibility of the end groups to each other. However, they did not face a contradiction in fitting the kinetics, because they limited their analysis to molar mass less than 52000 g/mol. Duh [16] accounted for this role of crystallization, but ignored the esterification reaction (Eq. 3.2), did not directly measure concentrations of the end groups, and limited his analysis to IV less than 1.3 dL/g. Jabarin [36] and Wu et al. [23] reported that maximum SSP rate in pelletized PET is achieved when [COOH]: [OH] = 0.5. Schaaf et al. [37] suggested an optimum at [COOH]:[OH] = 0.3 to 0.6 for maximum SSP rate. Chen and Chen [3] indicated that a high OH concentration is preferred in fine samples, while high COOH is preferred in granulated PET. However, during SSP of

PET of IV = 0.25 dL/g, Duh [4] recently found monotonically decreasing SSP rates with increasing acid end groups in the starting PET.

Table 3.1: End-group depletion during SSP of PET.

	Authors	**Characteristics of initial PET**	**SSP Conditions**	**Initial and final $\overline{M_n}$ (g/mol) or IV (dL/g)**	**Initial and final [OH] (meq/kg)**	**Initial and final [COOH] (meq/kg)**
1	Chen and Chen [3]	16-18 mesh particles	240 °C 6 hr 60 mtorr	21000 52000	56 21	38 16
2	Karayannidis et al. [29]	Precipitated PET	230 °C 8 hr 30 mtorr	0.7 1.5	56 24	43 08
3	Zhi-Lian et al. [14]	1.5 mm thick	225 °C 30 hr N_2	22000 32400	Not measured	20 11.5
4	Wu et al. [23]	0.25 mm particles	235 °C 4 hr 1 torr	18000 36000	Not measured	30 3

The depletion of acid end-groups is generally attributed to the esterification reaction (Eq. 3.2). Though it is generally believed, that besides H_2O and EG, only that cyclic oligomers are removed by vacuum or inert gas besides water and EG [28], an additional possibility is the sublimation of acid end-groups containing species such as terephthalic acid (TA) and monohydroxyethyl terephthalate (MHET) at the high SSP temperatures under vacuum. An analysis of the sublimate during SSP will allow us to determine if such sublimation play a significant role.

3.1.3 Effect of nature and flow rate of carrier gas

Several authors have reported [1, 8, 14, 15, 26] that with increasing rate of carrier gas flow, the rate and the extent of post-polymerization increases, before leveling out at high flow rates. However, only Hsu [8] and Huang and Walsh [15] provided information on the gas velocity (perhaps the most direct parameter responsible for the mass transfer coefficient on the gas side) employed by them. Huang and Walsh [15] concluded that while nitrogen flow of 0.8 cm/s was sufficient to achieve maximum SSP rate in 1.1-2.7 mm particles at 190 °C, nitrogen flow at 2.5 cm/s was required to achieve the maximum reaction rate at 220 °C. Hsu [8] found that for SSP of 0.18-0.25 mm particles ($\overline{M_n}$ = 16500 g/mol) at 250 °C for 7 hr, nitrogen flow at 2 cm/s lead to $\overline{M_n}$ of 58000 g/mol. However, use of helium or carbon dioxide under same conditions lead to $\overline{M_n}$ of 81000 g/mol and 90000 g/mol respectively. Hsu attributed this to the influence of carrier gas diffusion on the diffusivity of EG in the polymer, and to the interaction of the carrier gas with EG. Devotta and Mashelkar [13] quantified these effects in terms of the influence of the associated free volume changes on the diffusivities. Mallon et al. [38] found no discernible effect of carrier gases during SSP of 0.1 mm PET particles at 226 °C. Though Aharoni [6] indicated that nitrogen under reduced pressure performs better than either nitrogen sweep or high vacuum alone, Fakirov [8] suggested no significant influence of reaction medium (vacuum vs. nitrogen sweep) during SSP. A detailed analysis of such effects, if any, is not available. Chang et al. [28] found that vacuum (as compared to nitrogen sweep) gave better IV retention and less acid end-group production during annealing of PET (20-30 mesh, IV=0.72 dL/g) for 2 hr at 181 °C.

In this chapter we compare the kinetics of SSP to ultra high molecular weight PET under vacuum and under N_2 sweep. Not only the IV, but also the acid and hydroxyl end-groups concentrations are monitored using our recently developed NMR based technique (chapter 2). The results are analyzed in terms of the kinetics of the two simultaneous reactions producing EG and water (Eqs. 3.1 and 3.2), and additionally proposed reactions producing higher molar mass aromatic condensates. This possibility is examined by collection and analysis of the sublimate during the SSP process.

3.2 Experimental

3.2.1 Materials

PET chips were obtained from Wilton Research Center (ICI, UK), and the following characteristics were determined at Twaron Research (Arnhem): $\overline{M_n}$ =20,500 g/mole, DEG = 0.69 wt. %.

Chloroform ($CHCl_3$, 99.9%), deuterated chloroform ($CDCl_3$, 99.9 atom D %), phenol, tetrachloroethane (TCE, 97%), dimethyl sulfoxide (DMSO, d6, 99 atom D %), hexafluoroisopropanol (HFIP, 99%), α,α,α-trifluorotoluene (TFT, 99%), 4-

pyrrolidinopyridine (98%), trifluoroacetic acid (TFA, 99%) and bishydroxyethyl terephthalate (BHET) were obtained from Aldrich. Phenol (99%), NaOH (98%), EG (98%), dicyclohexyl carbodiimide (DCC, 99%), and TA (99%) were obtained from Merck. All chemicals were used as received.

3.2.2 NMR Analysis

A 400 MHz Varian Mercury Vx 400 was used to carry out the ^{1}H NMR and ^{19}F NMR measurements, using DMSO, $CDCl_3$, or a $CDCl_3$ mixture with HFIP or TFA as the solvents.

3.2.3 Intrinsic Viscosity (IV) of PET

The relative viscosity (η_{rel}) of solutions of PET in a phenol-TCE mixture (1:1, by weight) at concentration (c = 0.5 g/dL) was determined using an Ubbelohde viscometer at 30 °C. Intrinsic viscosity (IV) was estimated from this single point measurement of η_{rel}, using the following approximation for linear flexible chains [39]:

$$IV=(1/c)\,[2\,(\eta_{rel}-1)-2\ln(\eta_{rel})]^{1/2} \qquad (3.11)$$

Table 3.2: Coefficients of IV-$\overline{M_n}$ relationships (Eq. 3.12) for PET in phenol:TCE (1:1 by wt.).

Author	**T (^{o}C)**	***K*x10^4**	***A***	**$\overline{M_n}$ range x 10^{-3} (g/mole)**
Koepp and Werner [40]	20	7.55	0.685	3-30
Conix [41]	25	2.1	0.82	5-25
Griehl and Neue [42]	20	1.27	0.86	5-21 (non-fractionated)
Griehl and Neue [42]	20	0.9	0.87	5-21 (fractionated)

IV can be related to $\overline{M_n}$ using the IV-$\overline{M_n}$ relationship:

$$IV = K\overline{M}_n^{\,a} \qquad (3.12)$$

Several workers have reported the coefficients *K* and *a* for measurements in the same mixed solvents, and these are summarized in Table 3.2.

3.2.4 Liquid Chromatography – Mass Spectrometry (LC-MS)

The LC-MS system was from Agilent (1100 series, MS type 61946D), using the column Supersphere RP18e, 150x3 mm, particle diameter 4 μ. The sample was dissolved in a mixture of HFIP/THF (1:10), and the following elution (0.4 mL/min) profile was used: MeOH/H_2O/THF=50/50/0 for 10 min, then MeOH/H_2O/THF =100/0/0 for 5 min, then wash out with THF. An electrospray interface (ESI) was used to ionize the molecules. The drying gas temperature was 350 ^{o}C and flow rate was 10 L/min. The applied voltage on the capillary was 4 kV. The nebuliser pressure was 50 psi. Data were acquired in positive mode.

3.2.5 Solid-state polymerization in N_2 (SSP-N_2)

PET chips (average weight 0.045 g) were pressed for 1 min into thin disks (diameter ~1.5 cm, thickness ~180 micron) between two stainless steel plates heated to 160 ^{o}C, and these thin chips were used in all SSP experiments reported in this thesis. These PET chips were suspended in a cylindrical (id = 27 mm) glass reactor immersed into a preheated salt-bath, whose temperature was feedback controlled with a thermocouple placed in the reactor. Nitrogen gas flowing at the rate of 1 L/min (room temperature and pressure) was dried by passing through an anhydrous $CaSO_4$ column (W.A. Hammond Drierite, Xenia, Ohio), preheated by passing through a glass coil immersed in the same bath, and introduced at the bottom of the reactor. The nitrogen gas passed around the thin chips at a superficial velocity of 5 cm/s. Effectively higher velocities of 17 cm/s and 59 cm/s were achieved by keeping the nitrogen volumetric flow rate unchanged, but restricting the nitrogen flow through smaller cross-sections (id = 15 mm, 8 mm) of the reactor. The chips were first dried in a reactor at 165 ^{o}C for 6 hr. The chips were then transferred to another identical reactor, but maintained at 250 ^{o}C, and withdrawn after the desired time of reaction.

3.2.6 Sublimate collection during SSP-N_2

The SSP was conducted as above for 6 hr at 250 ^{o}C using thin PET chips (1 g), the outgoing gases were passed through a cold trap (glass coil, immersed in liquid nitrogen, path length = 0.3 m, id = 7 mm), and then bubbled through $CHCl_3$ before being let out to the exhaust. No sublimate was observed on the reactor walls, the transfer lines, and in the cold trap. The $CHCl_3$ in the bath could be evaporated without leaving any residue.

3.2.7 Solid-state polymerization in vacuum (SSP-vacuum)

Thin PET chips were placed in a glass made 150 mL round bottomed flask connected to a vacuum pump maintaining 10 mtorr pressure. The flask was immersed till its neck into a preheated, temperature controlled salt bath. The chips were first dried at 165 ^{o}C for 6 hr. The flask was then transferred to an identical bath but maintained at 252 ^{o}C (resulting in 250 ^{o}C inside the flask), and the flask was withdrawn after the desired time of reaction.

3.2.8 Sublimate collection during SSP-vacuum

The SSP was conducted with thin PET chips (1 g) as above for 3 hr at 250 ^{o}C. The sublimate was accumulated as a white film-like deposit on the cooler sections of the flask (i.e. on walls at the mouth of the flask just outside of the salt-bath), and was collected by scrapping with a spatula.

3.2.9 Determination of acid end-groups in PET

The fluoroderivatization of the acid end-groups was carried out by DCC mediated esterification with HFIP (see chapter 2):

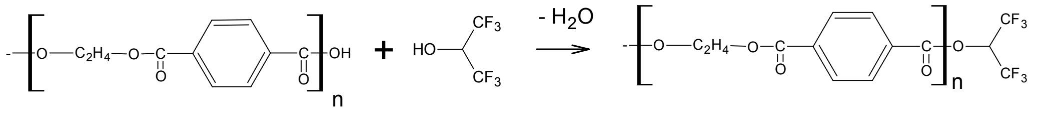

(3.13)

One chip of PET (0.045 g) was dissolved in a mixture of HFIP (0.2 g) and $CDCl_3$ (1.00 g) at room temperature. Firstly, part (0.1 g) of a solution of 4-pyrrolidinopyridine (0.001 g) in $CDCl_3$ (1 g) was added and subsequently, part (0.2 g) of a solution of DCC (0.0075 g) in $CDCl_3$ (1.5 g) was added. Finally, part (0.1 g) of a solution of TFT (0.01 g) in $CDCl_3$ (2 g) was added to the above reaction mixture to give the sample for ^{19}F NMR analysis. Integration of the δ -73.41 [d, 6F] peak for the fluoroester relative to the δ -62.9 [s, 3F] peak of TFT allowed quantification of the acid end-groups.

3.2.10 Determination of hydroxyl end-groups in PET

The hydroxyl end-groups were fluoroderivatized by esterification with TFA (chapter 2)

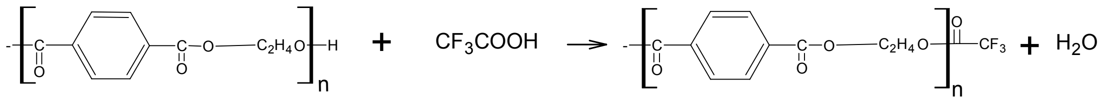

(3.14)

One chip of PET (0.045 g) was dissolved in a mixture of TFA (0.2 g) and $CDCl_3$ (1.0 g). Part (0.1 g) of a solution of TFT (0.01 g) in $CDCl_3$ (2 g) was added to the above reaction mixture. ^{19}F NMR analysis was carried out after standing for 72 hr. Integration of the δ -75.2 [s, 3F] peak for the fluoroester relative to the δ -62.9 [s, 3F] peak of TFT allowed quantification of the hydroxyl end-groups.

3.2.11 Preparation of TA and MHET mixture

BHET (3 g) was dissolved in EG (100 mL) and water (20 mL), and then NaOH solution (10 wt%, 3 g) was added [43]. The mixture was heated to 70 ^{o}C for 0.5 hr, cooled to room temperature, and more NaOH solution (5 g) was added. After 2 hr, sulfuric acid was added, after which a mixture of TA and MHET precipitated. The precipitate was washed three times with water and filtered, and finally dried. ^{1}H NMR in $CDCl_3$-HFIP mixture (95:5, by weight): MHET: δ=8.137 (s, 4H), 4.032 (t, 2H) 4.516 (t, 2H). ^{1}H NMR in DMSO: TA: δ 8.05 (s, 4H) ppm , MHET: δ 8.096 (d, J = 4.0, 4H), 3.735 (t, 2H), 4.327 (t, 2H).

3.2.12 Fluoroesterification of acid mixture or sublimate

0.002 g of the TA and MHET mixture (section 3.2.11), or of the sublimate (section 3.2.8), was added to 1 g of $CDCl_3$-HFIP mixture (95:5, by weight). 4-pyrrolidinopyridine (0.0001 g) and DCC (0.001 g) were each added as solution in $CDCl_3$ (0.1 g). ^{1}H NMR peaks at δ 8.256 (s, 4H), 6.01 (septet, 2H) correspond to the diester of TA,

(3.15)

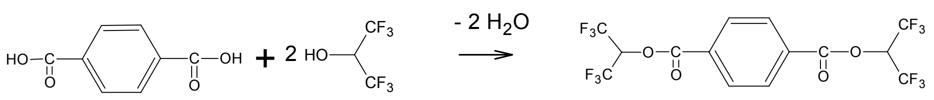

and the peaks δ 8.19 (d, 4H, J=2.8), 6.01 (septet, 1H), 4.02 (t, 2H), 4.52 (t, 2H) correspond to the fluoroester of MHET:

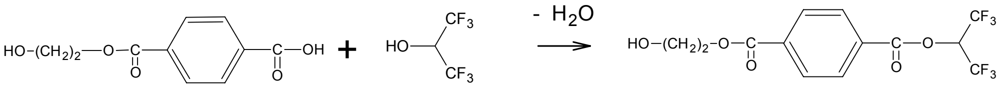
HO–(CH2)2—O—C(=O)—C6H4—C(=O)—OH
+
HO—CH(CF3)2
- H2O
HO–(CH2)2–O—C(=O)—C6H4—C(=O)—O—CH(CF3)2

(3.16)

3.3 Results and Discussion

The IV vs. time data for SSP of the 180 μ thick disks at 250 ^{o}C are shown in Fig. 3.1. Initially, the IV increases quickly during SSP-vacuum, and then nearly flattens out at a maximum IV of 2.75 dL/g at 6 hr. This kinetic data imply a much faster SSP as compared with the previously reported experiments. For example, Hsu [8], Rinehart [21], Ito et al. [23] and Boiko and Marikhin [24] reported the time required for reaching IV ~ 2.4 dL/g (or $\overline{M_n}$=130,000 g/mol) as 35 hr, 5 hr, 7 hr, and 10 hr respectively, as compared to 3 hr in our SSP-vacuum experiments. Further, we notice from Fig. 3.1 that the SSP proceeds faster in vacuum as compared to SSP under nitrogen sweep. This is also indicated by the faster depletion of the end-groups during SSP-vacuum as compared to SSP-N_2 (Fig. 3.2).

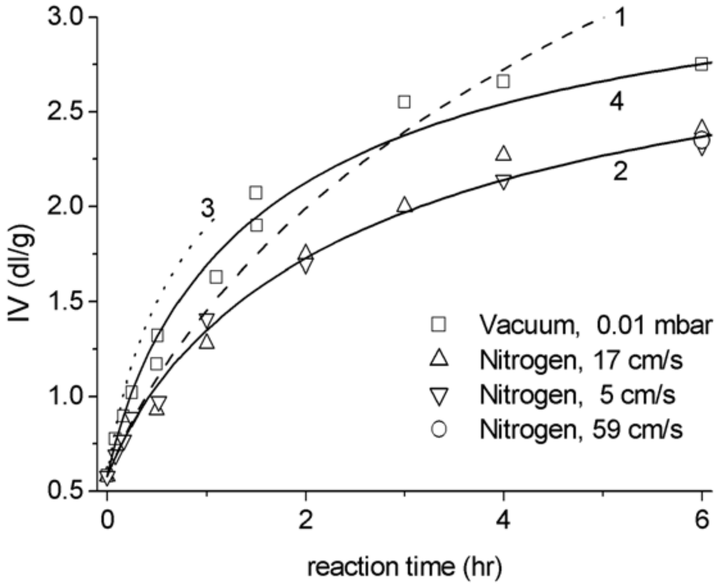

Figure 3.1: Increase in IV with time of SSP reaction in 180 μ thick PET chips at 250 ^{o}C in vacuum (10 mtorr) or under nitrogen flow (at the indicated gas velocities). Curve 1: fit to SSP-N_2 (5 cm/s) data up to 1 hr while considering all end-groups to be active (Eq. 3.6 ~ 3.10). Curve 2: fit to all SSP-N_2 (5 cm/s) data while accounting for a part of the acid and hydroxyl end-groups to be inactive (Eq. 18, 19). Curve 3: prediction for SSP-vacuum assuming kinetics control (Eq. 3.29 ~ 3.31) for removal of aromatic condensates. Curve 4: fit to SSP-vacuum data assuming mass transfer control (Eq. 3.32~3.34) for removal of aromatic condensates.

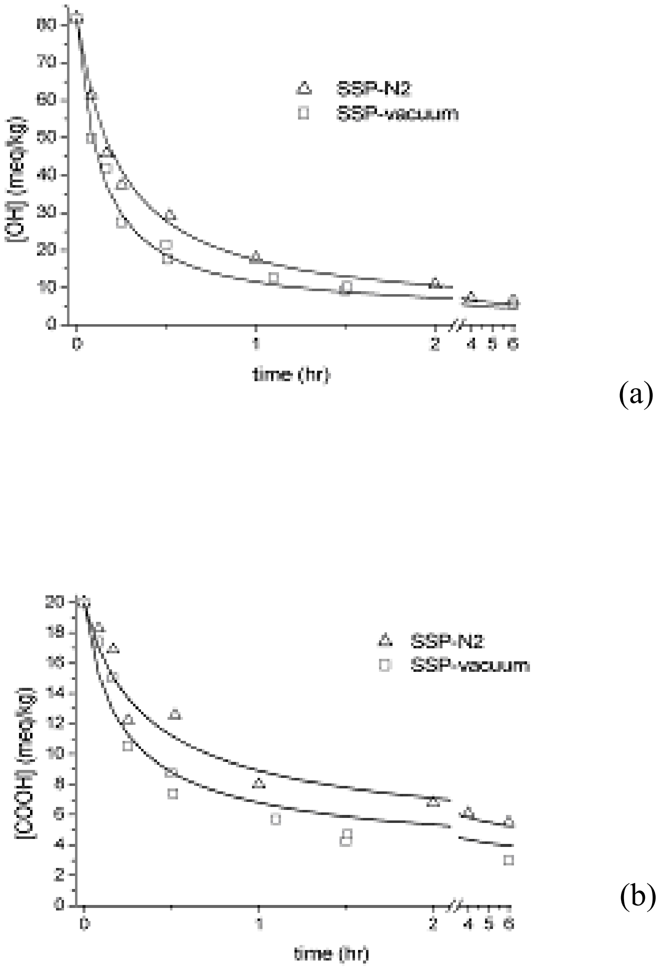

Figure 3.2: Depletion of the (a) hydroxyl and (b) acid end-groups with time of SSP reaction in 180 μ *thick PET chips at 250 °C in vacuum (10 mtorr) or under nitrogen flow (5 cm/s). The upper lines represent the fits to SSP-*N_2 *(5 cm/s) data while accounting for the inactive end-groups, and the lower lines represent the fit to SSP-vacuum data assuming mass transfer controlled removal of aromatic condensates.*

The results of Figs. 3.1 and 3.2 are replotted in Fig. 3.3 to show the dependence of the end-group concentrations on IV. The overlap of this dependence for SSP-N_2 and SSP-vacuum (Fig. 3.3) indicates that even though the overall rate of reaction is enhanced by vacuum (Figs. 3.1, 3.2), the pattern of end-group vs molecular weight remains similar between SSP-N_2 and SSP-vacuum .

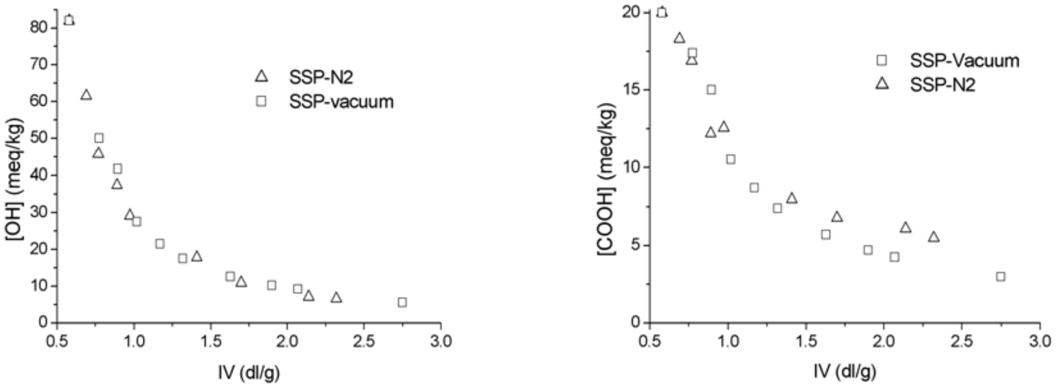

(a) (b)

Figure 3.3: Depletion of the (a) hydroxyl and (b) acid end-groups with increase in IV during SSP reaction in 180 μ thick PET chips at 250 ^oC in vacuum (10 mtorr) or under nitrogen flow (5 cm/s).

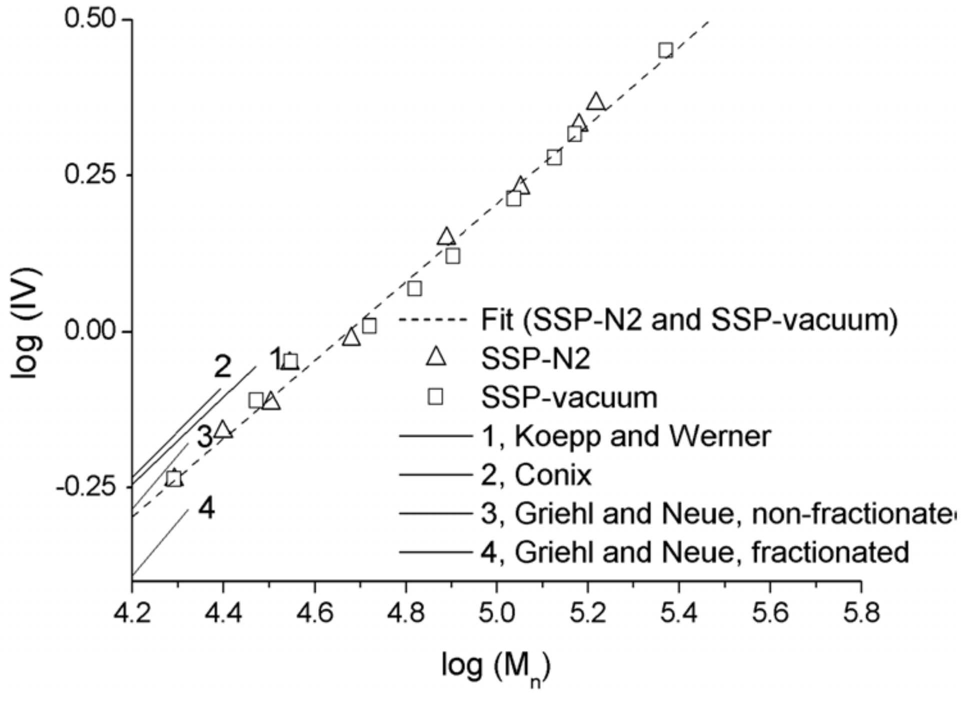

Figure 3.4: LogIV-$\overline{M_n}$ relationship between the measured IV (section 3.2.3) and $\overline{M_n}$ (determined from the end-group measurements of section 3.2.9 and 3.2.10) of the PET samples obtained during SSP-N_2 and SSP-vacuum. The dotted line is the least square fit on the logarithmic plot, resulting in Eq. 3.17. The continuous lines correspond to previously reported relations (Eq. 3.12, Table 3.2).

Fig. 3.4 shows the relation between the measured IV (Fig. 3.1) and the $\overline{M_n}$ calculated (Eq. 3.8) from the measured end-group concentrations. A least-square straight-line fit on the logarithmic plot yields the following Log (IV-$\overline{M_n}$) relation in phenol-TCE (1:1 by wt) at 30 ^{o}C :

$$IV = 1.175x10^{-3}\overline{M}_n^{0.627} \quad \text{for} \quad 0.58 < \text{IV} < 2.75 \text{ dL/g} \qquad (3.17)$$

which is shown as a dotted line in Fig. 3.4. For comparison, also shown (as continuous lines) are the previously reported IV- $\overline{M_n}$ relations (Eq. 3.12, Table 3.2). The differences between the previously reported measurements and our results could be related to the following: different temperatures for viscosity measurement, limited accuracy of the IV and end-group concentration measurements, different extent of additional (such as vinyl) end-groups present in the PET used, a smaller range of $\overline{M_n}$ (< 30,000 g/mol) examined by the previous workers, limited accuracy of the IV-η_{rel} approximation (Eq.3.11), etc.

3.3.1 SSP-N$_2$ kinetics and crystallization induced chain-end immobility

We notice from Fig. 3.1 that the kinetics of SSP-N$_2$ is not affected by increasing the nitrogen flow velocity beyond 5 cm/s, indicating that gas phase mass transfer is not the rate controlling step under these conditions. In case of thick PET (half thickness, *L* $>\sqrt{D/(kC)}$, where *D* and *C* are the condensate diffusivity and concentration, and *k* is the corresponding rate constant [11]), the SSP can be limited by the outward diffusion of the condensates EG and water through the polymer. Calculation with $D_{EG} = 3.1x10^{-6}$ cm^2/s [21], k = 0.0115 kg/meq-hr (this chapter), and *C*=82 meq/kg (this chapter) suggests that such diffusion limitations are negligible at the chip thickness of 180 μ employed in this work. Hence, the observed rate of our SSP reaction must be limited by the intrinsic reaction kinetics, and we will like to represent our SSP kinetics data in terms of the reactions (1) and (2). We realize that several possible side reactions can result in additional consumption/production of the hydroxyl and acid end-groups, and lead to formation of vinyl and diethylene glycol end-groups, acetaldehydes, and crosslinks [2,13]. However, considering the moderate temperature (as compared to melt polymerization) and inert atmosphere (e.g. oxygen is known to accelerate degradation rate [2]) involved in our work, we keep our kinetics analysis simple by ignoring these side reactions and additional end-groups, and their influence on $\overline{M_n}$ (Eq. 3.8) and hence on the Log IV-$\overline{M_n}$ relationship (Eq. 3.12).

First, the kinetics data ([OH](t) and [COOH](t)) in the initial stage (IV up to 1.5 dL/g) of SSP-N_2 (5 cm/s) are fitted with the kinetics expressions Eq. 3.10 (using the CONSTANT_RELATIVE_VARIANCE model of the gPROMS software, PSE Enterprises, UK) to estimate the rate constants: k_1 = 0.0111 kg/meq-hr and k_2 = 0.0264 kg/meq-hr. These values can be compared with Kang's analysis [21] of the experiments of Chen and Chen [3] resulting in k_1 = 0.009 kg/meq-hr and k_2 = 0.0143 kg/meq-hr at 230 ^{o}C, though most likely with a different catalyst composition. The fitted curve 1 (Fig. 3.1) deviates from our experimental values at the larger time (t > 1 hr). This is because the reaction rate at this time is strongly influenced by inability of a part of the end-groups to participate in the condensation reactions (Eqs. 3.1 and 3.2). Zhi-Lian et al. [14], Wu et al. [23] and Kang [21] did not notice such inconsistency because their experimental observations were limited to $\overline{M_n}$ less than 52000 g/mol. Duh [16] accounted for such inactive groups, but its enormous impact was not visible in their analysis limited to IV less than 1.3 dL/g. Our fitted results (curve 1 of Fig. 3.1) indicate that the SSP-N_2 data at such IV (< 1.3 dL/g) can easily be represented even while neglecting the effect of such inactive groups. Though the concentration of such groups is small, they make up an increasing fraction of the total number of end-groups with progress of SSP. The inability of a part of the end-groups to participate in the polycondensation reactions can be either due to chemical degradation, leading to unreactive chain ends (such as vinyl end group), or due to the reactive ends being unable to approach each other. Such limited extent of mobility of some chain-ends could be a result of their restriction by relatively short chain segments linking them to crystalline parts, or a result of their incorporation in crystalline parts as defects. We note from Fig. 3.2 that the OH and the COOH end-groups are still detectable (by fluoroderivatization and ^{19}F NMR), at substantial concentrations of 5 meq/kg and 3 meq/kg respectively, at the end of our SSP-vacuum where the observed reaction rate is very low compared to the SSP rate expected if some of these were not temporarily inactivated (Fig. 3.1). We verified this by the following experiment: starting with the PET sample of IV = 2.75 dL/g (obtained by SSP-vacuum, t = 6 hr as in Fig. 3.1), a continued SSP-vacuum at 250 °C for an additional 4 hours resulted in no further increase in IV. Four of these PET chips were placed on aluminium foils, and heated under vacuum to melt at 270 °C. After allowing further polymerization in melt for 1.5 hr, the chips were examined for IV. The measured IV = 2.97 dL/g represents a re-initiation of the polymerization in melt. We conclude that melting at the apparent end of reaction during SSP results in release of the crystalline restraints on the mobility of the temporarily inactivated acid and hydroxyl end-groups, allowing post polymerization to start again.

This suggests that a kinetic analysis of SSP should take into account this apparent inactivity of a fraction of the OH and COOH end-groups. We consider both the transesterification and the esterification reactions as we monitor both the OH and the COOH end-groups during the SSP:

$$R_{EG} = 2k_1([OH]-[OH]_i)^2 \tag{3.18}$$

$$R_{H2O} = k_2([COOH]-[COOH]_i)([OH]-[OH]_i) \tag{3.19}$$

where $[OH]_i$ and $[COOH]_i$ are the (unknown) concentrations of the temporarily inactivated OH and COOH end-groups during SSP. The IV(t), [OH](t) and [COOH](t) data in the entire range of SSP-N_2 (5 cm/s) are now fitted using the gPROMS software with the kinetics expressions Eq. 3.6~3.8 and 3.18~3.19 to estimate the rate constants: k_1 = 0.0115 kg/meq-hr, k_2 = 0.034 kg/meq-hr and the inactive end-group concentrations $[OH]_i = 3.1$ meq/kg and $[COOH]_i = 2.8$ meq/kg. The corresponding calculated [OH](t), [COOH](t) and IV(t) profiles are shown as curve 2 in Fig. 3.1, and as upper lines in Figs. 3.2a and 3.2b, and we conclude a satisfactory match with the experimental measurements till IV =2.3 dL/g obtained by us during SSP-N_2.

We may compare our estimated inactive end-group concentrations (C_i) with the following relation of Duh [16]

$$C_i = 43.31 + 1.0723C_o - 4.683\times10^{-2}T - 2.0755\times10^{-3}C_oT \tag{3.20}$$

for 200 °C ≤ T ≤ 230 °C

where $C_o = [OH]_o + [COOH]_o = 102$ meq/kg is the initial concentration of the reactive groups in PET pellets. When extrapolated to 250 ^{o}C, Eq. 3.20 yields an inactive end-group concentration of 17.5 meq/kg. This is far in excess of the $[OH]_i + [COOH]_i = 5.9$ meq/kg obtained by us, and indicates that this relation (Eq. 3.20) cannot be extrapolated to the SSP conditions employed by us.

3.3.2 SSP-Vacuum

Fig. 3.1 indicates that under otherwise identical conditions, SSP proceeds significantly faster in vacuum as compared to the SSP under N_2 sweep. We do not expect an influence of the inert surrounding media on the intrinsic reactions, but an influence on mass transfer of the condensates by one of the following mechanisms is a possibility:

(1) faster removal of water or EG when vacuum is applied
(2) removal of other end-group containing molecules under vacuum

As discussed in section 3.3.1, removal of water and EG through the polymer and the surrounding medium is not the rate limiting step during our SSP, and hence hastening of these steps during SSP-vacuum cannot explain the observed increase in the overall reaction rate during SSP-vacuum as compared to SSP-N_2. Our following observation of the solid deposits (sublimate) on the cold parts of the reactor walls during SSP-vacuum (section 3.2.8) and not during SSP-N_2 (section 3.2.6) points to the possibility (2) above, and we decided to carry out an analysis of the constituents of the sublimate. Higher vacuum levels resulting in supersaturation of solutes are known [44, 45] to enhance diffusive devolatilization of solutes from polymer matrices.

3.3.2.1 Characterization of sublimate from SSP-vacuum

^{1}H NMR spectrum of the sublimate (section 3.2.8) in a $CDCl_3$-HFIP (95:5 by wt) mixture is shown in Fig. 3.5a. The singlets at δ 8.08 and 4.69 are attributed [46] to the cyclic oligomers of PET. The singlet at δ 8.115 (4 H) and the triplets at δ 4.035 (4H) and δ 4.505 (4 H) are attributed to BHET, and we verified this by addition of additional BHET that resulted in enhancement of these peaks. The singlet at δ 8.137 is attributed to MHET (section 3.2.11). This was confirmed by a DCC-mediated esterification of the

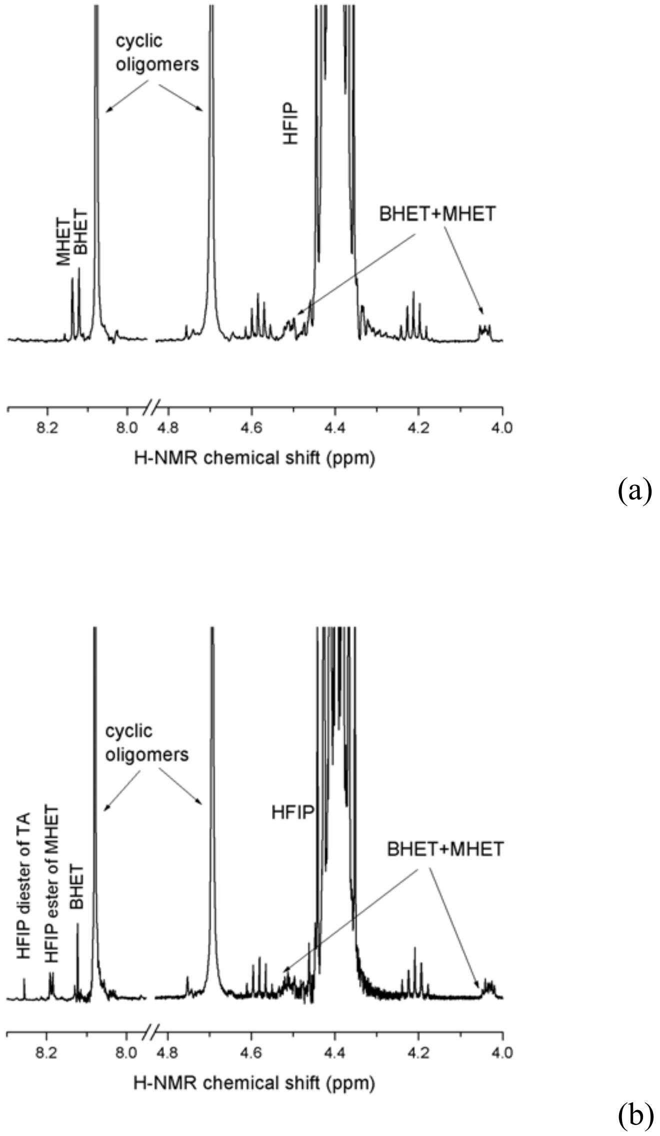

Figure 3.5: ^{1}H NMR of the sublimate obtained during SSP-vacuum, (a) as obtained in section 3.2.7, and (b) after esterification with HFIP (section 3.2.12).

sublimate with HFIP (section 3.2.12), when a doublet at δ 8.19 ($J = 2.4$) featured (Fig. 3.5b) corresponding to the hexafluroisopropyl ester of MHET (section 3.2.12). In addition, a singlet at δ 8.256 featured (Fig. 3.5b) corresponding to diester of TA (section 3.2.12), indicating that TA was constituent of the sublimate, but was not detected in the ^{1}H NMR of the sublimate (Fig. 3.5a) because it is insoluble in the $CDCl_3$-HFIP mixture. The composition of the sublimate so determined, is shown in Table 3.3. During LC-MS (section 3.2.4) of the SSP-vacuum sublimate, the species eluted at 2.88 min and 3.13 min were detected to have molar mass of 243 and 277 g/mole, respectively, corresponding to ionized MHET and BHET, thus further verifying the presence of MHET and BHET in the sublimate.

Table 3.3: Composition of the SSP-vacuum (250 ^{o}C, 3 hr) sublimate (section 3.2.8) as determined by ^{1}H NMR (Fig. 3.5).

Constituents	**Mole fraction (aromatic rings)**
cyclic oligomers (trimers)	0.92
BHET	0.035
MHET	0.037
TA	0.007

3.3.2.2 Reactions responsible for the aromatic condensates in sublimate

The extraction of cyclic oligomers at high vacuum during melt polymerization reactions is well known [27]. These cyclic oligomers (primarily trimers) are believed to be formed mainly by transesterification of hydroxyl chain-ends [47, 48]. Added presence of TA, MHET and BHET in the sublimate during SSP-vacuum indicates that these are formed as condensates during SSP by the following reactions, and their removal from the PET chips by high vacuum enhances the rate of the rise of IV during SSP-vacuum as compared to SSP-N$_2$:

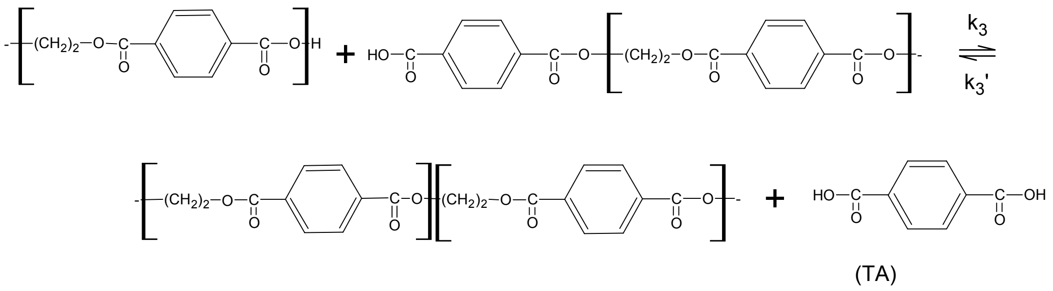

(3.21)

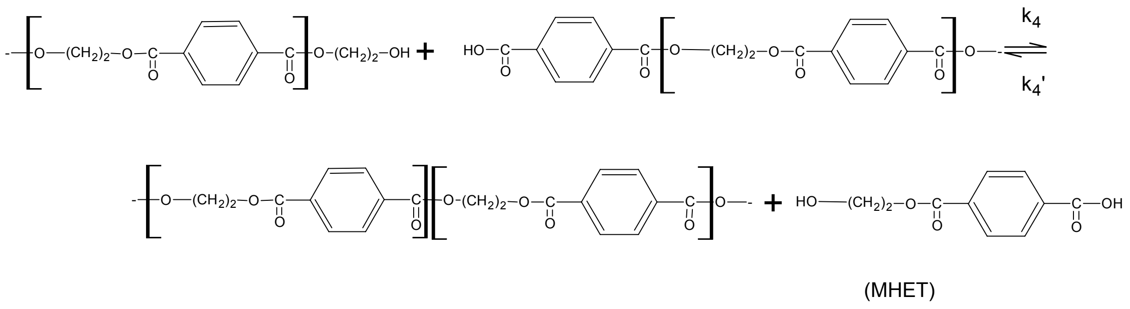

(3.22)

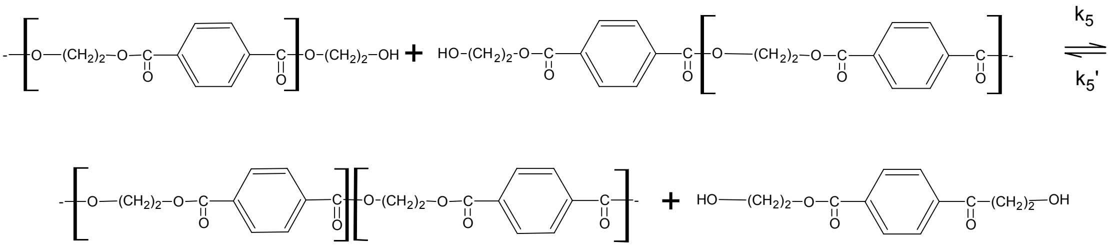

(BHET)

(3.23)

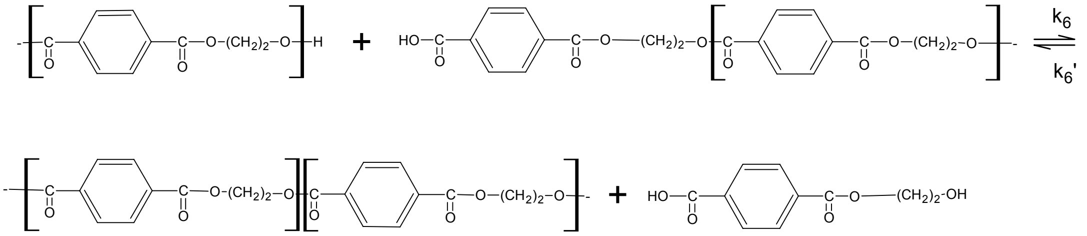

(MHET)

(3.24)

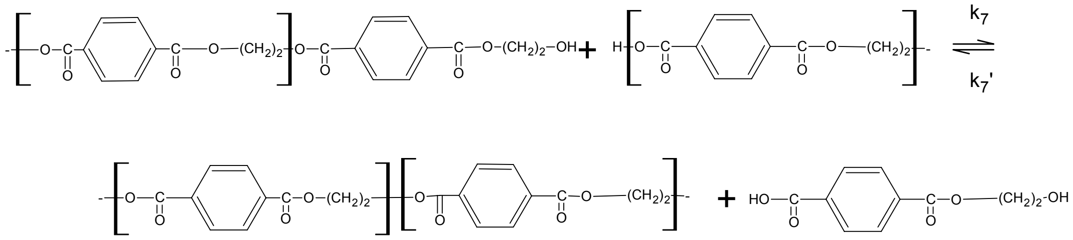

(MHET)

(3.25)

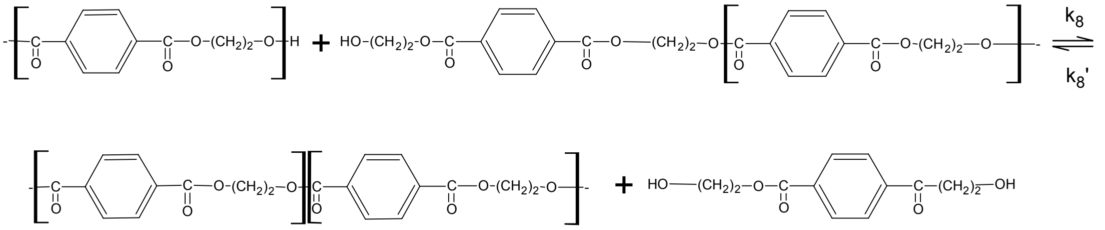

(BHET)

(3.26)

Though these are essentially the well-known intermolecular glycolysis, acidolysis and transesterification reactions [49,50], their importance in the overall progress of polymerization has not been realized in the past. If an instantaneous removal of TA, MHET and BHET during SSP was possible, incorporation of these reactions in the kinetic scheme along with (trans)esterification reactions (Eqs. 3.1 and 3.2) would lead to the following modification of the reaction kinetics (Eqs. 3.6 and 3.7):

$$\frac{d[OH]}{dt} = -2R_{EG} - R_{H2O} - 2R_{BHET} - R_{MHET} \tag{3.27}$$

$$\frac{d[COOH]}{dt} = -R_{H2O} - R_{MHET} - 2R_{TA} \tag{3.28}$$

where the EG and water production rates would continue to be described by Equation 3.15 and 3.16, and we can estimate the maximum rates of production (and removal) of TA, MHET and BHET in the absence of the reverse reaction as:

$$R_{TA} = 2k_3([COOH]-[COOH]_i)^2 \tag{3.29}$$

$$R_{MHET} = (k_4 + k_6 + k_7)([COOH]-[COOH]_i)([OH]-[OH]_i) \tag{3.30}$$

and

$$R_{BHET} = 2(k_5 + k_8)([OH]-[OH]_i)^2 \tag{3.31}$$

where we have again assumed the reaction rates to be dependent only on the reactive chain-ends. We further approximate $k_3 = k_4 = k_5 = k_6 = k_7 = k_8 \approx k_1$, as Kotliar [50] estimated the polycondensation and redistribution rates to be comparable (at 254 ^{o}C). Solving the initial value problem posed as Eqs. 3.27~3.31 as well as Eqs. 3.18~3.19 using the $k_1, k_2, [OH]_i, [COOH]_i$ values as obtained from SSP-N$_2$ experiments, we find the predicted IV(t) profile (curve 3 in Fig.3.1) at short time (< 1 hr) to be much faster than the SSP-vacuum observations of Fig. 3.1. Thus, as expected, the rate of removal of the aromatic condensates TA, MHET and BHET must be far short of their maximum possible production rate estimated from the kinetics of the forward reaction alone (Eqs.

3.29~3.31). Hence, the net contribution of the reactions (Eqs. 3.18~3.23) to the progress of SSP-vacuum can be expected to be controlled by the rate of mass transfer of the aromatic condensates.

3.3.2.3 Mass transfer controlled removal of aromatic condensates during SSP-vacuum

A realistic analysis should consider simultaneously the reaction kinetics, and mass-transfer (both through the polymer and the surrounding medium, as influenced by the reduced pressure [44, 45]) of the aromatic condensates. However, this is formidable in the absence of data such as all kinetic rate constants (Eqs. 3.21~3.26) and diffusivities and mass-transfer coefficients, and we simply lump these effects [51] by writing the rates of removal of TA, MHET and BHET in terms of the corresponding (unknown) overall mass transfer coefficients k_{TA}, k_{MHET} and k_{BHET} :

$$R_{TA} = k_{TA}[TA] \tag{3.32}$$

$$R_{MHET} = k_{MHET}[MHET] \tag{3.33}$$

and

$$R_{BHET} = k_{BHET}[BHET] \tag{3.34}$$

We shall further consider the concentrations of TA, MHET and BHET in the PET chips during SSP-vacuum to be determined by (pseudo) equilibrium considerations. Using equal reactivity hypothesis and probabilistic arguments [52] we can arrive at the following:

$$\frac{[TA]}{[P]} = \frac{[COOH]}{[COOH]+[OH]}(1-p_{COOH}) \tag{3.35}$$

$$\frac{[MHET]}{[P]} = \frac{[COOH]}{[COOH]+[OH]}p_{COOH}(1-p_{OH}) \tag{3.36}$$

$$\frac{[BHET]}{[P]} = \frac{[OH]}{[COOH]+[OH]}p_{OH}\,p_{COOH}(1-p_{OH}) \tag{3.37}$$

where $[P]=\frac{[COOH]+[OH]}{2}$ refers to molar concentration of all (macro) molecular species in the PET undergoing SSP, $p_{COOH}=\frac{[COO]}{[COO]+[COOH]}$ and $p_{OH}=\frac{[COO]}{[COO]+[OH]}$ refer to the fraction of the reacted COOH and OH groups in the PET, and [COO] refers to the concentration of the ester groups. Under the simplification $[COOH]<<[COO]$ and $[OH]<<[COO]$, this leads us to:

$$[TA]=\frac{[COOH]^2}{2[COO]} \tag{3.38}$$

$$[MHET]=\frac{[COOH][OH]}{2[COO]} \tag{3.39}$$

$$[BHET]=\frac{[OH]^2}{2[COO]} \tag{3.40}$$

Further, considering the presence of inactive end-groups, [OH] and [COOH] in the Eqs. 3.35~3.40 should be replaced by $([OH]-[OH]_i)$ and $([COOH]-[COOH]_i)$ respectively. We will now like to determine the yet unknown mass transfer coefficients by fitting the SSP-vacuum data in the form of IV(t), [OH](t) and [COOH](t) (Fig. 3.2a and 3.2b) with the rate expressions Eqs. 3.18~3.19, 3.27~3.28, 3.32~3.34 and 3.38~3.40. With the limited experimental data available here, it seems unreasonable to try to estimate the three different mass transfer coefficients. In the absence of a more suitable interrelation, we make a somewhat gross approximation $k_{TA}=k_{MHET}=k_{BHET}=k(say)$, and then use gPROMS to fit the SSP-vacuum data (Fig. 3.1 and 3.2), thereby estimating the overall mass transfer coefficient $k=405$ /hr, or the corresponding surface area based mass transfer coefficient $k'=kL=0.06$ cm/min. The corresponding calculated IV(t), [OH](t) and [COOH](t) profiles for SSP-vacuum are shown as curve 4 in Fig. 3.1, and as lower lines in Fig. 3.2a and 3.2b. We conclude a satisfactory match with the experimental measurements till IV = 2.75 dL/g obtained by us, suggesting that the enhancement in overall reaction rate during SSP-vacuum as compared to SSP-N_2 can be attributed to the mass transfer controlled removal of the end-group containing aromatic condensates during SSP-vacuum. While our experimental measurements indicate leveling out of the IV increase during SSP at 6 hr, the predicted curves still show an increasing trend. This may be because the so termed inactive end-groups are not all inherently inactive to begin with, but some are rendered inactive during the SSP by the progressing crystallization. Though a theoretical modeling of such an effect is not possible at present, its consideration would have predicted a sharper slowdown in the SSP reaction, and perhaps in a better agreement with our experimental observations.

3.4 Conclusions

We have analyzed the kinetics of SSP of thin PET chips at 250 ^{o}C in two different reaction environments: fast flowing nitrogen and high vacuum. The post polymerization begins with efficient removal of EG and water as condensates, but slows down considerably at IV > 1.3 dL/g due to the restricted mobility of a part of the chain-ends due to crystalline constraints. This is verified by detection of a substantial concentration of the hydroxyl and acid end-groups at IV=2.75 dL/g at the end of SSP-vacuum, and further post-polymerization only after melting to impart mobility to these end-groups. An analysis of the sublimate during SSP-vacuum shows that TA, MHET and BHET are removed from the PET chips at the high temperature and vacuum applied. These aromatic molecules carrying functional end-groups are considered to be produced by acidolysis, glycolysis and transesterification reactions. Their removal as a sublimate during SSP under vacuum provides an additional pathway for the progress of SSP, albeit limited by mass transfer even in the thin PET chips considered here.

References

[1] Schaaf E, Zimmerman H, Dietzel W, Lohmann P. Acta Polymerica 1981; 32: 250.
[2] Ravindranath K, Mashelkar RA. Chem Engng Sci 1986; 41: 2197.
[3] Chen S-A, Chen F-L. J Polym Sci, Part A: Polym Chem 1987; 25: 533.
[4] Duh B. J Appl Polym Sci 2002; 83: 1288.
[5] Marechal E. Polyesters: Synthesis and Chemical Aspects. In: Fakirov S, editor, Handbook of Thermoplastic Polyesters, New York: Wiley; 2002. Vol. I, p. 1.
[6] Aharoni SM. Industrial Scale Production of Polyesters, In: Fakirov S, editor, Handbook of Thermoplastic Polyesters. New York: Wiley, 2002. vol. I, p. 56.
[7] Wendling PR. US patent 4532319, 1985.
[8] Hsu L-C. J Macromol Sci-Phys 1967; B1(4): 801.
[9] Chen FC, Griskey, RG Beyer GH. AIChEJ 1969; 15: 680.
[10] Jabarin SA, Lofgren EA. J Appl Polym Sci 1986; 32: 5315.
[11] Ravindranath K, Mashelkar RA. J Appl Polym Sci 1990; 39: 1325.
[12] Fakirov S. In: Schultz JM, Fakirov S. editors, Solid State reactions in Linear Polycondensates. In: Solid State Behavior of Linear Polyesters and Polyamides. New Jersey: Prentice Hall, 1990. p. 1.
[13] Devotta, I Mashelkar RA. Chem Engng Sci 1993; 48: 1859.
[14] Zhi-Lian T, Gao Q, Nan-Xun H, Sironi C. J Appl Polym Sci 1995; 57: 473.
[15] Huang B, Walsh JJ. Polymer 1998; 39: 699.
[16] Duh B. J Appl Polym Sci 2001; 81: 1748.
[17] Gaymans RJ, Amrithraj J, Kamp H. J Appl Polym Sci 1982; 27: 2513.
[18] Kaushik A, Gupta SK. J Appl Polym Sci 1992; 54: 507.
[19] Warner SB, Lee J. J Polym Sci, Polym Phys Ed 1994; 32: 1759.
[20] Srinivasan R, Almonacil C, Narayan S, Desai P, Abhiraman AS. Macrmolecules 1998; 31: 6813.
[21] Kang, C-K. J Appl Polym Sci 1998; 68: 837.
[22] Mallon FK, Ray WH. J Appl Polym Sci 1998; 69: 1233.
[23] Wu D, Chen F, Li R, Shi Y. Macromolecules 1997; 30: 6737.
[24] Boiko YM, Marikhin VA. Polymer Science USSR, Ser. A 2000; 42: 1169.
[25] Medellin-Rodriguez FJ, Lopez-Guillen R, Waldo-Mendoza MA. J Appl Polym Sci 2000; 75: 78.
[26] Gao Q, Nan-Xun H, Zhi-Lian T, Gerking L. Chem Engng Sci 1997; 52: 371.
[27] Chang TM. Polym Engng Sci 1970; 10: 364.
[28] Chang S, Sheu M-F, Chen SM. J Appl Polym Sci 1983; 28: 3289.
[29] Karayannidis GP, Kokkalas DE, Bikiaris DN. J Appl Polym Sci 1995; 56: 405.

[30] Kokkalas DE, Bikiaris DN, Karayannidis GP. J Appl Polym Sci 1995; 55: 787.

[31] Duh B. Polymer 2002; 43: 3147.

[32] Gupta SK, Kumar A. Reaction Engineering of Step Growth Polymerization. New York: Plenum, 1987. p. 285.

[33] Ito M, Takahashi K, Kanamoto T. J Appl Polym Sci 1990; 40: 1257.

[34] Ziabicki A. Text Res J 1996; 66: 705.

[35] Huang B, Tucker PA, Cuculo JA. Polymer 1997; 38: 1101.

[36] Jabarin SA. Polymer Material Encyclopedia 1996; 8: 6078.

[37] Schaaf E et al. East Ger patent 139,129: 1979

[38] Mallon F, Beers K, Ives A, Ray WH. J Appl Poym Sci 1998; 69: 1789.

[39] Solomon OF, Ciuta IZ. J Appl Polym Sci 1962; 6: 683.

[40] Koepp HM, Werner H. Makromol Chem 1959; 32: 79.

[41] Conix A. Makromol Chem 1958; 26: 226.

[42] Griehl W, Neue S. Faserforsch Textiletechn 1954; 5: 423.

[43] Hotten BW. Ind Engng Chem 1957; 49: 1691.

[44] Biesenberger JA, Sebastian DH. Polymer Devolatilization. In: Principles of Polymerization Engineering. New York: Wiley, 1983. p. 573.

[45] Ravindranath K, Mashelkar RA. Chem Engng Sci 1988; 43: 429.

[46] Byrant JJL, Semlyen JA. Polymer 1997; 38: 2475.

[47] Peebles LH, Huffman MW, Ablett CT. J Polym Sci (A-1) 1969; 7: 479.

[48] Ha WS, Choun YK. J Polym Sci, Polym Chem 1979; 17: 2103.

[49] Ravindranath K, Mashelkar RA. Chem Engng Sci 1986; 41: 2969.

[50] Kotliar AM. J Polym Sci, Macromol Rev 1981; 16: 367.

[51] Maffettone PL, Astarita G, Cori L, Carnelli L, Balestri F. AICHE J 1991; 37: 724.

[52] Peebles LH. Molecular weight distributions in polymers, 1st Ed., Interscience, New York: 1971.

Chapter 4 Solvent assisted post-polymerization of PET

4.1 Introduction

High molecular weight grades of PET are desired for potential applications for high modulus high strength fibers through solution spinning. Solid-state polymerization to IV greater than 1.5 dL/g often requires reaction temperatures close to the PET melting point, as well as reduction of the effective PET diffusion length to less than 1 mm through film formation or porosity generation. The problems associated with fusion of these fine particles at these high temperatures demand special solids handling procedures.

4.1.1 Role of crystallization during SSP

The extent of crystallinity and the crystalline morphology are known to influence the rate of SSP [1, 2, 3]. For example, it is believed that the end groups, and hence the chemical reactions, given in Eq. 3.1 and Eq. 3.2, during SSP, are restricted to the amorphous phase of PET. This enhances the effective end group concentration in the amorphous phase and hence the reaction rate [4]. Several authors have followed the kinetics of SSP while monitoring the reduction in the OH and the COOH end-group concentrations with progress of SSP to moderate molecular weights [5, 6, 7, 8, 9]. The role of crystallization induced end group concentration enhancement can be considered to be imbedded in their effective rate constants. An additional consideration that becomes increasingly important during SSP to high IV is the role of crystallization in limiting the accessibility of the end-groups to each other. Duh [10] accounted for this role of crystallization, but ignored the esterification reaction (Eq. 3.2), and did not directly measure concentrations of the end-groups, and limited his analysis to IV values less than 1.3 dL/g. However, he did not face a contradiction in fitting the kinetics, because his analysis was limited to molar mass less than 52000 g/mol. We showed in chapter 3 that the rapid slowdown in SSP kinetics at IV greater than 1.3 dL/g could be represented by transesterification and esterification reactions (Eqs. 3.1 and 3.2) only when accounting for the part of the acid and hydroxyl end groups ($[COOH]_i$ and $[OH]_i$) to be rendered temporarily inactive, resulting in rate expressions Eqs (3.15 and 3.16) instead of Eqs. 3.6 and 3.7.

A temporary inactivation of a part of the end groups through mobility restriction could arise either due to relatively short chain segments linked to crystalline parts, or as a result of their incorporation in crystalline parts as defects. Though the concentration of such groups is small, they make up an increasing fraction of the total number of end-groups with progress of SSP.

4.1.2 Solvent assisted polymerization of PET

As discussed in section 4.1.1, the polymerization rates in the solid state are often limited by the low diffusivity of water and EG out of the chips and by the low mobility of the reactive hydroxyl and carboxyl end groups of the polymer chains. A recent innovation for obtaining ultra high molecular weight (UHMW) PET is the swollen state polymerization (SwSP) [11, 12, 13, 14]. Here, the polymerization of PET chips is carried out by swelling in a suitable solvent that does not dissolve the chips. The rate of such SwSP is higher than SSP at the same temperature, and found to depend on the nature of solvent and the extent of swelling. More importantly, the highest achievable IV by SwSP is found to be dependent on several parameters, e.g. solvent used [11], particle size [12, 13,15], initial IV [15], degree of swelling [11, 13,16], catalyst concentration [16,17] and reaction temperature [12, 15, 16]. For example, Tate and Watanabe [13] found that while PET fibres could be post polymerized in swollen state in hydrogenated terphenyl at 236 °C for 15 hr to IV = 3.1 dL/g, PET granules (3 mm) could not be polymerised to IV greater than 2.1 dL/g. Ha et al. [15] found that porous and fibrous PET of starting IV = 0.62 dL/g could be similarly post polymerized in swollen state in hydrogenated terphenyl at 230 °C for 6 hr to IV = 1.82 dL/g, but not higher. Wang et al. [16] found that PET of starting IV = 0.62 dL/g could not be post polymerized in swollen state in a diphenyl ether - biphenyl (DPE-BP) mixture at 200 °C to IV values exceeding 1 dL/g. The enhancement in polymerization rate by swelling with a solvent may be due to the increased surface area (high mass transfer rates of condensates), enhanced diffusivity of condensate molecules (enabling their easy removal), increased mobility of reactive chain ends (accelerating their collisions), and intrinsic catalytic effects of solvent presence/participation in reaction. Since Parashar et al. [17] found the SwSP rates to be larger than SSP rates even in very thin PET chips where the condensate diffusion (mass transfer) limitation was eliminated, they attributed the increased post polymerization rates of thin PET chips during SwSP to the increased mobility of the chain ends due to the presence of the solvent [17]. However, the same solvent that assists chain mobility at low IV can increase PET crystallization by solvent induced crystallization [11,13]. In line with the crystallization induced limitation during SSP, the high degree of crystallization during SwSP perhaps brings in stronger limitations in the highest IV values achievable during SwSP. If so, it is interesting to examine if the post polymerization can be carried out to higher IV in solutions, thus eliminating the limitation imposed by solvent induced crystallization. Since the toxicity of the thermal fluids (such as DPE, BP) is small, post polymerization in these solvents can be especially interesting if the high molecular weight PET polymerized in these solvents can be directly spun into high modulus high strength fibers. Tate et al. [18] reported extrusion of PET (IV = 2 dL/g) melt plasticized with 1-methyl naphthalene (20 wt%) at 270 ^{o}C, followed by solvent evaporation and drawing to a draw ratio of about 6, resulting in tensile modulus and strength of 2 GPa and 30 GPa respectively. Rogers [19] reported solution spinning of a 30% solution of PET of IV = 1.71 dL/g into filaments that could be drawn into fiber of modulus as high as 90 g/dtex.

In this chapter, we follow the progress of SwSP by monitoring not only the IV, but also the acid and hydroxyl end-groups concentrations using our recently developed NMR based technique (chapter 2). The results are analyzed in terms of the kinetics of the two simultaneous reactions producing EG and water (Eqs. 3.1 and 3.2), and the limiting IV obtained is explained in terms of the crystallization induced temporary inactivation of part of the end groups with consideration of concentration enhancement effect due to crystallization at the same time. Solution polymerization of PET in the same solvents is then examined to eliminate the role of crystallization.

4.2 Experimental

4.2.1 Materials

PET chips (IV = 0.42 dL/g) were obtained from Wilton Research Center (ICI, UK). Chloroform ($CHCl_3$, 99.9%), deuterated chloroform ($CDCl_3$, 99.9 atom D %), hexafluoroisopropanol (HFIP, 99%), α,α,α-trifluorotoluene (TFT, 99%), 4-pyrrolidinopyridine (98%), trifluoroacetic acid (TFA, 99%) and bishydroxyethyl terephthalate (BHET) were obtained from Aldrich. Dicyclohexyl carbodiimide (DCC, 99%), DPE

(98%), BP (99%) were obtained from Merck. All chemicals were used as received. DPE and BP were mixed in the weight ratio (73.5:26.5), and dried over molecular sieves (4 A) over three days to obtain the mixed solvent DPE-BP.

4.2.2 NMR Analysis

A 400 MHz Varian Mercury Vx 400 was used to carry out the ^{19}F NMR measurements, using $CDCl_3$ mixture with HFIP or TFA as the solvents.

4.2.3 Intrinsic Viscosity (IV) of PET

The relative viscosity (η_{rel}) of solution of PET in a phenol-TCE mixture (1:1, by weight) at concentration (c = 0.5 g/dL) was determined using an Ubbelohde viscometer at 30 °C. IV was estimated from this single point measurement of η_{rel} and using the following approximation for linear flexible chains [20]:

$$\mathrm{IV}=1/c\ [2(\eta_{\mathrm{rel}}-1)-2\ln(\eta_{\mathrm{rel}})]^{1/2} \tag{4.3}$$

which can be related to $\overline{M_n}$ using the IV-$\overline{M_n}$ relationship [21, 22, 23]:

$$IV = K\overline{M}_n^{\ a} \tag{4.4}$$

4.2.4 Differential Scanning Calorimetry (DSC)

The melting characteristics of the samples were examined using a Perkin-Elmer differential scanning calorimetry system DSC-7. The heat of melting and heat of crystallization were determined from the corresponding peak area during the heating scan at 20 °C min^{-1}.

4.2.5 WAXD

The crystallized PET samples were dried by evaporation under vacuum at room temperature. The WAXD measurements were obtained with a Rigaku D/Max-B diffractometer, using Cu K_α radiation at 40 kV and 30 mA. The samples were measured with a step size of 0.02 ° (2θ) and a dwell time of 2 (s) in a range from 8 till 60° (2θ).

4.2.6 Swollen state polymerization (SwSP)

As shown in Fig. 4.1, the reaction apparatus is a vertical glass tube (25 cm long, id = 27 mm), fitted with a helical coil for bubbling nitrogen, and a condenser for refluxing the solvent. The reactor was immersed in a salt bath maintained at 195 ^{o}C, and the solvent DPE-BP (15 mL) was added. Nitrogen gas flowing at the rate of 2 L/min (room temperature and pressure) was dried by passing through an anhydrous $CaSO_4$ column (W.A. Hammond Drierite, Xenia, Ohio), preheated by passing through a glass coil immersed in the same bath, and introduced at the bottom of the reactor. PET chips (average weight 0.045 g) were pressed for 1 min into thin disks (diameter ~1.5 cm, thickness ~180 micron) between two stainless steel plates heated to 160 ^{o}C. These PET chips (0.8 g) were dried overnight under vacuum at 150 ^{o}C, and suspended (by hanging independently from metallic wires) into the solvent mixture in the reactor. The PET chips are taken out at the desired reaction time, and dried under vacuum.

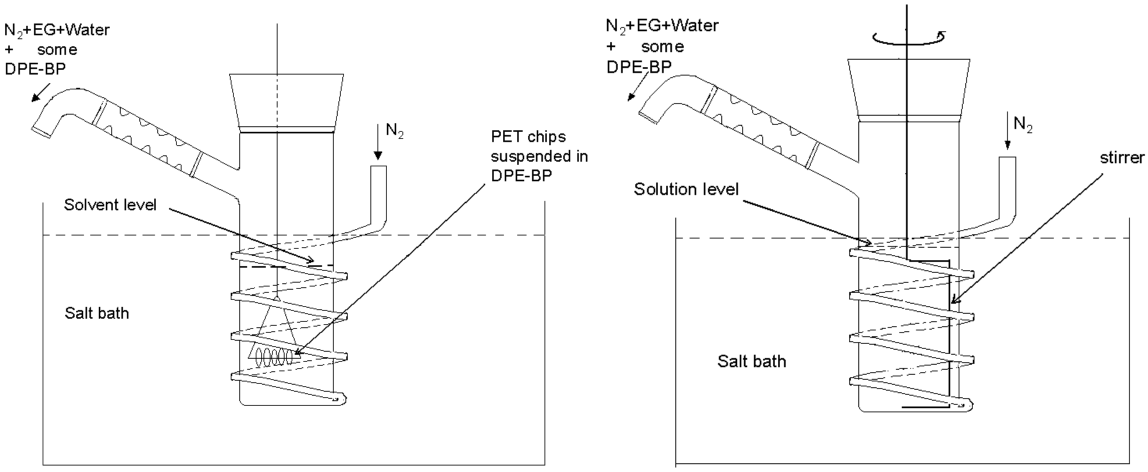

Figure 4.1: Schematic of apparatus used for post polymerization of PET in swollen state (left) and in solution (right).

4.2.7 Solution polymerization (SolP)

Similar to SwSP, the reaction apparatus is a vertical glass tube (25 cm long, id = 27 mm), fitted with a helical coil and a condenser. In addition, it is fitted with a custom-made anchor type stirrer driven by an electric motor (Fig. 4.1). The reactor was immersed in a salt bath maintained at 250 ^{o}C, and the solvent mixture DPE-BP (25 mL) was added. Nitrogen gas flowing at the rate of 2 L/min (room temperature and pressure) was dried by passing through an anhydrous $CaSO_4$ column (W.H. Hammond Drierite, Xenia, Ohio), preheated by passing through a glass coil immersed in the same bath, and introduced at the bottom of the reactor. PET chips (10.8 g), predried overnight under vacuum at 150 ^oC, were added to the reactor while stirring at 200 rpm, while the PET chips dissolved within 5 min. The condenser allowed reflux of the solvent even at the high nitrogen flow rate, and the small amount of the escaping solvent as well as the reaction condensates were further condensed with a long water cooled condenser, collected, and weighed. The concentrated PET solution sample was withdrawn with the stirrer after detaching the motor. The solution solidified immediately, and was dried under vacuum at 150 ^oC for 6 hr.

4.2.8 Solid state polymerization in vacuum (SSP-vacuum)

Thin PET chips were placed in a glass made 150 mL round bottomed flask connected to a vacuum pump maintaining 10 mtorr pressure. The flask was immersed till its neck into a preheated, temperature controlled salt bath. The chips were first dried at 165 ^oC for 6 hr. The flask was then transferred to an identical bath, but maintained at 252 ^oC (resulting in 250 ^oC inside the flask), and the flask was withdrawn after the desired time of reaction.

4.2.9 Determination of acid end-groups in PET

The fluoroderivatization (chapter 2) of the acid end-groups was carried out by DCC mediated esterification with HFIP (Eq. 2.1). One chip of PET (0.045 g) was dissolved in a mixture of HFIP (0.2 g) and $CDCl_3$ (1.00 g) at room temperature. Firstly, part (0.1 g) of a solution of 4-pyrrolidinopyridine (0.001 g) in $CDCl_3$ (1 g) was added and subsequently, part (0.2 g) of a solution of DCC (0.0075 g) in $CDCl_3$ (1.5 g) was added. Finally, part (0.1 g) of a solution of TFT (0.01 g) in $CDCl_3$ (2 g) was added to the above reaction mixture to give the sample for ^{19}F NMR analysis. Integration of the δ -73.41 [d, 6F] peak for the fluoroester relative to the δ -62.9 [s, 3F] peak of TFT allowed quantification of the acid end-groups.

4.2.10 Determination of hydroxyl end-groups in PET

The hydroxyl end-groups were fluoroderivatized by esterification with TFA (chapter 2) (Eq. 2.2). One chip of PET (0.045 g) was dissolved in a mixture of TFA (0.2 g) and

$CDCl_3$ (1.0 g). Part (0.1 g) of a solution of TFT (0.01 g) in $CDCl_3$ (2 g) was added to the above reaction mixture. ^{19}F NMR analysis was carried out after standing for 72 hr. Integration of the δ -75.2 [s, 3F] peak for the fluoroester relative to the δ -62.9 [s, 3F] peak of TFT allowed quantification of the acid end-groups.

4.2.11 Size exclusion chromatography (SEC)

The samples were analyzed with Size Exclusion Chromatography (SEC) combined with Triple detection. The SEC system consists of a K501 pump and 2x PSS PFG linear XL 7µ 300 x 8 mm columns. The eluent was hexafluoroisopropanol, flow rate 0.6 mL/min. The concentration was about 2 mg/mL.

4.3 Results and Discussion

4.3.1 SwSP kinetics and crystallization limited chain-end mobility

The IV vs. time data for SwSP of the originally 180 μ thick pressed chips (after swelling 30% with DPE-BP) at 195 °C are shown in Fig. 4.2. Initially, the IV increases quickly from 0.42 to 1.2 dL/g in 5 hr, and then nearly flattens out at a maximum IV of 1.4 dL/g at 12 hr. Also shown in the figure are the kinetics data for SSP under the same conditions, but without the solvent. We notice that the SwSP proceeds much faster than SSP at the same temperature.

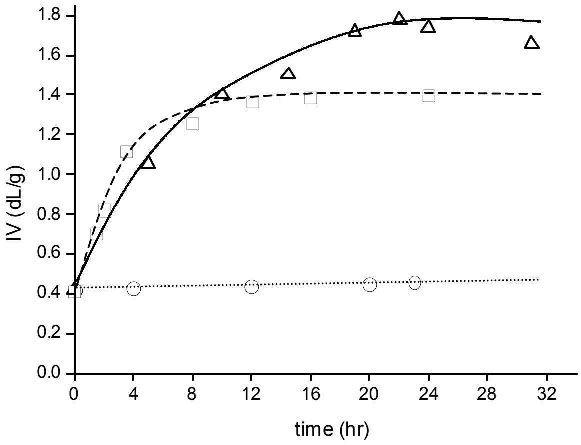

Figure 4.2: Increase in IV with time of (a) SwSP (squares, -----) in pressed PET chips at 195 °C in DPE-BP. (b) SolP (triangles, ——) at 30 wt% in DPE-BP (c) SSP (circles, dotted line) in 180 μ thick PET chips at 195 °C under nitrogen. The lines are smoothly drawn to guide the eyes.

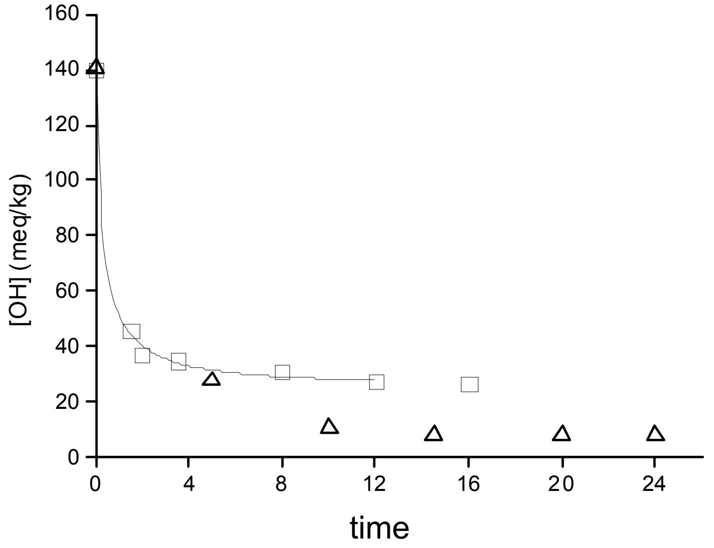

(a)

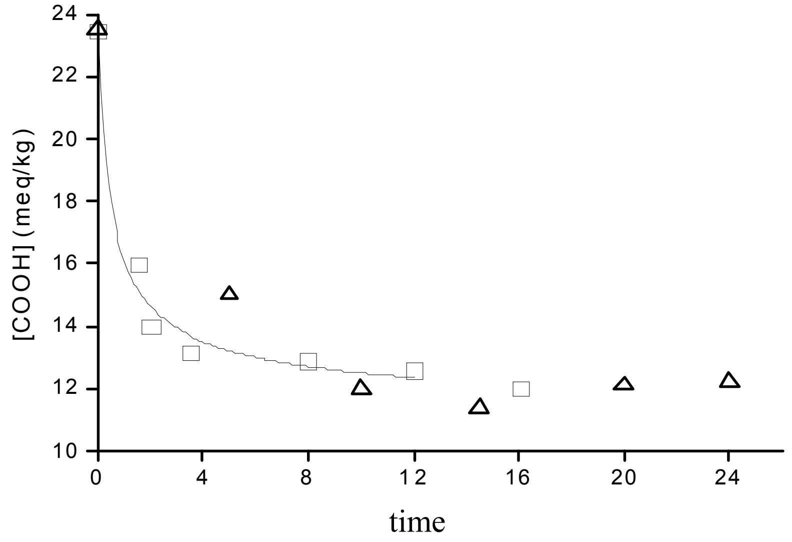

(b)

Figure 4.3: Depletion of the (a) hydroxyl and (b) acid end-groups with post polymerization during SwSP at 195 °C (squares) and SolP at 250 °C (triangles). The lines represent the fits to SwSP data while accounting for the inactive end-groups.

Swelling of the pressed PET chip (0.045 g) to their equilibrium swollen weight (0.08 g) took place in less than 1 min after dipping in the hot DPE-BP, indicating a PET concentration of 56 wt% in the swollen chip. In case of thick PET (half thickness, $L > \sqrt{D/(kC)}$, where D and C are the condensate diffusivity and concentration, and k is the corresponding rate constant [24], the SwSP can be limited by the outward diffusion of the condensates EG and water through the polymer. Calculation with $D_{EG} = 3.1x10^{-6}$ cm^2/s in PET alone [7] (D_{EG} can be higher in swollen PET), $k =$ 0.017 kg/meq-hr (this chapter), and C=163 meq/kg (this chapter) suggests that such diffusion limitations are negligible at the swollen chip thickness of less than 350 μ employed in SwSP. Hence, the observed rate of our SwSP reaction must be limited by the intrinsic reaction kinetics, and we will like to represent our SwSP kinetics data in terms of the reactions (Eq. 3.1) and (Eq. 3.2). Fig. 4.3 shows our measurements of the depletion of end groups with progress of the SwSP, as determined by fluoroderivatization of the acid and the hydroxyl end groups, followed by F-NMR (chapter 2). We first tried to represent the kinetics data ([OH](t) and [COOH](t)) of SwSP with the kinetics expressions Eqs. 3.3~3.7. However, the flattening of [OH](t) and [COOH](t) curves at ~ 12 hr even when substantial [OH] and [COOH] end groups are present, could not be explained in terms of these second order rate expressions. As discussed in our earlier work on SSP, this could be related to inability of a part of the end-groups to participate in the condensation reactions (Eqs. 3.1 and 3.2), perhaps due to crystallization induced mobility restrictions. Though the concentration of such groups is small, they make up an increasing fraction of the total number of end-groups with progress of the SwSP. The inability of a part of the end-groups to participate in the polycondensation reactions can be either due to chemical degradation leading to unreactive chain ends (such as vinyl end-groups), or due to the reactive ends being unable to approach each other. Such limited extent of mobility of some chain-ends could be a result of their being restricted by relatively short chain segments linking them to crystalline parts, or a result of their incorporation in crystalline parts as defects. We note from Fig. 4.3 that the OH and the COOH end-groups are still detectable (by fluoroderivatization and ^{19}F NMR), at substantial concentrations of about 25 meq/kg and 10 meq/kg respectively, at the end of our SwSP. We further verified this by the following experiment: the PET sample of IV = 1.4 dL/g (obtained by SwSP, t = 15 hr as in Fig. 4.2), was dried at 150 ^{o}C under vacuum for 6 hr, heated to melt on aluminium foil at 270 ^{o}C under vacuum for 4 hr. The measured IV = 2.4 dL/g of that sample suggests a re-initiation of the polymerization in melt. We conclude that the melting after SwSP results in release of the crystalline restraints on the mobility of the temporarily inactivated acid and hydroxyl end-groups, allowing post polymerization to start again.

This suggests that a kinetic analysis of SwSP should take into account this apparent inactivity of a fraction of the OH and COOH end-groups. The [OH](t) and [COOH](t) data for SwSP are now fitted (using the CONSTANT_RELATIVE_VARIANCE model of the gPROMS software, PSE Enterprises, UK) with the kinetics expressions Eqs. 3.3~3.5 and 3.15~3.16 to estimate the rate constants: k_1 = 0.00642 kg/meq-hr, k_2 = 0.017 kg/meq-hr and the inactive end-group concentrations $[OH]_i = 25.1$ meq/kg and $[COOH]_i = 10.9$ meq/kg. The corresponding calculated [OH](t), [COOH](t) profiles are shown as curve in Fig. 4.3, and we conclude a satisfactory match with the experimental measurements obtained by us during SwSP. The lower value of the highest IV (= 1.4 dL/g) achievable by SwSP as compared to SSP (highest IV ~ 2.8 dL/g, chapter 3), and the much higher $[OH]_i$ meq/kg and $[COOH]_i$ meq/kg values as compared to SSP at 250 ^{o}C ($[OH]_i = 3.1$ meq/kg and $[COOH]_i = 2.8$ meq/kg) hint at stronger crystallization induced limitations to chain end mobility during the SwSP at 195 ^{o}C as compared to the SSP at 250 ^{o}C. This could be related to the solvent induced crystallization in PET, and hence we decided to monitor this by DSC and WAXD.

Fig. 4.4 shows the DSC thermograms during heating of dried the SwSP product (dotted line, IV ~ 1.4 dL/g) and an SSP product (solid line, IV = 1.42 dL/g, sample from SSP at 250 ^{o}C as described in chapter 3). The higher melting temperature T_m = 260 ^{o}C of the SSP product as compared to T_m = 251 ^{o}C for the SwSP product corresponds to the annealing of the former during the SSP at the higher temperature (250 ^{o}C). The higher heat of melting (ΔH_m= 60 J/g) for the SwSP product as compared to (ΔH_m= 51 J/g) for the SSP product indicates that the extent of crystallization ($x_c = \Delta H_m/\Delta H_c$, where ΔH_c = 125.6 J/g is the crystalline heat of melting of PET [25]) is indeed higher in the SwSP product.

Figure 4.5 shows a comparison of the WAXD diffractograms of the above SSP sample and the dried SwSP sample. These spectra have already been corrected for background scattering, and amorphous spectrum has been subtracted while fitting the peaks by Gaussian components. The peaks are indexed according to the known assignments of the triclinic unit cell dimensions for PET [26,27,28,29]. The similar peak positions of the SSP and the SwSP samples indicate that the crystalline forms are identical. Calculations from WAXD spectra showed (x_c = 0.64) for the SwSP sample and (x_c = 0.51) for the SSP sample. Thus, both the DSC and the WAXD data indicate solvent induced crystallization of PET during SwSP in DPE-BP, and hence its possible role in the progress of post polymerization.

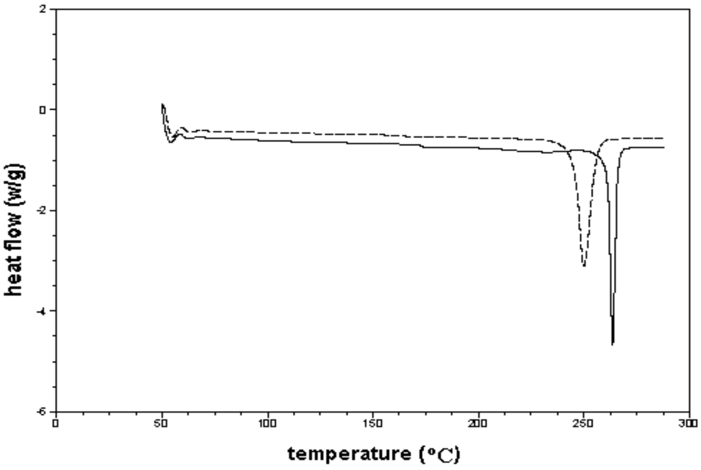

Figure 4.4: DSC heating scans of SwSP (dotted line) and SSP product (solid line).

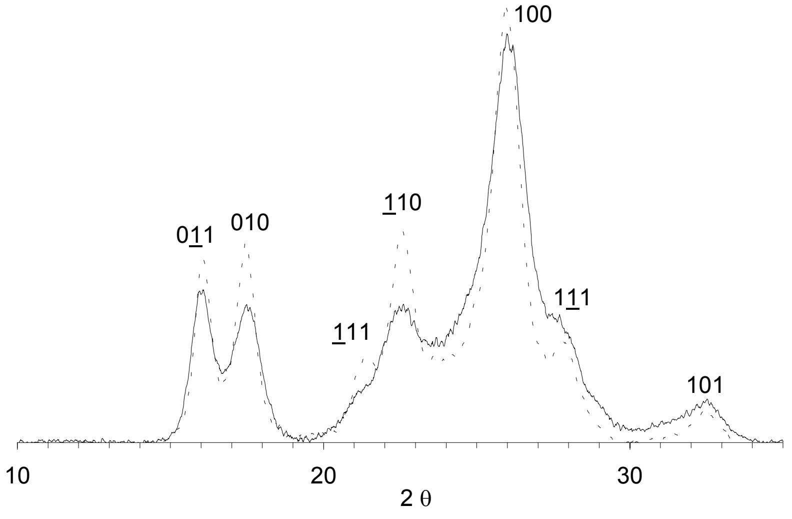

Figure 4.5: WAXD scans of SwSP (solid line) and SSP product (dotted line).

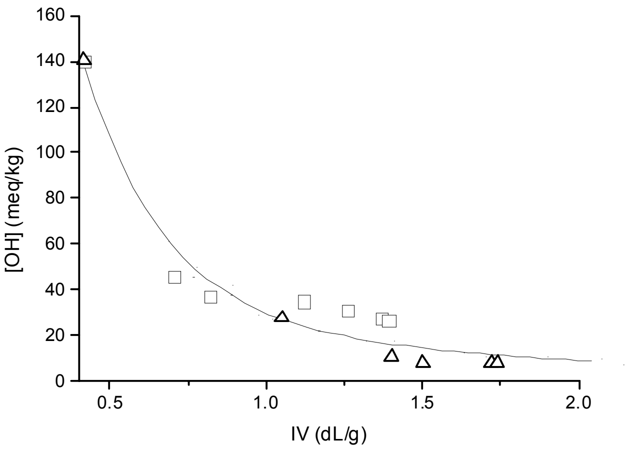

(a)

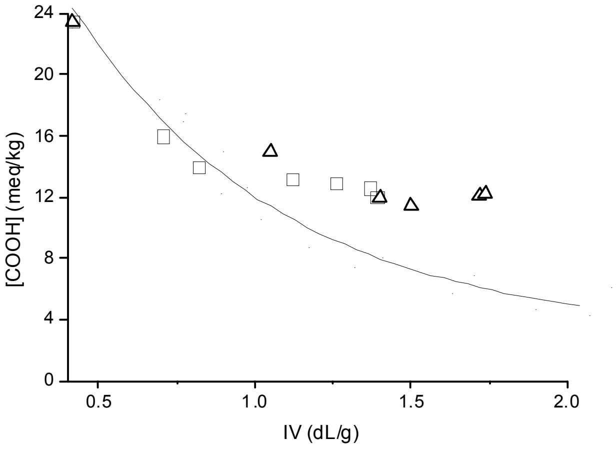

(b)

Figure 4.6: Depletion of the (a) hydroxyl and (b) acid end-groups with increase in IV during SwSP at 195 ^{o}C (squares) and SolP at 250 ^{o}C (triangles). The lines represent the SSP data from Fig. 3.3.

In Fig. 4.6 we replot the concentrations of the hydroxyl and the acid end groups, as functions of the IV rise during the SwSP. Also shown in the figure as solid lines is a smooth fit to the corresponding data for SSP (250 ^{o}C) (chapter 3). Fig. 4.6 indicates that the concentration of the hydroxyl end groups in the SwSP product is comparable to the SSP product at similar IV, but the concentration of the carboxylic acid end groups is higher in the SwSP product as compared to the SSP product of the same IV. Since IV is more strongly determined by the higher molecular weight fraction, the higher concentration of the acid end groups in the SwSP products can be due to a possible higher concentration of the acid end group carrying low molecular weight linear polymers. If low molecular weight linear polymers are indeed present in larger amounts in the SwSP product, these would result in its wider molar mass distribution (MWD) as compared to SSP product of the same IV. We tried to analyze this possibility by comparing SEC of PET of IV = 1.37 and 1.40 dL/g obtained by SSP (solid line) and SwSP (dashed line) respectively (Fig. 4.7). It shows that the SSP product has wider molar mass distribution, which seems contradictory to the expectation. However, the SEC facility available to us was unable to fractionate and detect species of molar mass lower than about 3000 g/mol. There is still a possibility that the expectation is right if the amount of oligomers with molar mass less than 3000 g/mol that exist in SSP are only a tiny bit more than that exists in SwSP product.

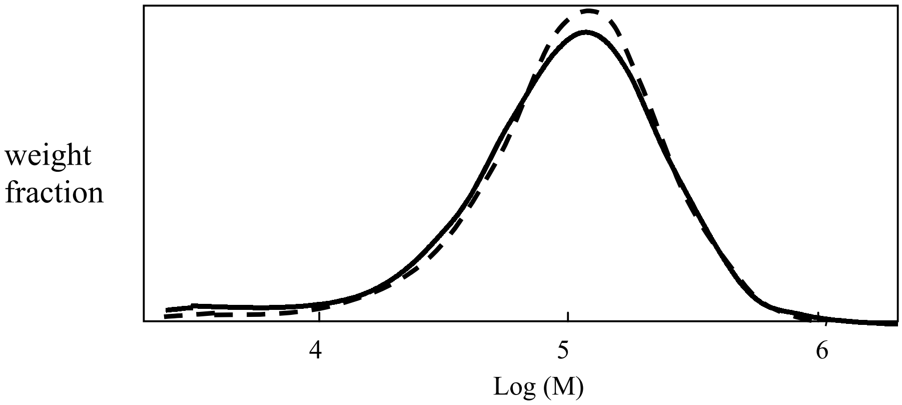

Figure 4.7: SEC plots of PET of IV = 1.37 and 1.40 dL/g obtained by SSP (solid line) and SwSP (dashed line) respectively. The respective $\overline{M_w}$ *values are 132000 and 134000, and the* $\overline{M_w}/\overline{M_n}$ *values are 2.66 and 2.25. The SEC measurements were carried out at Akzo Nobel (Arnhem) using PET concentration of about 2 mg/mL in HFIP flowing at 0.6 mL/min.*

4.3.2 SolP

Since it appears that the extent of SwSP in DPE-BP is limited by the high extent of crystallization, we decided to evaluate if such a limitation can be eliminated by carrying out the post polymerization by dissolving the PET in the same solvent. Since DPE-BP dissolves PET at about 205 °C, and the boiling points of DPE and BP are 259 °C and 255 °C respectively, we carried out the solution polymerization at 250 °C while starting with a PET concentration of 30 wt%. Most of the solvent evaporating with the bubbling nitrogen was refluxed by the condenser mounted on the reactor. However, a small part of the solvent (5 mL in 24 hr), along with the condensates having lower boiling points (EG: T_b = 196 ^oC, water: T_b = 100 ^oC), was carried over to condense in another water cooled condenser and not returned to the reactor (Fig. 4.1). Fig. 4.2 shows the IV vs. time data for post polymerization of PET of IV = 0.42 dL/g in the solution in DPE-BP at 250 ^oC. The initial rate of rise of IV during the SolP at 250 ^oC at 30 wt% concentration is comparable to SwSP at 195 ^oC at ~56 wt% concentration. However, while the SwSP is hindered beyond IV ~ 1.4 dL/g at ~ 12 hr, the SolP continues till IV ~ 1.8 dL/g until ~ 20 hr. The lower value of the maximum limiting IV in case of SwSP (with lower amount of solvent as compared to SolP) indicates that this limitation is not dictated by the a chemical influence of the solvent DPE-BP, but perhaps to a physical influence in the solid state, thus possibly through crystallization.

We are aware of only two reported attempts, albeit somewhat unsuccessful, of post polymerization of PET in solutions. Izard and Auispos [30] found that the solution polymerization of PET in DPE–BP proceeded to IV not higher than 0.72 dL/g. Similarly, Ha et al. [15] found that while solution polymerization of PET of IV = 0.62 dL/g at 220 ^oC resulted in no IV increase in solvents benzophenone, DPE and terphenyl, the IV increased to 0.87 dL/g in 15 hr in the solvent BP. While an obvious advantage of SSP is the avoiding of working with solvent, an important advantage of SolP as compared to SwSP and SSP processes for the very high molecular weight PET is the ease of handling a solution polymerization in a standard stirred reactor, as compared to handling of thin films or fine particles while avoiding their fusion during SSP and SwSP at temperatures close to the melting points. Finally, further processing of such high IV PET into fibers necessarily demands solubilization in suitable solvents. Since DPE-BP has been found to be a suitable solvent for such processing [19], the use of these solvents during the post polymerization step poses no disadvantage as it would allow direct spinning of the solution polymerized high IV PET. While withdrawing the samples from the reactor at the end of the SolP with a stiff wire, we noticed that filaments were drawn out with the wire, thus indicating the sufficient elasticity and the direct spinnability of the SolP product. We found that these filaments got from IV 1.8 dL/g solution (diameter ~200 μ) could be dried overnight at 150 ^oC under vacuum, and then drawn at 250 ^oC to a draw ratio of 7, resulting in fibers of modulus 11 GPa and strength of 0.47 GPa (section 5.2.11). We believe that it may be possible to enhance final fiber properties by employing an optimization of fiber spinning from the as polymerized solution.

4.4 Conclusions

We have carried post polymerization of PET in presence of the solvent mixture diphenyl ether – biphenyl (DPE-BP). As compared to SSP, the incorporation of solvent during SwSP at 195 ^{o}C enhances the initial rate of reaction due to the solvent induced mobility, but slows down dramatically at IV > 1.2 dL/g due to the restricted mobility of a part of the chain-ends due to crystalline restraints. This is verified by detection of substantial concentrations of the hydroxyl and acid end-groups even at the end of the SwSP, the high extent of crystallization of the SwSP product, and further post-polymerization only after melting to impart mobility to these end-groups. At a higher temperature, PET can be dissolved in the same solvent, permitting post polymerization in solution. The solution polymerization at 250 ^{o}C with PET concentration of 30 wt% proceeds from IV = 0.42 dL/g to 1.8 dL/g in a single step, and is thus a potentially attractive route for obtaining a solution of high molecular weight PET, suitable for direct processing into fibers and films.

References

[1] Gantillon B, Spitz R, McKenna. Macromol Mat Engng 2004; 289: 88.

[2] Kim TY, Lofgren EA, Jabarin SA. J Appl Polym Sci 2003; 89: 197.

[3] Fakirov S. In: Schultz JM Fakirov S, editors, Solid State reactions in Linear polycondensates. In: Solid State Behavior of Linear Polyesters and Polyamides. New Jersey: Prentice Hall, 1990, p. 1.

[4] Medellin-Rodriguez FJ, Lopez-Guillen R, Waldo-Mendoza MA. J Appl Polym Sci 2000; 75: 78.

[5] Chen S-A, Chen F-L. J Polym Sci, Part A: Polym Chem 1987; 25: 533.

[6] Zhi-Lian T, Gao Q, Nan-Xun H, Sironi C. J Appl Polym Sci 1995; 57: 473.

[7] Kang, C-K. J Appl Polym Sci 1998; 68: 837.

[8] Wu D, Chen F, Li R, Shi Y. Macromolecules 1997; 30: 6737.

[9] Karayannisis GP, Kokkalas DE, Bikiaris DN. J Appl Polym Sci 1995; 56: 405.

[10] Duh B. J Appl Polym Sci 2001; 81: 1748.

[11] Tate S, Watanabe Y, Chiba A. Polymer 1993; 34: 4974.

[12] Tate S, Ishimaru F. Polymer 1995; 36: 353.

[13] Tate S, Watanabe Y. Polymer 1995; 36: 4991.

[14] Burke ALC, Marier G, DeSimone JM. Polym Mater Sci Eng 1996; 74; 248.

[15] Ha WS, Oh SK, Youg JH. J Korean Fiber Society 1990; 27: 66.

[16] Wang L-x, Chen F, Wu D-c, Huang L-k, Ma Z-y, Xiang S-w. J Sichuan University (Engng Sc Ed) 2001; 33: 77.

[17] Parashar MK, Gupta RP, Jan A, Agarwal US. J Appl Polym Sci 1998; 67: 1589.

[18] Tate S, Chiba A, Tani K. Polymer 1996; 37: 4421.

[19] Rogers V. EP 0336 556, 1989.

[20] Solomon OF, Ciuta IZ. J Appl Polym Sci 1962; 6: 683.

[21] Koepp HM, Werner H. Makromol Chem 1959; 32: 79.

[22] Conix A. Makromol Chem 1958; 26: 226.

[23] Griehl W, Neue S. Faserforsch Textiletechn 1954; 5: 423.

[24] Ravindranath K, Mashelkar RA. J Appl Polym Sci 1990; 39: 1325.

[25] Fakirov S, Fischer EW, Hoffman R, Schmidt GF. Polymer 1977; 18: 1121.

[26] Fakirov S, Fischer EW, Schmidt GF. Makromolekulare Chemie 1975; 176: 2459.

[27] Bunn CW. in Ch. 11 in Fibers from Synthetic polymers, Ed. R. Hill, Elsevier, Amsterdam, 1953.

[28] Johnson, JE. Journal of Applied Polymer Science, 1959; 2(5): 205.

[29] Von Kilian, H. G., Halboth, H. and Jenckel, E. *Kolloid-Zeitschrift,* 1960; 172(2): 166.

[30] Izard EF, Auspos LA, USP 2597643, 1952.

Chapter 5 Crystallization of PET from dilute solutions

5.1 Introduction

Poly(ethylene terephthalate) (PET) is one of the commercially most important polymers, the major applications being textile fibers, soft drink bottles, injection molding, tire cord filaments and industrial fibers. While PET of IV ~ 0.6 dL/g, obtained by melt polymerization, is sufficient for textile fiber applications, the other applications demand solid state polymerization (SSP) to IV ~ 1.0 dL/g [1-6]. An even higher extent of post polymerization to IV as high as 3 dL/g is desired for its solution spinning leading to potentially high modulus/high strength fibers [7-9].

Crystallization of polymers from the melt and concentrated solutions leads to crystallites that are highly interconnected by trapped entanglements and tie molecules. However, when a dilute solution of a crystallizable polymer is cooled under controlled conditions, the polymer may crystallize as single crystals. Since the discovery of polyethylene crystallization from dilute solutions into lamellar crystals, crystallization of several other important polymers such as polyvinyl chloride, carrageenen, polyamides and syndiotactic polystyrene has been carried out in solution, and found to display special chain conformations leading to a variety of crystalline morphology [10].

While suspensions of lamellar crystals are often formed, crystallization from solutions under suitable conditions can result in thermoreversible gelation wherein small crystallites serve as crosslink points between flexible polymer molecules forming the network [11, 12]. For example, cooling of PE in xylene solution results in a suspension of crystals, stirring of the solution at high concentration results in formation of transparent elastic gels with a shish-kebab crystalline morphology. These gels can offer potential of processing into useful materials, such as ultra strong fibers [13]. Reversible gelation can also occur in absence of crystallization through other forms of interchain binding [14].

Several workers have examined solvent-induced crystallization in PET [15, 16, 17, 18]. In addition, crystallization of PET from solutions in oligomeric PEO has been studied in recent years, albeit only for concentrated (10-30%) solutions [19, 20, 21]. Oh et al.

[22] studied the influence of PET concentration (5-50%) and molecular weight (IV = 0.6–2.13 dL/g) on the crystallization and melting transitions in nitrobenzene. Crystallization of PET on a microscope grid during solvent evaporation from dilute solutions in benzyl alcohol at room temperature was reported to result in fibrillar growth, albeit by laydown of molecules along the growing fibril [23]. Crystallization kinetics of PET from solutions N-methyl-2-pyrrolidinone at elevated temperatures was studied, but without reference to crystal morphology [24]. Sun et al. [25] examined the crystallization potential of PET extracted from a suddenly quenched solution in phenol, and concluded that the higher crystallization potential of the so freeze-dried PET as compared to solution cast PET is related to the reduced entanglements in the former. Considering the possible influence of crystal architecture and on polymer properties, we here examine crystallization behavior of PET from its solution in the thermic fluid: the mixed solvent of diphenyl ether and biphenyl.

5.2 Experimental

5.2.1 Materials

Cylindrical PET chips (diameter 1.1 mm, length 2.8 mm, IV ~ 2.0 dL/g) were obtained from Acordis Research (Arnhem, Netherlands), and predried at 150 °C under vacuum for 4 hr before use. Diphenyl ether (99%) and biphenyl (99%) from Merck were used as received, and mixed at 26.5:73.5 (wt:wt) ratio to make the mixed solvent (BP-DPE). The solvent mixture BP-DPE was dried over molecular sieves for at least 2 days.

5.2.2 Detection of phase transition by light scattering

Predried PET was dissolved at the desired concentration in the BP-DPE mixture by stirring under argon atmosphere in a 20 mL glass bottle, at 240 °C in a molten salt bath. A preheated (240 °C) glass capillary with rectangular cross section (Vitrotube 3520 made by VitroCom Inc., wall thickness 0.2mm, inner size 0.2 mm, width 2.0mm) was introduced with its open end downwards, so as to dip the open end into the solution. When part of the solution seeped into the glass capillary by capillary action, the capillary was withdrawn and sealed at the open ends. The capillary was mounted on a hot stage (Linkam THMS600/TMS93) and laser light (Melles Griot 05-LHR-991, 30 mW, 632 nm) was shined on it from a distance of 10 cm, while the scattering was measured with a silicon PIN type photodiode detector (Centrovision, Model BPW 34) placed at 10 cm from the sample and connected to an XY plotter (Kipp & Zonen, Model BD 40). The sample was subjected to the following program with the hot stage: heating from 60 °C to 240 °C at 20 °C min^{-1}, isothermal for 5 minutes, cooling at 20 °C min^{-1} to 50 °C, and isothermal for 5 minutes, and heating at 20 °C min^{-1} to 275 °C.

5.2.3 Isothermal crystallization from solution

PET was dissolved at the desired concentration in the BP-DPE by stirring in a test tube at 240 °C in a molten salt bath over 1 hr. The test tube was transferred to a silicon oil bath maintained at 170 °C. With passage of time, the solution turned turbid and the test tube was withdrawn from the hot bath after 2 hr when no further increase in turbidity could be observed.

5.2.4 Film formation and drawing from solution-crystallized PET

PET (1.0 g) was dissolved in DPE-BP at the desired concentration (0.2 wt%) at 240 °C, crystallized isothermally at 170 °C, and filtered using a Whattman 595 filter. Excess solvent was allowed to drain over 1 hr. The loosely interconnected gel so left on the filter paper is laid out in the form of a 2 mm thick sheet on another filter paper supported by a metal wire mesh placed in a glass petri-dish. The sheet was covered with another filter paper and then with another wire mesh, to maintain the dimension of the sheet. Acetone was added to the petri-dish to allow extraction of the solvent DPE-BP overnight. After pouring out the solvents, the petri-dish was transferred to a vacuum oven, and maintained at 100 °C for 24 hr. Dried film of thickness 0.15 mm was then easily separated form the filter papers and the wire-meshes.

A small part of the film was subjected to IV measurement. Since the film was brittle, it was subjected to constrained annealing between stainless steel plates at 220 °C for 2 min. A sharp blade was used to cut out 1 mm wide strips, which were quickly drawn using a hotbench (Kofler Heizbank, Model 7841) at 250 °C to draw ratio of about 5 to 6. The drawn samples were weighed to determine their cross section, and tested for their tensile properties using a Zwick Z010 with 20 N load cell, sample span of 1 cm and extension rate of 0.5 cm min^{-1}.

5.2.5 DSC

The melting and crystallization characteristics of the samples were examined using a Perkin-Elmer differential scanning calorimetry system DSC-7. The heat of melting and heat of crystallization were determined from the corresponding peak area during heating and cooling scans at 20 ^{o}C min^{-1}.

5.2.6 WAXD

The crystallized PET samples were dried by evaporation under vacuum at room temperature. The WAXD measurements were obtained with a Rigaku D/Max-B diffractometer, using Cu K_{α} radiation at 40 kV and 30 mA. The samples were measured with a step size of 0.02 ^{o} (2θ) and a dwell time of 2 (s) in a range from 8 till 60^{o} (2θ).

5.2.7 FTIR

FTIR analyses were performed using a Biorad FTS 6000 spectrometer on three samples of PET (1% PET gel, pure solvent, crystallized PET film, and amorphous PET film). The samples were measured as thin films between KBr plates. The spectra were recorded with a resolution of 2 cm^{-1}, and averaged over 72 scans. Subtraction of the solvent spectrum from the 1% gel spectrum was done later.

5.2.8 Scanning electron microscopy

Following the isothermal crystallization from solution (section 2.3), a sample of the turbid suspension was withdrawn with a spatula, mounted on a freshly cleaved mica sheet, and dried by evaporation at 70 ^{o}C in a vacuum oven. The SEM was carried out on a Philips field-emission environmental scanning electron microscope XL30 ESEM-FEG, which was equipped with a field emission electron source. The acceleration voltage used for image acquisition was 2 kV.

5.2.9 Transmission electron microscopy (TEM)

Following the isothermal crystallization from solution (section 5.2.3), a droplet of the turbid suspension was cast onto a copper TEM grid coated with a thin layer of amorphous carbon, dried by evaporation at 70 ^{o}C in a vacuum oven overnight. Bright-field (BF) TEM morphology observations and acquisition of selected-area electron diffraction (SAED) patterns were conducted on a JEOL JEM-2000FX transmission electron microscope operated at 80 kV. Traditional negative plates were used to record all the images. Then, the negatives were digitized using a high-resolution scanner (Agfa DUO scanner), working in the gray mode with 8 bits/channel of gray scale.

5.2.10 Preparation of solid-state crystallized PET

Highly crystalline PET chips were prepared from PET chips (IV ~ 0.6 dL/g) by pressing at 150 ^{o}C into 180 μ films, and then precrystallization at 165 ^{o}C for 6 hr followed by solid state polymerization at 250 ^{o}C for 4 hr to IV = 2.2 dL/g [6].

5.2.11 Fiber formation from concentrated PET solution

A concentrated solution (30 wt%) of PET (IV = 1.8 dL/g) in DPE-BP at 250 ^{o}C was obtained by solution polymerization (chapter 4). Filaments (diameter ~ 200 μ) were drawn out by quickly withdrawing a metal wire tip dipped in this solution. These filaments were dried overnight at 150 ^{o}C under vacuum, and then drawn at 240 ^{o}C using the hotbench (Kofler Heizbank, Model 7841) to a draw ratio of 7. The drawn samples were weighed to determine their cross section, and tested for their tensile properties using a Zwick Z010 with 20 N load cell, sample span of 1 cm and extension rate of 0.5 cm min^{-1}.

5.3 Results and Discussion

The most common thermoreversible gelation in polymer solutions is due to crystallization occurring due to undercooling. The onset of crystallization (T_c) may depend on many factors such as cooling rate and polymer concentration, besides the polymer-solvent characteristics. The melting temperature (T_m) of these crystals may depend on T_c, and is greater than T_c. Presence of solvent can decrease T_m. Another phenomen that can lead to gelation is the liquid-liquid phase separation, which can precede crystallization of the concentrated phase. We are interested in examining the gelation taking place during cooling of dilute PET solutions using the DPE-BPE eutectic mixture as the solvent..

5.3.1 Detection of phase transition

When a polymer crystallizes from a dilute solution, the solid crystallites so formed may remain suspended in the solvent, giving a turbid appearance. Formation of such crystallites, or a liquid-liquid phase separation can both be detected by examining the scattering behavior of polymer solutions. Fig. 5.1 shows the scattering response to incident laser beam on the PET solutions of various concentrations during a cooling and a heating cycle. During the cooling cycle, the onset of scattering is seen at ~ 165 ^{o}C, possibly indicating the crystallization of PET at this T_c. During the subsequent heating cycle, the scattering intensity decreases at T_m ~ 204 ^{o}C, indicating the possible melting of PET crystallites. The same transitions could be observed repeatedly during additional cooling and heating cycles, indicating thermoreversible nature of the involved processes. The T_m and T_c at the employed scanning rate (20 ^{o}C/min) are nearly independent of the polymer concentration.

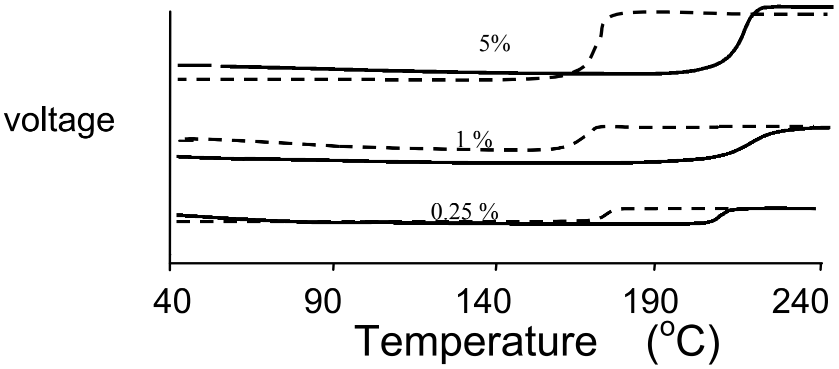

Figure 5.1: Scattering during heating and cooling of PET solution of shown concentrations, in response to incident laser beam. Temperature profile: heating from 40 ^{o}C to 240 ^{o}C at 20 ^{o}C/min (solid lines) , isothermal for 2 min, cooling at 20 ^{o}C/min to 40 ^{o}C (dashed lines). In this experimental setup, the scattering intensity goes up when the voltage goes down, and vise versa.

Gelation characteristics of dilute PET solutions during cooling is also determined visually. PET solutions in DPE-BP at 240 ^{o}C at three different concentration, 0.25, 1 and 5% were step-cooled from 240 ^{o}C by transferring to constant temperature bath maintained at170 ^{o}C. Fig. 5.2 shows the appearance of these solutions after 1 hr at 170 ^{o}C. While a settling suspension of a loosely interconnected swollen gel is seen in the 0.25% case, gelation is seen in the 1 and 5% solutions throughout the system. When the 0.25% solution suspension was poured out from the test tubes into a petri dish, we detected ~ 0.2 cm size translucent gel lumps suspended in the solvent. This gel was very soft as it could be easily deformed with a spatula, possibly indicating a low degree of entanglement between the crystallites. However, the 1% gel could support its own weight for 10 min at room temperature, as found by inverting the test tube.

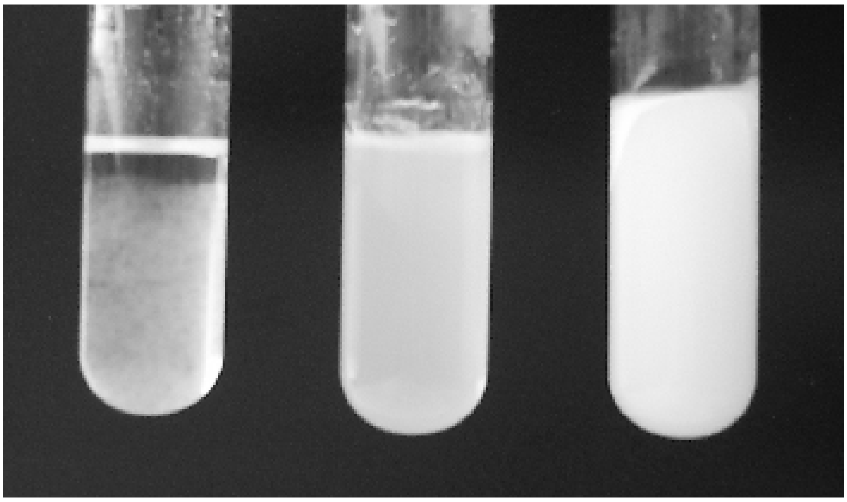

Figure 5.2: Appearance of PET gels obtained by cooling PET solution of concentrations (0.25, 1.0 and 5%, from left to right) to 170 ^oC. IV of the PET is 2.0 dL/g.

5.3.2 Crystallization characteristics of PET from solution in DPE-BP

Fig. 5.3 shows the DSC scans of a gel obtained by natural cooling of a 10% PET solution in DPE-BP. All the PET samples used have the IV of 2.0 dL/g. Following the first heating to 275 ^oC, the subsequent cooling scan shows an exotherm with peak at 159.6 ^oC (T_c, ΔH_m=5.55 J/g solution), corresponding to the crystallization of PET. The low value of this T_c as compared to T_c~200 ^oC of bulk PET can be attributed to higher degree of supercooling required to crystallize in presence of solvent. The subsequent heating scan shows an endotherm at 204.6 ^oC (T_m), corresponding to melting of these PET crystals. The low value of the T_m as compared to bulk PET (T_m ~ 250 ^oC) can be attributed to the presence of solvent during the DSC scan. The peaks at T_c and T_m are integrated to determine the heat of crystallization and heat of melting as 5.55 and 5.21 J/g, thus corresponding with the expected value for a sample containing 10% PET with degree of crystallization x_c of about 50%, since the crystalline heat of melting of PET is 125.6 J/g [26]. The T_c and T_m values correspond very well with the scattering transitions (Fig. 5.1), indicating that the scattering is most likely resulting from crystallization.

It is interesting to determine if the crystallization precedes phase separation, or the crystallization occurs in the more concentrated phase following phase separation. If a liquid-liquid phase separation precedes crystallization, then one would expect the phase separation temperature to depend on the polymer concentration. However, onset of scattering (Fig. 5.1) and crystallization (Fig. 5.2) at 165 °C during the cooling scan, irrespective of the polymer concentration in the range 0.25-10% indicates lack of such dependence at these concentrations. In addition, if a liquid-liquid phase separation precedes crystallization, then crystal size is expected to be limited by the dimension of the concentrated phase. As we will see from microscopic examination, the crystals grown in dilute solutions (0.25%) display fibrillar morphology of very high aspect ratio, which is an unlikely result of liquid-liquid phase separation.

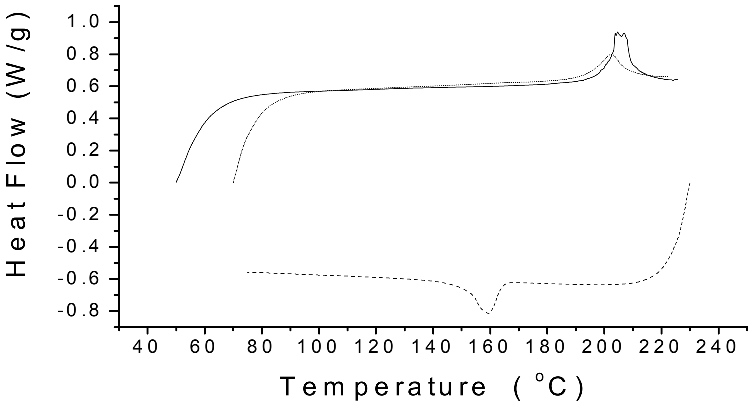

Figure 5.3: DSC scans of a 10% PET gel in DPE-BP. First heating (50 °C to 230 °C, solid line), cooling (230 °C to 70 °C, lower dashed line) and second heating (70 °C to 230 °C, upper dotted line) scans are shown.

The PET gel samples obtained by isothermal crystallization (170 °C) from solutions of three different concentrations (0.25, 1, and 5%) were dried by evaporation at room temperature under vacuum and subjected to DSC analysis. These three samples showed melting endotherms (Fig. 5.4) with peaks at 252.4, 252.7 and 251.6 °C, and with ΔH_m as 63.7, 64.4 and 64.1 J/g respectively. During subsequent cooling and heating of the 0.25% sample, we observe $T_c \sim 189$ °C and $T_m \sim 252$ °C with ΔH_c and ΔH_m each of 38 J/g. These values are similar to the values for bulk crystallized PET, indicating that the structure formed during solution crystallization is lost during melting, as expected. In comparison, the ΔH_m of the dried gel samples during first heating was much higher (~

64 J/g) and corresponds to x_c ~ 51%. Such high degree of crystallization can be obtained in bulk PET samples also by annealing at T ~ T_m for several hours [27], during gelation from concentrated solutions (10-30%), in oligomeric PEO [19, 20, 21], or during crystallization under high pressure [28, 29].

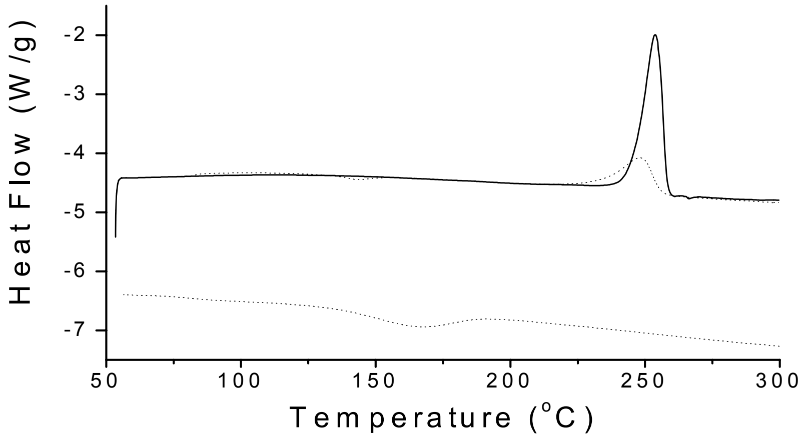

Figure 5.4: DSC scans of an isothermally (170 ^{o}C) crystallized 0.25% PET gel in DPE-BP, after drying at room temperature under vacuum. First heating (50 ^{o}C to 300 ^{o}C, solid line), cooling (300 ^{o}C to 50 ^{o}C, lower dotted line) and second heating (50 ^{o}C to 300 ^{o}C, upper dotted line) scans are shown.

5.3.3 Morphology of PET crystallized from solution in DPE-BP

Molecular packing of molecules in crystals can be determined by WAXD and electron diffraction. The following triclinic unit cell dimensions for PET have been reported [30-33] : a = 0.448 nm, b = 0.585 nm, c = 1.075 nm, α = 99.5^{o}, β=118.4^{o}, γ=111.2^{o}. For the $0\underline{1}1$, 010, $\underline{1}11$, $\underline{1}10$, 011, 100, $1\underline{1}1$ and 101 planes, the d-values are 0.537, 0.497, 0.4085, 0.386, 0.370, 0.340, 0.314, and 0.267 nm respectively. The chain alignment is along c axis, along which the chain is nearly fully extended in a nearly planar conformation in the bc plane.

Fig. 5.5 shows a comparison of the WAXS diffraction patterns of the solid state crystallized sample with the sample crystallized from 0.25% solution. These spectra have been corrected for CuK$_{\alpha2}$ and background scattering, and the amorphous spectrum has been subtracted while fitting the peaks by a Pearson-VII profile. The peaks are indexed according to the above known assignments. The similar peak positions of the solid-state and solution crystallized samples indicates that the crystalline forms are identical. An important difference, however, between the two samples is the broadening of the peaks for the solution crystallized sample. Fig. 5.5 illustrates clear broadening of the $0\underline{1}1$ and 010 peaks in the 0.25% solution crystallized sample as compared to the SSP sample, even as the X-ray determined degree of crystallization in the two samples is comparable (51% for SSP sample and 53% for solution crystallized sample), indicating smaller crystal size along b and c axis in the dilute solution crystallized PET as compared to SSP PET.

Calculation of the crystallite size $\overline{D}$ can be achieved by means of the Scherrer equation:

$$\overline{D} = \frac{0.9\lambda}{B\cos\theta} \tag{5.1}$$

where B is the Full Width at Half Maximum (FWHM) of the reflection peak. The FWHM of a peak is a convolution of the specimen and instrument broadening. This allows us to calculate the corresponding crystallite dimensions as 7.9 nm respectively for the solution crystallized sample, as compared to 10.3 nm for the solid state crystallized sample. The smaller crystallite size of the solution crystallized sample is in agreement with its lower $T_m \sim 252\ ^oC$ as compared to $T_m \sim 260\ ^oC$ for the solid state crystallized sample. In particular, a much smaller crystallite dimension along c-axis suggests thinner lamellae in the solution crystallized samples, and is perhaps a function of the temperature of crystallization (degree of supercooling). Smaller crystallite sizes for PET crystallized from oligomeric PEO, as compared to melt crystallized PET, was also observed by SAXS by Wang et al. [19]. When the solution crystallized sample was annealed at 150 ^oC for several hours and then at 250 ^oC for 10 min, the corresponding crystallite dimension increased to 9.7 nm. The limitations on the crystallite dimension growth from annealing could also come from the fibril diameter, as we shall see from electron microscopy.

The DSC results showed higher crystallinity for the solution crystallized samples (x_c = 0.51) than for the solid state crystallized sample (x_c = 0.38). This is in qualitative agreement with the calculations from WAXD spectra which showed (x_c = 0.6) for the solution crystallized sample and (x_c = 0.51) for the solid state crystallized sample. Higher crystallinity for PET crystallized from oligomeric PEO was also observed by

Xue et al. [21] and Wang et al. [19] In addition, we find that the fractional contribution of the area under the $0\underline{1}1$, 010 and 100 peaks to the total area under the crystalline curve are 0.15, 0.14 and 0.28 for the solution crystallized sample, as compared to 0.09, 0.11 and 0.34 for the solid state crystallized sample. Origin of this difference could lie in orientation of the WAXD samples. However, 2-D pictures of the analyzed samples showed no orientation as inferred from the uniform intensity along the ring pattern. So origin of the difference remains a puzzle.

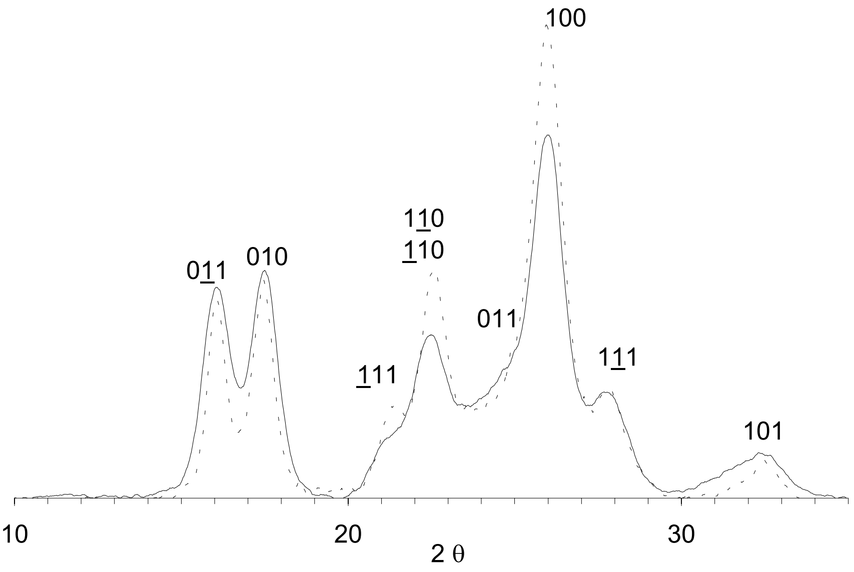

Figure 5.5: Crystalline component of wide angle x-ray diffractometer scans. Solid line: an isothermally (170 ^{o}C) crystallized 0.25% PET gel in DPE-BP, after drying at room temperature under vacuum. Dashed line: solid state crystallized PET.

Figure 5.6a shows the scanning electron micrograph of the PET crystals obtained by isothermal crystallization (170 ^{o}C) of PET from a 0.25% solution in DPE-BP, followed by solvent evaporation on a mica sheet. The entire polymer appears to be present as fibrillar structures extending to lengths of several microns and width ~ 50-100 nm. While the fibrillar structure is formed in the bulk solution, their aggregation into a sheaf like structure could be a result of the solvent evaporation process during the SEM sample preparation. The high aspect ratio (> 100) of the crystals can explain the gelation of the solution by network formation at such a low concentration, as was also proposed for i-PS in decalin [34]. Formation of high aspect ratio fibrils can be explained by preferentially rapid growth of crystals along a certain lattice direction. The fibril ends in Figure 5.6 appear blunt, rather than tapered as observed by Veld et al. [23] for crystallization on substrate while evaporating solvent. The blunt ends indicate that the crystal growth had occurred by laydown of molecules across the growing end. For the case of high PET concentration (5%), the SEM image (Fig. 5.6b) displays a continuous porous network of PET lamellar crystals, perhaps resulting from evaporation of the solvent distributed in a co-continuous manner.

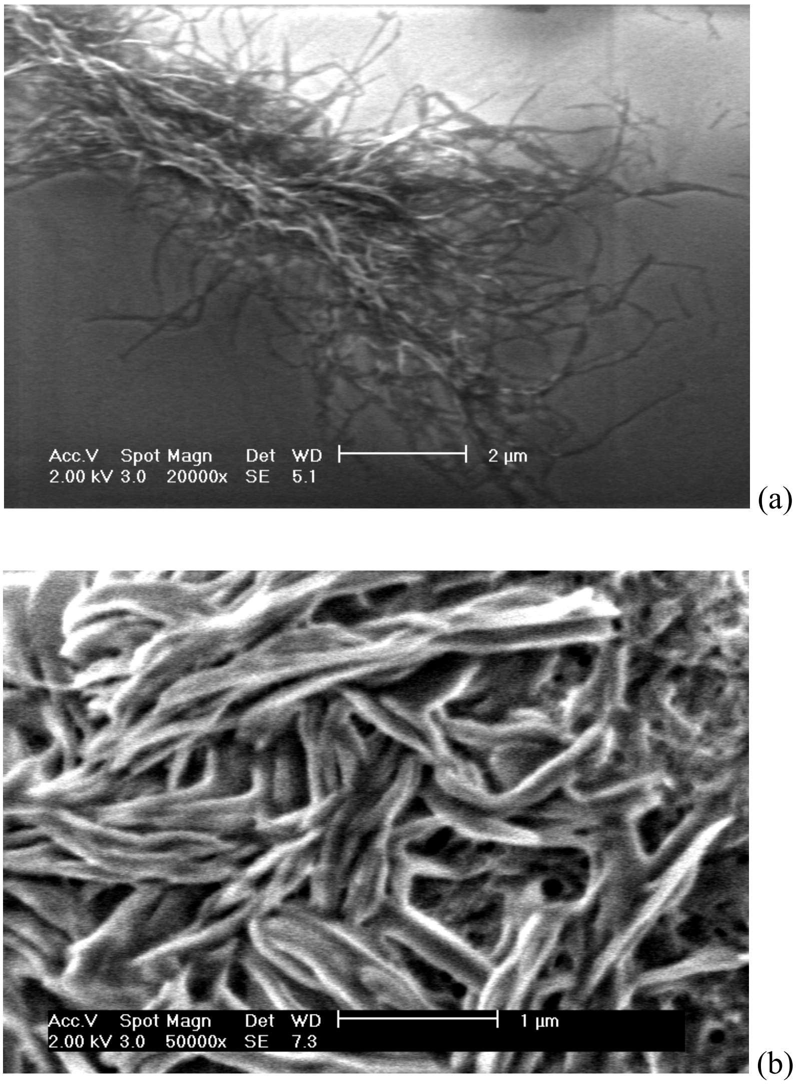
Acc.V Spot Magn Det WD 2 µm
2.00 kV 3.0 20000x SE 5.1
(a)
Acc.V Spot Magn Det WD 1 µm
2.00 kV 3.0 50000x SE 7.3
(b)

Figure 5.6: SEM images of an isothermally (170 ^{o}C) crystallized (a) 0.25% and (b) 5% PET solutions in DPE-BP after drying at room temperature under vacuum

It is known that lamellar crystals of nylon-66 can be grown from dilute solutions in lathlike shapes of thickness 5-6 nm [35, 36] and nylon 10,10 was found to crystallize into lathlike, spindle like and planar sheet shapes [37]. Yang et al. [38] reported formation of micro fibrillar crystals (diameter 5-8 nm, length 50-300 nm) of nylon 10,10 also by atomizing its very dilute solution (0.0025-0.01%) and then crystallizing on amorphous carbon. While a fibrillar structure of polymer crystals exists extensively in natural and synthetic polymers crystallized in bulk [39], nanoscale separated fibrillar crystals have also been observed e.g. through self assembly of peptides [40, 41], templating in porous matrices [42], electrospinning [43], dense grafting on linear backbones [44, 45]. When induced by externally induced flow, crystallization from dilute solutions into fibrillar morphology is observed for several homopolymers e.g. polyethylene [46, 47], polyvinyl alcohol [48], polyethylene oxide [49], cis-1,4-polybutadiene [50], amylose [51], and Bombyx mori L. silk fibroin [52]. Alternatively, precipitation-crystallization of rigid highly aromatic (rodlike LC) polymers is known to result in fibrillar morphology with the chains alignment along the long axis of the fibrils [53, 54]. In contrast, here the PET microfibrils are obtained by crystallization within dilute quiescent solution, and thus not on substrates during solvent evaporation, and not under external fields.

The PET crystals grown from dilute solution (0.2%) were deposited on a carbon coated Cu-grid, and examined by TEM. The fibrillar morphology (length several microns and width ~20 nm) of the solution grown crystals was observed again in the Bright Field (BF) TEM image (Figure 5.7). The electron diffraction pattern of a selected area marked in Fig. 5.7 is shown as an inset in the same figure. There are at least three diffraction rings, corresponding to the *d*-spacings of 0.51, 0.43 and 0.35 nm (inner to outer ring). The innermost and the outermost rings are easily assigned as reflections from the 010 and 100 planes of known PET crystal structure [30]. However, we are unable to assign the intermediate ring to a specific plane, as it could belong to $\underline{1}11$ or $\underline{1}10$ reflections expected at 0.4085 and 0.386 nm respectively. The position of the 010 arcs perpendicular to the fibrillar axis suggests that the crystalline *b*-axis is normal to the fibrillar axis. The position of the somewhat diffused 100 arcs on the outermost ring along the fibrillar axis suggests that the growth direction of the crystals is along the *a*-axis. This is consistent with the relatively blunt ends of the fibrils observed in the SEM (Fig. 5.6(a)) and BF-TEM images (Fig. 5.7), as the crystal growth occurred by laying down the chain across the growing end, i.e. by adding chains by folding successively in the *a*-plane (or the *b*-*c* plane) [55]. The absence of the $0\underline{1}1$ reflection may suggest c-axis alignment perpendicular to the supporting substrate. However, such a preferential alignment of *c*-axis is difficult to explain as the crystallization and fibril formation took place in bulk, thus in the absence of a surface influence. A larger fibril dimension along a principle result in the possible flat strips settling on their wider sides during solvent evaporation. However, imperfections during their settling would result in fibril width projection's variation over its length, which is seen for some fibrils in the SEM (Fig. 5.6(a)) and BF-TEM (Fig. 5.7) images. The then expected 011 reflections in the electron diffraction could be either very weak or overlapping with the neighboring 010 reflection.

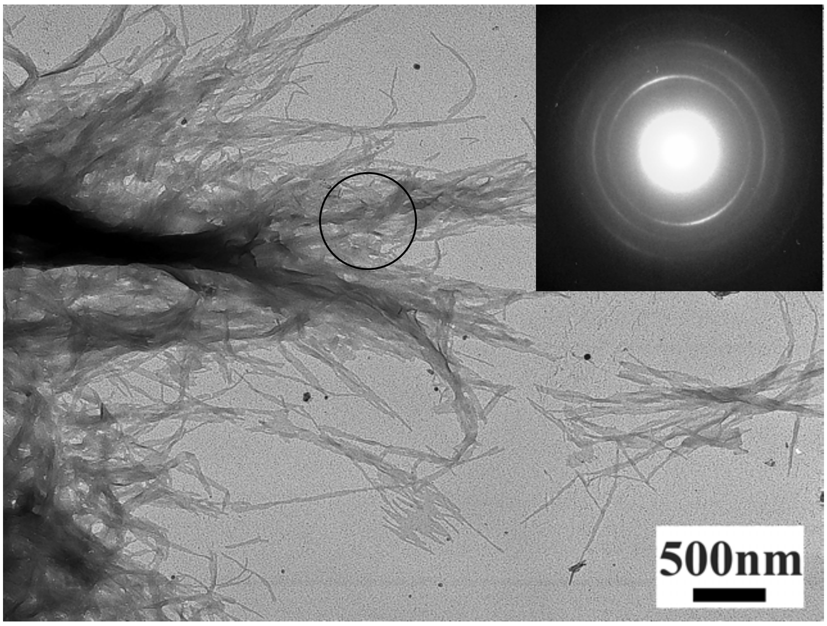

Figure 5.7: Bright field TEM image of an isothermally (170 °C) crystallized 0.25% solution DPE-BP after drying at room temperature under vacuum. Inset: electron diffraction pattern of the selected area marked as circle.

Based on the original work of Ward [56], showing that IR can detect the transformation of the gauche conformation of the glycol moiety to trans conformation on crystallization, Cole et al. [57] obtained basis spectra for the gauche and the trans conformation. For example, the absorption bands at 1471, 1340 and 849 cm^{-1} were attributed to CH_2 bending, wagging and rocking motion under the trans conformation. Fig. 5.8 compares the PET spectrum from 1% gel with the spectra of crystalline and amorphous PET films. The spectrum of the solvent is subtracted from that of the 1%

PET gel. This gives rise to some spectral features at about 1590, 1490, 1240, and 750-650 cm^{-1}. The spectra of the gel sample and of the crystalline PET sample predominantly show the presence of the absorption band at 1471, 1340 and 849 cm^{-1}, which are not detected in the amorphous PET spectrum, indicating the presence of a high amount of trans glycol conformation. In addition, the absorption band at 973 cm^{-1}, assigned to the trans glycol C-O stretching, is clearly present. An increase in trans conformation was also reported for i-PS on crystallization from solution [58].

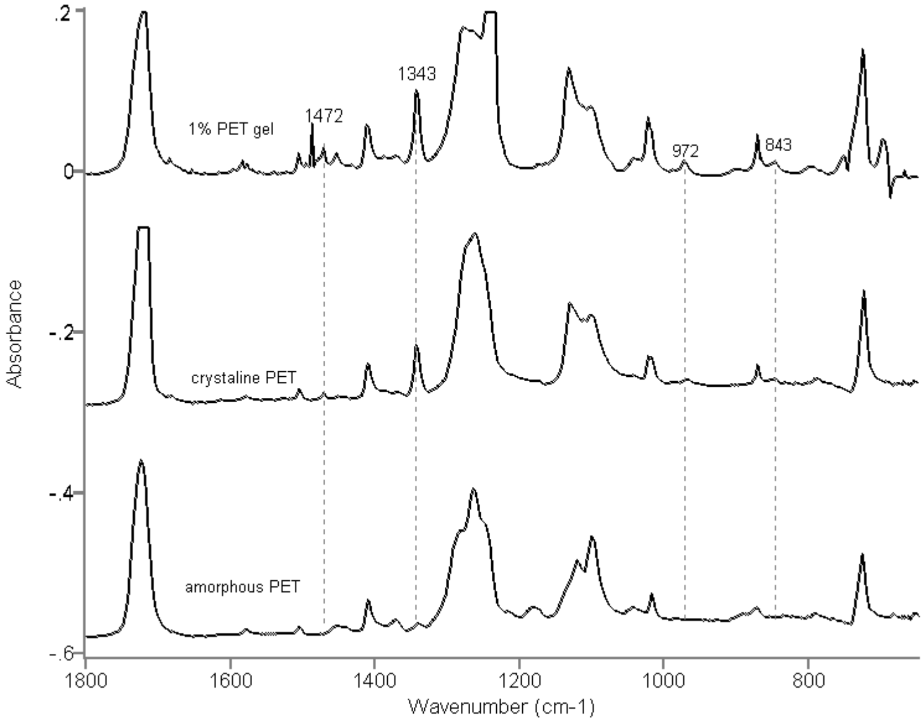

Figure 5.8: FTIR spectra of (a) an isothermally (170 °C) crystallized 1% PET gel in DPE-BP, (b) a solid state crystallized PET and (c) an amorphous PET quenched from melt into liquid nitrogen.

5.3.4 Mechanical properties of PET crystallized from dilute solution

The PET crystals grown from dilute solution (0.2%) were filtered and then dried at 100 °C to a film of thickness 0.15 mm. The film was very brittle, even for this high molecular weight PET, indicating disentanglement between crystallites. Since a low degree of entanglement between folded chain crystals can offer the possibility of a large extension to break while unfolding, we wished to carry out drawing studies on these PET films. This was, however, hindered by the brittleness, of the samples, and ductility could be introduced only by annealing between heated plates at 220 ^{o}C for 2 min. A lower temperature was not effective in imparting sufficient ductility. Suspecting thermal/hydrolytic degradation of the high molecular weight PET during its solubilization in DPE-BP, and during the subsequent annealing, we carried out IV measurement on the annealed sample. The measured value (2.1 dL/g) was comparable to that of the original sample, indicating no molecular weight degradation. The extent of crystallinity of this annealed sample was determined by DSC as 43%, indicating some extent of melting from x_c = 51% before the annealing. The ductile PET samples so obtained could be drawn only at 250 ^{o}C, to a draw ratio of 5~6.

We prepared three fiber samples for stress-strain measurement: (a) from HFIP solution through room temperature evaporation and drawn 6 times at 100 ^{o}C, (b) from dilute DPE-BP solution at 170 ^{o}C, dried, and drawn 5 times at 250 ^{o}C and (c) by pulling filament from concentrated (30 wt%) DPE-BP solution at 250 ^{o}C, drying, and then drawing 7 times at 240 ^{o}C. The stress-strain curves of three samples during the subsequent mechanical analysis are shown in Fig. 5.9. For the sample (b), the elastic modulus, breaking strength and elongation to break are E = 5.3 GPa, σ_b = 0.35 GPa and ε_b=9 % respectively. In comparison, for a film cast at room temperature from the same PET sample's solution (5 wt%) in HFIP, and then drawn to a similar draw ratio (5~6), the E, σ_b and ε_b values of were 11 GPa, 0.41 GPa and 6.6%. We also carried out filament formation from concentrated PET solution (30 wt%, section 5.2.11), followed by overnight drying under vacuum at 150 ^{o}C, and then drawing at 240 ^{o}C to a draw ratio of 7. The corresponding E, σ_b and ε_b values of were again similar, i.e. 11 GPa, 0.47 GPa and 8 % (Fig. 5.9). Thus, it appears that disentangled crystallization, if any achieved for sample (b) during the crystallization from dilute solution in DPE-BP, was not effective in enhancing the drawability of PET. The inherent nature of the inter-segmental interaction in PET crystals (e.g. compared to polyethylene) could hinder their unfolding. Presence of somewhat porous structure left by solvent removal could have limited the sample uniformity and hence drawability. Partial loss of disentanglement could have occurred during the annealing step required to render the brittle film drawable (section 5.2.4). Several of these limitations can be eliminated by carrying out thin filament extrusion from a fiber spinning machine, see Chapter 6.

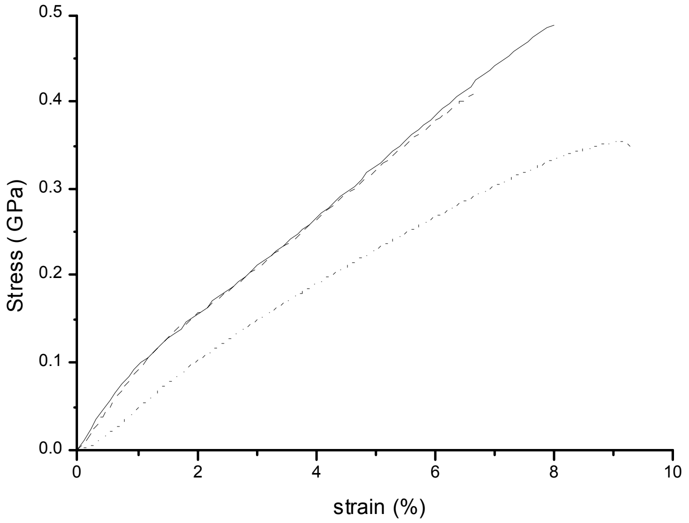

Figure 5.9: Tensile behavior of PET crystallized from (a) from HFIP solution through room temperature evaporation (-------) and drawn 6 times at 100 °C and (b) from dilute DPE-BP solution at 170 °C (··········), dried, and drawn 5 times at 250 °C (c) by pulling filament from concentrated (30 wt%) DPE-BP solution at 250 °C (———), drying, and then drawing 7 times at 240 °C.

5.4 Conclusions

The crystallization behavior of high molecular weight PET from solution in a DPE-BP mixture. When in dilute solution (0.25-10%), the PET undergoes crystallization at T_c~ 165 °C during cooling, and melting at T_m~ 204 °C during heating, with the T_c and T_m remaining nearly independent of PET concentration. Though the degree of crystallization is high (~ 50% by DSC, ~ 60% by WAXD), the crystallite sizes are somewhat smaller as compared to solid state crystallized PET. Crystallization within dilute solutions (0.25%) results in fibrillar crystals, with the chain alignment perpendicular to the fibril axis. The very high aspect ratio of the crystals is perhaps responsible for the gelation on cooling of even the dilute solutions. Films made from the dilute solution crystallized PET could be drawn 5 times at 250 °C, resulting in only moderate values of modulus and strength, suggesting the need for further process optimization.

References

[1] Schaaf E, Zimmerman H, Dietzel W, Lohmann P. Acta Polymerica 1981; 32: 250.
[2] Ravindranath K, Mashelkar RA. Chem Engng Sci 1986; 41: 2197.
[3] Chen S-A, Chen F-L. J Polym Sci, Part A: Polym Chem 1987; 25: 533.
[4] Duh B. J Appl Polym Sci 2002; 83: 1288.
[5] Marechal E. Polyesters: Synthesis and Chemical Aspects. In: Fakirov S, editor, Handbook of Thermoplastic Polyesters, New York: Wiley; 2002. Vol. I, p. 1.
[6] Ma Y, Agarwal US, Sikkema DJ, Lemstra PJ. Polymer 2003; 44: 4085.
[7] Ito M, Takahashi K, Kanamoto T. J Appl Polym Sci 1990; 40: 1257.
[8] Ziabicki A. Text Res J 1996; 66: 705.
[9] Huang B, Tucker PA, Cuculo JA. Polymer 1997; 38: 1101.
[10] Geil PH. Polymer Single Crystals, Wiley-Interscience, New York, 1963, Ch. IV.
[11] Berghmans H. Calorim Therm Anal Polym 1994; 207.
[12] Keller A. in Structure-Property Relationship of Polymeric Solids, Ed. A. Hiltner, plenum, 1983.
[13] Lemstra PJ Krisbaum R. Polymer 1985; 26: 1372.
[14] Petka WA, Harden JL, McGrath KP, Wirtz D, Tirrell DA. Science 1998; 281: 389.
[15] Bai S, Hu J, Pugmire RJ, Grant DM, Taylor CMV, Rubin JB, Peterson EJ. Macromolecules 1998; 31: 9238.
[16] Makarewicz PJ, Wilkes GL. J polym Sci Polym Phys Ed 1978; 16: 1529.
[17] Jameel H, Noether HD, Rebenfeld L. J Appl Polym Sci 1982; 27: 773.
[18] Ouyang H, Shore S-H. Polymer 1999; 40: 5401.
[19] Wang ZG, Hsiao BS, Fu BX, Liu L, Yeh F, Sauer BB, Chang H, Schultz JM. Polymer 2000; 41: 1791.
[20] Xue G, Ji G, Li Y. J Polym Sci, Polym Phys 1998; 36: 1219.
[21] Xue G, Ji G, Yan H, Guo M. Macromolecules 1998; 31: 7706.
[22] Oh SK, Youg JH, Ha WS. J Korean Fiber Soc 1991; 28: 52.
[23] Van Veld RD, Morris G, Billica HR. J Appl Polym Sci 1968; 12: 2709.
[24] Vane LM, Rodriguez F. J Appl Polym Sci 1993; 49: 765.
[25] Sun B., Lu Y., Ni H, Wang C. Polymer 1998; 39: 159.
[26] Fakirov S, Fischer EW, Hoffman R, Schmidt GF. Polymer 1977; 18: 1121.
[27] Ronald CM. Polymer Eng Sci 1991; 31: 849.
[28] BaltaCalleja FJ, Ohm O, Bayer RK. Polymer 1994; 35: 4775.
[29] Koncke U, Zachmann HG, BaltaCalleja FJ. Macromolecules 1996; 29: 6019.
[30] Fakirov S, Fischer EW, Schmidt GF. Makromolekulare Chemie 1975; 176: 2459.

[31] Bunn CW. in Ch. 11 in Fibers from Synthetic polymers, Ed. R. Hill, Elsevier, Amsterdam, 1953.
[32] Johnson, JE. J Appl Polym Sci 1959; 2(5): 205.
[33] Von Kilian HG, Halboth H Jenckel E. Kolloid-Zeitschrift 1960; 172(2): 166
[34] Atkins EDT, Isaac DH, Keller A, Miyasaka K. J Polym Sci, polym Phys 1977; 15: 211.
[35] Hinrichsen G. Die Makromol Chemie 1973; 166: 291.
[36] Geil PH. Polymer Single Crystals, Wiley-Interscience, New York, 1963, Ch. IV.
[37] Yang X, Tan S, Li G, Zhou E. J Polym Sci, Polym Phys 2001; 39: 729
[38] Yang X, Li G, Zhou E. Polymer 2001; 42: 4713.
[39] Lu XF, Hay JN. Polymer 2001; 42: 9423.
[40] Aggeli A, Nyrkova IA, Bell M, Harding R, Carrick L, McLeish TCB, Semenov AN, Boden N. Proc National Ac Sc 2001; 98: 11857.
[41] Burkoth TS, Benzinger TLS, Urban V, Lynn DG, Stephen C, Thiyagarajan MP. J Am Chem Soc 1999; 121: 7429.
[42] Wilson JN, Bangcuyo CG, Erdogan B, Myrick ML, Bunz UHF. Macromolecules 2003; 36: 1426.
[43] Jun Z, Hou H, Schaper A, Wendorff JH, Greiner A. E-Polymers 2003; 9.
[44] Stephan T, Muth S, Schmidt M. Macromolecules 2002; 35: 9857.
[45] Jinsan K, Mc Hugh SK, Swager TM. Macromolecules 1999; 32: 1500.
[46] Pennings AJ. J Polym Sci, Polym Symp 1977; 59: 55.
[47] Rietveld J. McHugh AJ. J Polym Sci, Polym Phys Ed 1985; 23: 2339.
[48] Yamaura K, Karaki T, Matsuzawa S. Makromol Chemie 1974; 175: 247.
[49] Pelzbauer Z, Manley RSJ, J Macromol Sci, Phys 1970; 4: 761.
[50] Xu Y, Zhou E, Yu F, Qian B. Chinese J Polym Sci 1988; 6: 152.
[51] Bolhuis HH, Pennings AJ. J Macromol Sci, Phys Ed 1975; B11: 455.
[52] Yamaura K, Yosiroh O, Matsuzawa S. J Appl Polym Sci, Appl Polym Symp 1985; 41: 205.
[53] Kimura K, Endo S, Kato Y, Inaba T, Yamashita Y. Macromolecules 1995; 28: 255.
[54] Shimamura K, Uchida T. J Macromol Sci – Phys 2000; B39: 667.
[55] Uemura A, Isoda S, Tsuji M, Ohara M, Kawaguchi A, Katayama K. Bull Inst Chem Res, Kyoto U 1986; 64 (2): 66.
[56] Ward IM. Chem Ind 1957; 1102.
[57] Cole KC, Ajji A, Pallerin E. Macromolecules 2002; 35: 770.
[58] Girolamo M, Keller A, Migasaka K, Overbergh N. J Polym Sci, Polym Phys 1977; 15: 211.

Chapter 6 Spinning trial of high molecular weight PET

6.1 Introduction

As has been reviewed in Chapter 1, spinning of fibers from high molecular weight PET with intrinsic viscosity of more than 1.2 using solution-spinning, has been carried out successfully by many researchers, and fibers so obtained have very impressive properties in comparison with fibers made from standard molecular weight PET using the melt spinning method [1]. The spinning of high molecular weight PET has been investigated, and was carried out in cooperation with Donghua University in Shanghai which specializes in the fiber and textile area.

Spinning has been defined as the transformation of a liquid material into a solid fiber. There are two main methods for spinning fibers: melt spinning and solution spinning. Solution spinning can be further categorized into dry spinning and wet spinning and dry-jet wet spinning. In melt spinning, the molten polymer is extruded through a spinneret into a gaseous medium such as air where the fiber cools down producing solid, non-porous fiber. The filament is usually then drawn to orient the polymer molecules which also improves the mechanical properties of the fiber. Dry solution spinning involves the extrusion of a polymer dope (polymer dissolved in an appropriate solvent) into a heated zone where the solvent evaporates while the air is blown around. Wet spinning is identical to dry spinning except in the way the solvent is removed from the extruded filaments. Instead of evaporating the solvent, the fiber is spun into a liquid bath containing a solvent called the coagulant. Dry-jet wet spinning is a combination of dry and wet spinning. A polymer dissolved in a suitable solvent is extruded into a gap before entering a coagulation bath containing a coagulant that is miscible with the solvent but not with the polymer. This method helps prevent blockage of the spinneret and also allows some drawing of the fiber prior to coagulation.

The more recent process for spinning UHMWPE is called gel-spinning process [2]. It is basically solution spinning, more or less like dry-jet wet spinning. The filament after being extruded is gel-like and has special morphology with less molecular chain entanglements, thus can undergo super-drawing with total draw ratio as high as 100. In this work on solution spinning of high molecular weight PET, a process like gel-spinning route was adopted, aiming to achieve high draw ratios and higher stiffness and strength.

6.2 Experimental

Materials. High molecular weight PET (intrinsic viscosity=1.8 dl/g) was made using the solution polymerization method as discribed in chapter 4. The fibers were prepared by a solution spinning method using a mixed solvent of diphenyl ether and biphenyl (73.5/26.5, w/w)[3]. The PET solution was made by dissolving PET in a flask at 240 ^{o}C at the protection of nitrogen. The solution was fed into an extruder (MicroCompounder, DACA), and was extruded through a die with diameter of 0.7 mm at 220 ^{o}C into a gap (about 50 cm) before entering a water coagulation bath (Figure 6.1). The speed of take-up is about 1.5 m/min. The filament was then extracted by ethanol three times at room temperature for 20 minutes every time, and dried at 50 ^{o}C under vacuum for certain hours before drawing.

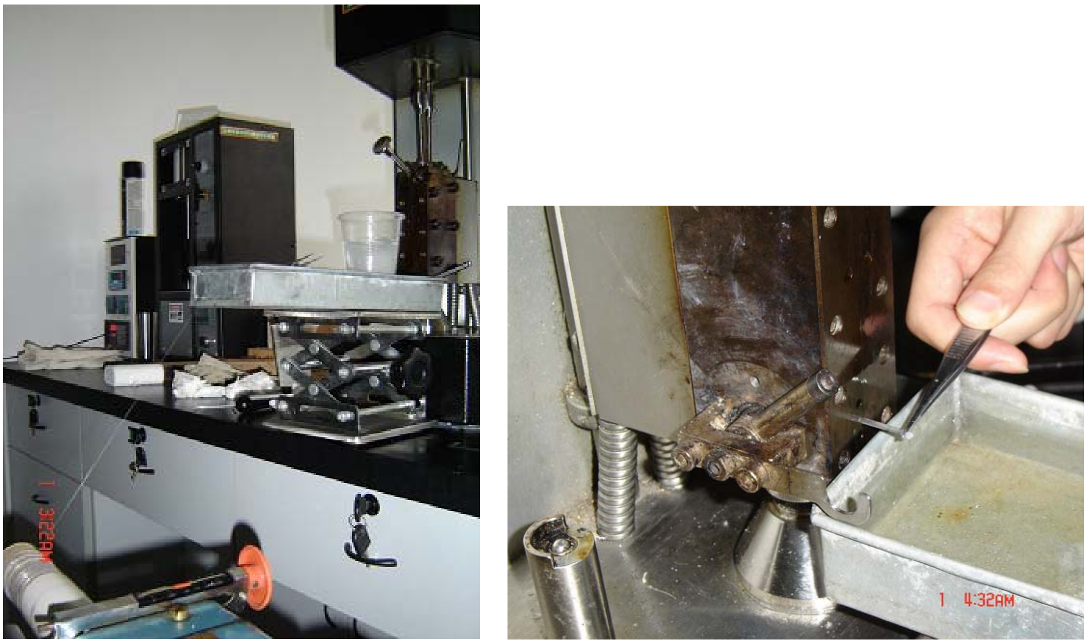

Figure 6.1 Solution spinning instruments.

Fiber drawing. A two-stage drawing method was adopted to achieve maximum mechanical and thermal property of PET fiber. Every stage is divided into two zones.

The temperatures in the two zones in the first stage are 70 °C and 90 °C , respectively; the temperatures in the second zones are 200 °C and 230 °C, respectively (Figure 6.2). The draw ratio was determined by the following equation:

$$DR=V_2/V_1 \tag{6.1}$$

DR is the draw ratio. V_2 is the speed of the take –up roll. V_1 is the speed of feed roll.

After the drawing process, the fiber undergoes the heat setting process to enhance its size stability and mechanical properties. During heat setting process, the fiber is treated for 3 minutes in ethylene glycol at 140 °C under stress [4].

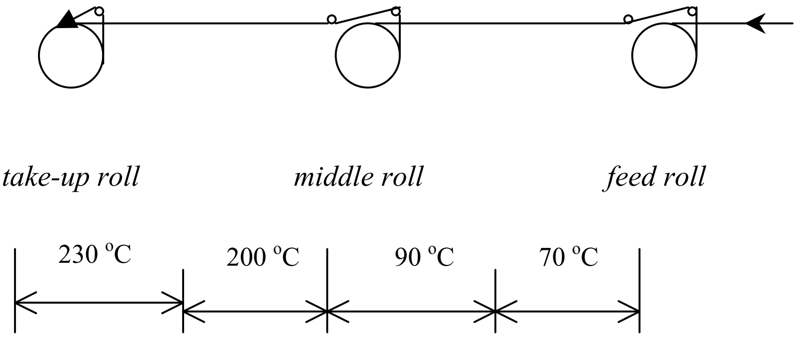

Figure 6.2: Fiber stretching scheme.

Measurements. The Differential Scanning Calorimetry (Perkin-Elmer DSC-2C) was performed for measuring the melting point and crystallinity of the fiber after drawn and before annealing. The tensile strength and modulus of annealed drawn samples was measured at room temperature and at a strain rate of $2x10^{-3}s^{-1}$ with a tensile testing machine (XQ 21, Shanghai). The modulus was determined from the tangent to the stress-strain curve at low strain (0.1%).During DSC measurement, the samples were heated from room temperature to 290 °C with heating rate of 20 °C/min. The melting point and crystallinity can be determined from DSC using the following equation:

$$\text{Crystallinity} = [\Delta H_m - \Delta H_c] / \Delta H_m^\circ \tag{6.2}$$

The term ΔH_m° is a reference value and represents the heat of melting if the polymer were 100% crystalline. For PET, the reference value of ΔH_m° is 125.6 J/g [5]. ΔH_m and

ΔH_c are enthalpy change of melting and enthalpy change of cold crystallization, respectively.

The morphology of the fiber was observed using Scanning Electron Microscopy (JSM－5600LV, JEOL, Japan). The fiber was spray-coated with gold before observation. Acceleration voltage used was 2KV.

6.3 Results and discussion

PET with IV of 1.8 corresponds to $\overline{M_w}$ of around 100,000 g/mol, therefore, melt spinning is not possible and solution spinning has to be employed. The lower the concentration, the lower of entanglement density. However, when the concentration is lower than certain value, there will be no coherent force between the polymer molecular chains and, as a result, the solution can not be spun into continuous fiber. In our spinning trial, we used three different concentrations to investigate the fiber spinning and have successfully spun the fibers at three concentrations (9%, 15%, 30%) (w/w).

The as-spun fiber without drawing has low mechanical strength because the chain orientation degree is very low. The more the times it can be drawn, the higher the chain orientation degree is, the higher the strength and modulus the fibers can have. The common technique for drawing fiber is using the multi-stage drawing by raising the temperature stepwise to achieve maximum draw ratio. A two-stage drawing was used in this spinning trial.

Before the drawing process, not all the solvent has to be removed. The small amount of solvent remaining in the fiber is beneficial for the drawing because solvent can act as a plasticizer. When content of solvent is too high, the molecular chain will slip past each other and the drawing is not effective on getting the chain orientation. Consequently, the resulted fiber has high elongation at break (higher than 20%) and low tensile strength. On the other hand, when the solvent content is too low, the fiber can easily break during drawing. Therefore, a minimum solvent content that can give continuous fiber-drawing has to be determined.

Table 6.1 Solvent content on the draw ability of fiber.

Vacuum drying time (minutes)	Solvent content (%)	Drawing stability	Mechanical properties in general
20	1.1%	Good	Poor
40	0.85	Good	Good
60	0.72	Good	Excellent
80	0.62	Poor	Poor

The data in Table 6.1 shows that 60 minutes of vacuum-drying is the optimum condition to have the right solvent content in fiber before drawing process. All fibers were treated under this condition before drawing in this study.

Figures 6.3a and b are the pictures of the fiber drawing equipment. The fiber is heated and drawn in the hollow stainless steel tunnel. The fiber feeding rate is 0.5 meter per minute. The maximum drawing speed was determined to calculate the draw ratio that can be achieved for various fibers.

Panasonic
High
RUN
Low
STOP

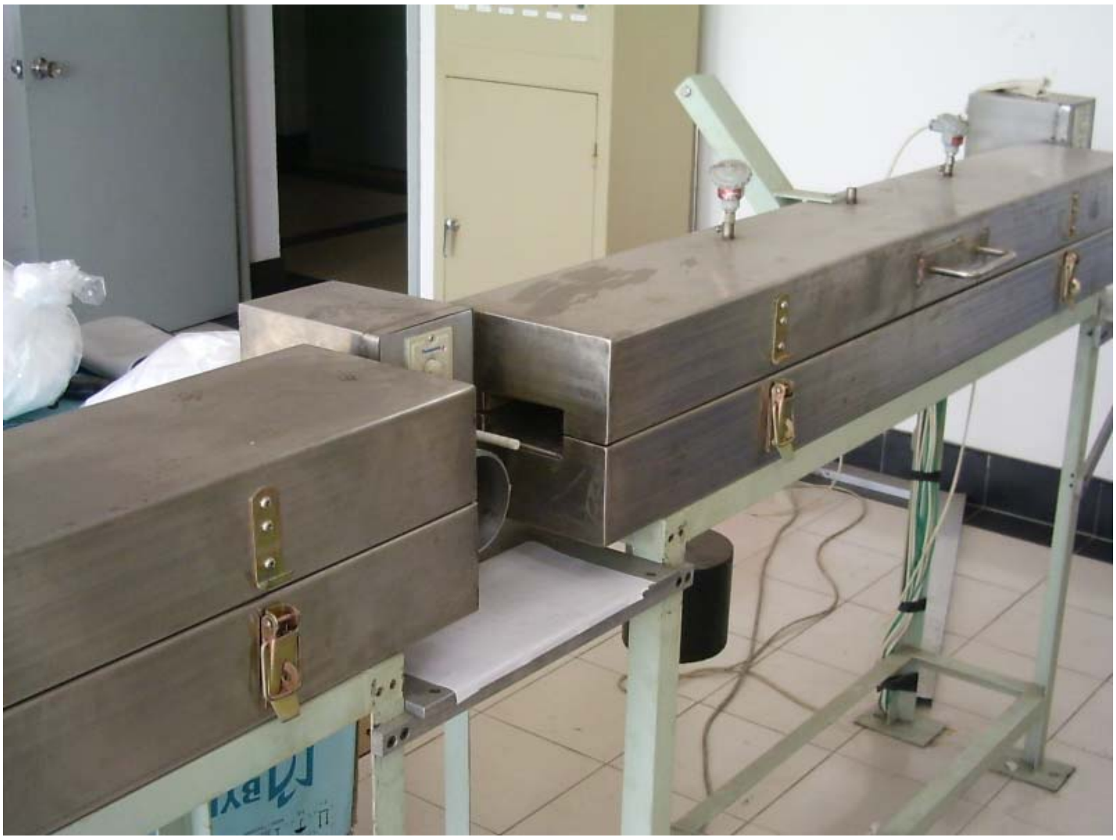

Figure 6.3ab Fiber drawing instruments.

Table 6.2 Drawing ability and mechanical property of fiber.

Concentration of spinning dope	First stage draw ratio	Second stage draw ratio	Total draw ratio	Tensile strength (GPa)	Tensile modulus (GPa)	Elongation at break (%)
10%	4	1.6	~ 6	0.8	13	17
15%	6	1.8	~ 12	1.4	23	11
30%	5	1.7	~ 9	1.2	21	13

It was found in our experiments that the PET fiber can not be spun continuously when the concentration is below 10% or above 50%. Table 6.2 shows that 15% PET concentration gives highest drawability and mechanical properties. Low concentration leads to lower entanglement density and higher draw ratio, and thus high tensile strength and modulus. However, continuous fiber spinning needs a spinning dope with certain viscosity, thus the concentration can not be too low. The minimum concentration is around 10% percent for PET with IV of 1.8. When the spinning dope concentration is just above 10%, the as-spun fiber has more defects and large size pores within the filament (Figure 6.4), therefore, the draw ratio can not be as high as it should be. Hence, the fiber mechanical property is not as good as when the concentration is 15%.

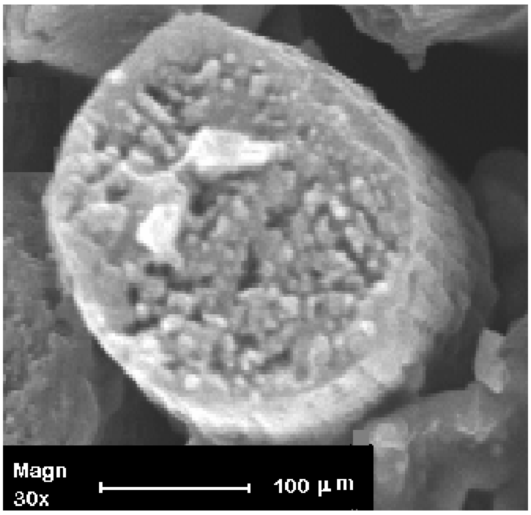

Figure 6.4 SEM image of cross section of PET as-spun fiber from 10% solution.

The SEM (Figure 6.5) was used to observe the morphology of the fiber achieved from 15% concentration spinning dope. The fiber has typical core-shell structure (Figure 6.5-B). The outside is a dense layer without any obvious pores (Figure 6.5-A). The inside has micro-pores left after the solvent is extracted (Figure 6.5-C). These pores will fuse and disappear after post-drawing the fiber (Figure 6.5-D, E).

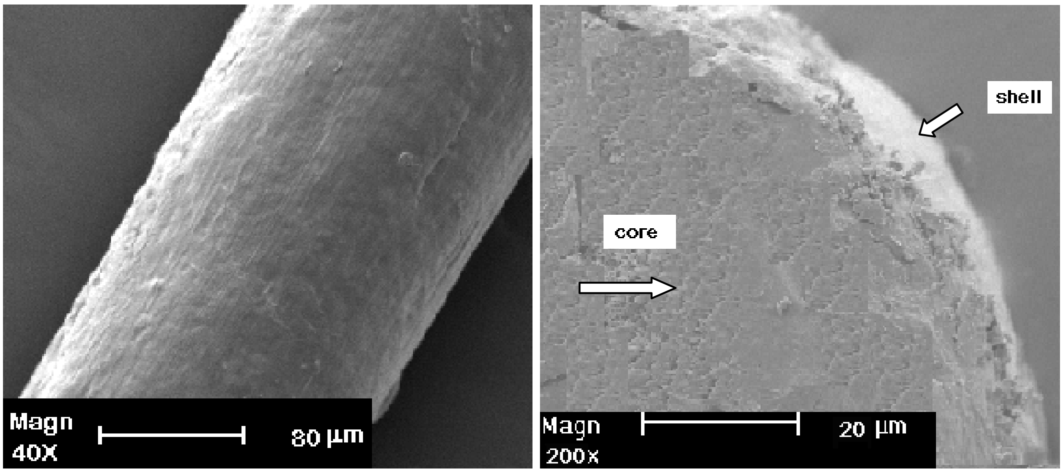

(a) (b)

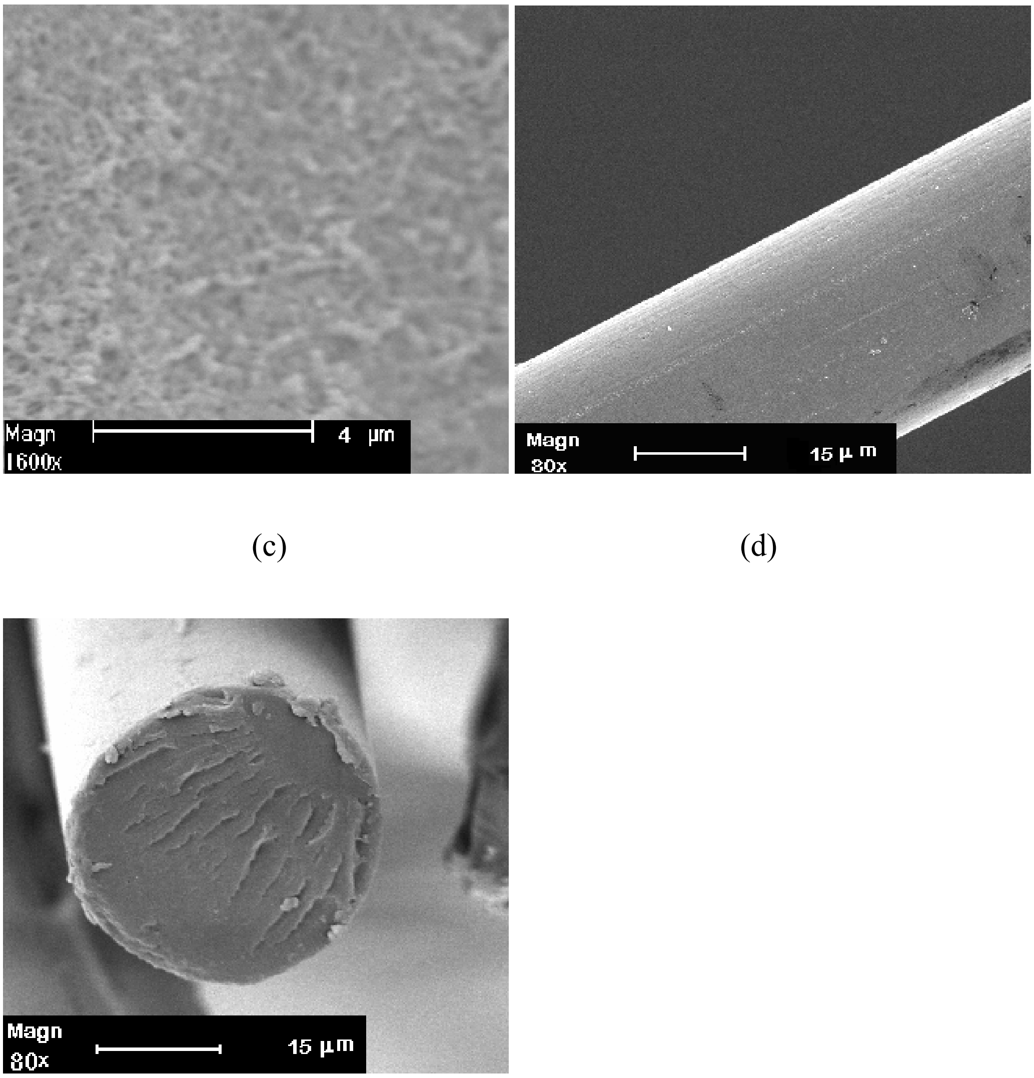

(c) (d)

(e)

Figure 6.5. SEM of fiber obtained from 15% concentration (a: surface of pre-draw fiber; b: cross section of pre-draw fiber; c: enlarged image of pre-draw fiber cross section; d: surface of after- draw fiber; e: cross section of after-draw fiber).

DSC was performed on the fiber spun from 15% concentration to study the crystallinity (Figure 6.6 and Table 6.3). The as-spun fiber has virtually no crystallinity and is basically in amorphous state. After first step drawing, the crystallinity increases to 43%. It shows that the as-spun fiber is easily to crystallize by drawing, suggesting that orienting molecular chains facilitated fast and perfect crystallization. The crystallinity increased to nearly 60% after the final drawing step. In comparison with PET chips, PET fiber has higher crystallinity and narrower melting range.

Table 6.3 Crystallinity of PET fiber vs. draw ratio. PET fiber comes from 15% percent solution spinning.

Draw ratio	ΔH_c (J/g)	ΔH_m (J/g)	Crystallinity (%)	Peak Melting Point (^oC)
0	39	42	2	251
5.9	1	56	44	257
11.2	0	75	60	262

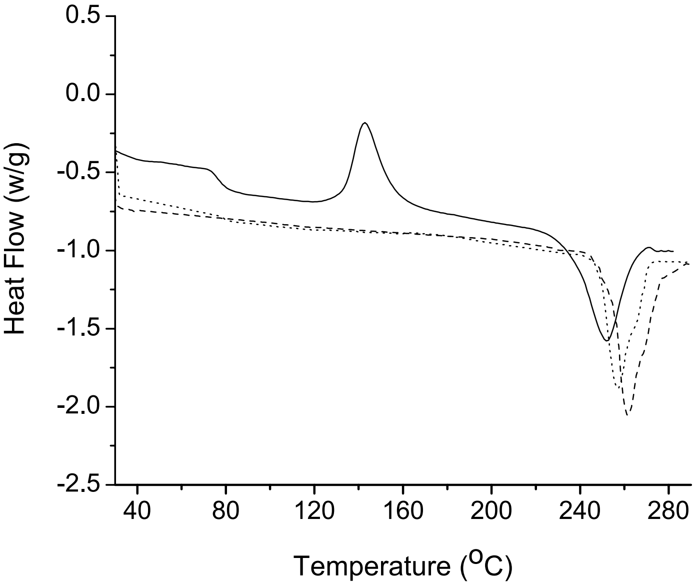

Figure 6. 6: DSC cure of 15% solution spinning fibers (solid line: as-spun fiber; dash line: fiber after first step post drawing; dot line: fiber after second step post-drawing).

6.4 Conclusions

High molecular weight PET with an IV of 1.8 dL/g can be spun successfully by solution spinning with as solvent the Diphenyl ether/Biphenyl mixture. The as-spun fiber before post-drawing has a shell-core morphology. The shell is dense and smooth and the core has micro pores. The as-spun fiber is amorphous with virtually no crystallinity. After drawing, the fiber has high crystallinity and high melting temperature and narrow melting range. The fibers after draw possess a crystallinity of as high as 60%. The total draw ratio can be over 11, much higher than that for melt spinning of PET and the mechanical properties are also well over fibers achieved by normal molecular weight PET, with a tensile strength of appr. 1.5 GPa, a tensile modulus > 20 GPa and elongation to break of 11%.

References

[1] Chapter 1, page 10.
[2] Paul S, Piet L. Journal of Materials Science 1980; 15(2): 505.
[3] Rogers V. EP 0336 556, 1989.
[4] Hu XC, Xie JB, Zhang TL, Yan JH. China Synthetic Fiber Industry 1998; 21(2): 5.
[5] Fakirov S, Fischer EW, Schmidt GF. Makromolekulare Chemie 1975; 176: 2459.

Chapter 7 Conclusions

In our pursuit for a process for high modulus and high strength (HMHS) fibers of UHMW PET, we targeted to examine the potential of a process that may use the same solvent to assist both the post polymerization and the subsequent solution spinning. If a solvent assisted post polymerization can be directly followed by fiber spinning, without intermediate solvent-polymer separation, then process cost reductions may result due to savings from elimination of the need for intermediate solvent evaporation and re-dissolution. Before examining the integrated process, we have first studied the post polymerization step in detail.

Since end-group determination is an important aspect of following step growth polymerization kinetics, we first developed a new method that allows quantitative determination of small concentrations of the acid and hydroxyl end-groups in PET. This is based on a room temperature carbodiimide mediated esterification of the acid end-groups with HFIP, and direct esterification of the hydroxyl end-groups with TFA, followed by quantification (by using α,α,α-trifluorotoluene as a secondary standard) of the respective fluoroester with well resolved peaks at isolated chemical shifts during ^{19}F NMR. As compared to the often used titration based techniques, our technique offers the advantages of very small sample size, small quantity of solvent, and quick and reliable measurements with elimination of difficulties with exact determination of the end-point during titrations.

We have examined the influence of reaction environment on the SSP of thin (180 μ) PET chips at 250 ^{o}C by following the IV increase and the end-group depletion. When the SSP reaction is carried out in vacuum, IV increases from 0.58 dL/g to 2.4 dL/g in 2.5 hr of reaction. The initially rapid reaction slows down considerably with time, and the IV raise nearly stops at 2.75 dL/g at 6 hr, though we still detect the acid and the hydroxyl end-groups at concentrations of 3 and 5 meq/kg, respectively. This suggests a role of crystallization in limiting the possibility of the end-groups to approach each other, thereby temporarily rendering them inactive. At this stage, raising the temperature to 270 ^{o}C to melt the PET in vacuum again increases the IV to 2.97 dL/g in 1.5 hr, perhaps due to the release of crystalline restraints in the melt allowing some these dormant end-groups to approach each other. We find that accounting for these temporarily inactive end-groups is a must for a good kinetic description of SSP to IV > 1.3 dL/g.

When nitrogen is used as a carrier gas, the reaction rate and the extent of molecular weight build-up are somewhat lower compared to SSP under vacuum. A sublimate is collected during SSP under vacuum, and we find it to be made up of terephthalic acid, monohydroxyethyl terephthalate, bishydroxyethyl terephthalate and cyclic oligomers. This indicates the presence of a new condensation mechanism during SSP under vacuum.

SSP of PET proceeds to IV as high as 2.75 dL/g, but only when carried out in well isolated thin films (enabling efficient condensate removal) and at temperatures close to T_m (reducing crystallization induced lack of chain segment mobility). This poses potential solids handling problems due to sintering of chips during a scale-up. Therefore, it appeared interesting to examine the recently reported SwSP route that uses a solvent to swell the PET, thus facilitating condensate and reactive end-group diffusion.

We have examined the influence of the solvent mixture DPE-BP on the post polymerization of PET in the swollen state. The initially rapid SwSP of thin chips (180 μ) at 195 °C slows down dramatically beyond IV = 1.2 dL/g in 5 hr, and is unable to proceed beyond 1.4 dL/g. This appears to be related to the temporarily restricted mobility of the end groups due to the observed solvent induced crystallization, because sufficient reactive end groups can be directly detected, and further post polymerization in melt state is possible.

When limitations due to crystallization are eliminated by carrying out post polymerization in 30 (wt)% PET solution in DPE-BP at 250 °C, the IV raise proceeds to 1.8 dL/g in a single step. We are not aware of any previous report of PET polymerization in solution to IV higher than 0.87 dL/g. Since solution polymerization eliminates the requirement of handling fine PET particles, it offers an attractive route to high molecular weight PET. The use of these solvents during the post polymerization step poses no disadvantage as it allows direct spinning of the solution-polymerized high IV PET.

The crystallization behavior of PET (IV ~ 2 dL/g) from solution in DPE-BP was examined. Reversible gelation of the polymer solution is observed during cooling of the solutions. Light scattering and DSC analysis are used to follow the heating and cooling processes, thus determining the crystallization temperature and the melting point, which are found to be nearly independent of the polymer concentration (0.25-5%). A higher degree of crystallization (> 50%) is observed in the PET crystallized from the solution at 170 ^{o}C. Morphological characteristics of the crystals obtained after solvent removal are determined by WAXD, FTIR, SEM and TEM examination. The crystallization of PET into unique high aspect ratio fibrillar morphology during cooling of the solutions explains their gelation even at low PET concentration. Thin films made from the so obtained PET could be drawn 5 times, resulting in fibers with only moderate values of modulus (5.3 GPa) and strength (0.35 GPa), even though the IV measurements indicated no loss of molecular weight during the solution processing. The spinning trial using the solution polymerization product with IV of 1.8 dL/g can be easily carried out by solution spinning method with DPE-BP as the solvent when the concentration is above 10% (w/w). The as-spun fiber from 15% solution can be drawn more than 10 times and give a fiber with its tensile modulus > 20 GPa and a tensile strength of appr. 1.5 GPa.

Technology assessment

Many attempts have been made in the past to obtain high modulus/high strength PET fibers by solution spinning of UHMW-PET. The UHMW-PET can be prepared by post-polymerization of fine PET particles in the solid state at temperatures close to T_m (chapter 3 and 4). However, a potential scale-up of such a process is hampered by the sintering of the fine particles. SwSP, a process introduced by workers at Toyobo in the 1980s, provides a potential alternative. However, we found that the maximum IV achievable during SwSP with DPE-BP is limited to less than 1.4 dL/g (chapter 4). In contrast, we have developed a solution polymerization process, in 30 wt% concentration in DPE-BP at 250 ^{o}C, leading to IV ~ 1.8 dL/g within 24 hr (chapter 4). This process has potential of being scaled up in reactors similar to those used for melt polymerization, and on similar time scales. Subsequent solution spinning into filaments can be carried out directly (chapter 4). Spinning trials, Chapter 6, without optimization demonstrate that fibers can be made with tensile Moduli > 20 GPa and a tensile strength of appr. 1.5 GPa. A proposed process is shown schematically below. This route involves the following steps:

- Solubilization of melt polymerised PET (IV ~0.6 dL/g) in DPE-BP in a stirred reactor maintained at 250 ^{o}C by heating fluid in the reactor jacket.
- Solution polymerization under vigorous nitrogen bubbling while stirring, first at high speed, and then reducing speed as the solution viscosity rises.
- On completion of reaction (as indicated by torque measurement on the stirrer), the UHMW-PET solution is transferred to a storage tank, also maintained hot.
- The solution is extruded through the spinneret into filaments that are passed through a coagulation bath, where most of the DPE-BP is removed.
- The as spun filaments may be dried and drawn at desired conditions.

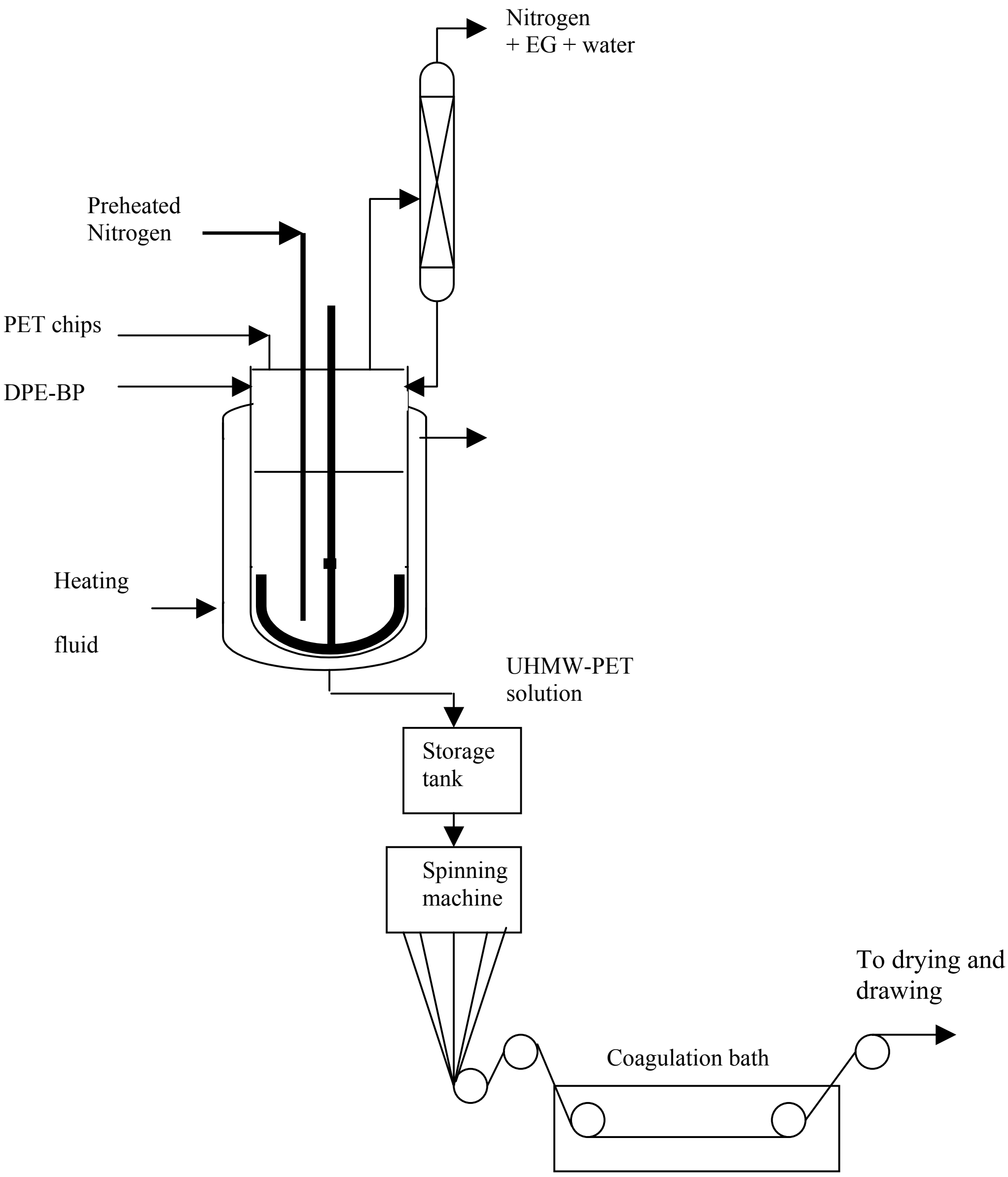
Nitrogen
+ EG + water
Preheated
Nitrogen
PET chips
DPE-BP
Heating
fluid
UHMW-PET
solution
Storage
tank
Spinning
machine
To drying and
drawing
Coagulation bath

Integrated process for SolP to UHMW-PET and its solution spinning

Our proposed integrated SolP-spinning process is compared with the earlier reported solution spinning processes for high modulus/high strength (HMHS PET) fiber. The earlier reported processes involve difficult dissolution of highly crystalline high molecular weight SSP product in aggressive solvents at high temperatures (Table 1.2, chapter 1), resulting in molecular weight degradation of the UHMW-PET. In comparison, the proposed process enables spinning directly with the same solvent that assists the SolP process. The solvent recovery and environmental costs are thus reduced. The diphenyl ether and biphenyl eutectic solvent mixture (DPE-BP) is easily available. Besides the reduction in the operating costs, the proposed process employs less equipment, and a reactor design similar to the melt polymerization reactors. Thus equipment investment costs may be reduced compared to the development of special reactors, demanding particle morphology designed to enable SSP at $T \sim T_m$. As discussed in chapter 4 and 5, the rather limited mechanical properties of our drawn fibers/films indicate need for further studies involving fine filament extrusion from fiber spinning machines, and optimization of the associated process parameters, see below.

Past processes	Proposed process
PET ↓ SSP or (SwSP in *solvent-1*) **UHMW-PET** ↓ solution spinning in *solvent-2* **Spun Fiber** ↓ drawing **High modulus high strength fiber**	**PET** ↓ SolP in *solvent-1* **UHMW-PET** ↓ solution spinning in same *solvent-1* **Spun Fiber** ↓ drawing **High modulus high strength fiber**
Limitations of the process: • SSP scale-up (fine PET, $T \sim T_m \Rightarrow$ sintering) • Aggressive *solvent-2* for UHMW PET ⇒ IV↓+ Intermediate drying + re-dissolution (SwSP)	**Process Advantages of the process*:*** *Same* solvent for SolP and processing ⇒ Reduced hydrolytic/thermal degradation Reduced energy + environmental costs

Comparison of the past and proposed process for HMHS PET fibers

Summary

Polyethylene terephthalate (PET) fibers are manufactured industrially by melt polymerization, followed by melt-spinning. The molecular weight of PET is represented in terms of the intrinsic viscosity [η]. The [η] values for PET textile fibers are about 0.6 dL/g, and for tire cords in the range of 0.8~1.2 dL/g. Solid state polymerization (SSP) has been described in the past as a route for post-polymerization of PET to high molecular weight PE. The effect of the reaction environment on the post polymerization characteristics has been studied in the thesis. Crystallization of PET is generally considered to assist the SSP process by confining the reactive end groups to the amorphous region, thereby increasing the reaction rate. However, it was found that crystallization limits the highest achievable [η] during SSP. By developing a fluoroderivatization and ^{19}F-NMR based technique, the presence of reactive acid and hydroxyl end groups could be detected, even when the polymerization can no more proceed during SSP. Further, melting of the crystals enables reinitiation of the post polymerization. It was found that the SSP in thin chips (0.18 mm) proceeds faster under vacuum than under nitrogen flow, because of the removal of acid and hydroxyl end group carrying aromatic species under high vacuum at 250 ^{o}C. The kinetics of the SSP process is modeled while accounting for these factors, and a good fit with the experimental data is obtained.

In the late 1980s, faster reaction by a swollen-state polymerization (SwSP) was reported wherein a solvent is used to swell (but not dissolve) the PET chips, thereby enhancing the reaction rate. It was found that SwSP in thermic fluid (diphenyl ether-biphenyl) at 195 ^{o}C cannot proceed to [η] beyond 1.4 dL/g. Once again, DSC and WAXD analysis show that the extent of crystallization is enhanced by the presence of solvent, and is responsible for this limit on the highest achievable [η]. When limitations due to crystallization are eliminated by carrying out post polymerization in solution at 250 ^{o}C, it proceeds to IV = 1.8 dL/g in a single step. Since solution polymerization eliminates the requirement of handling fine PET particles, it offers an attractive route to high molecular weight PET, particularly when the solution can be directly used for further processing e.g. into fibers. That PET crystallizes into unique high aspect ratio fibrillar morphology during cooling of the solution accompanys its gelation phenomenon even at low PET concentration. Fibers made from high molecular weight PET solutions could be drawn more than 10 times by multi-step drawing technique, resulting in high values of modulus and strength.

Samenvatting

Polyester vezels worden standaard vervaardigd via smeltspinnen waarbij polyester granulaat (chips) via een extruder wordt opgesmolten en door spinplaten geperst. Na afkoelen van de versponnen draden kunnen via naverstrekken de mechanische eigenschappen zoals E-Modulus en sterkte van de vezels worden verbeterd ten gevolge van de moleculaire oriëntatie in de vezelrichting.

Het is bekend in de vezelwereld dat bij een toenemend moleculairgewicht de eigenschappen zoals sterkte en stijfheid van vezels toenemen maar de verwerkbaarheid, in het geval van vezels, de verspinbaarheid vanuit de smelt, wordt bemoeilijkt evenals de (na)verstrekbaarheid. In het algemeen wordt dit gecorreleerd met het toenemend aantal warpunten (entanglements) per molecuul.

De oplossing voor dit probleem is om hoog-moleculaire polymeren te verspinnen vanuit (verdunde) oplossing. In het geval van polyester (PET) zijn diverse onderzoeken uitgevoerd om a) hoog-moleculair PET te vervaardigen en b) deze polyesters te verspinnen/verstrekken tot hoge-Modulus/hoge sterkte vezels. In dit proefschrift wordt het verhogen van het moleculairgewicht van PET via polymerisatie in de vaste fase SSP) uitvoerig gedocumenteerd op basis van experimenten en modellering. Het vigerend probleem is dat hoog-moleculair PET, gemaakt via nacondensatie (SSP) in de vaste fase weliswaar een hogere molecuulmassa bezit, maar tevens hoog-kristallijn is, en daarna moeten worden opgelost in agressieve oplosmiddelen om te kunnen verspinnen vanuit (verdunde) oplossing.

In dit proefschrift wordt een methode nagestreefd waarbij via solutie-polymerisatie hoog-moleculair gewicht PET wordt gemaakt met de optie van direct verspinnen vanuit hetzelfde oplosmiddel. Het oplosmiddel dat is gebruikt is een eutectisch mengsel van diphenyl ether en biphenyl, ook bekend als verwarmingsolie onder de naam Dowtherm®. Polymerisatie in dit oplosmiddel levert een PET met een weliswaar lagere molmassa dan via vaste stof nacondensatie, een IV van 1.8 in plaats van > 2, maar uit orienterende spinproeven bleek dat op basis van deze solutie-gepolymeriseerde PET, vezels te vervaardigen zijn op labschaal met een trekstrekte van ca. 1.5 GPa en een E-Modulus > 20 GPa. Hierbij dient te worden opgemerkt dat verdere optimalistie niet kon worden doorgevoerd vanwege het ontbreken van optimale spin- en strekapparatuur. Er is dus de nodige ruimte voor optimalisatie maar dan moet dit project vanuit de academische omgeving worden geïmplementeerd in een industriële omgeving waar opschaling en optimalisatie standaard is.

Curriculum vitae

Yunqian Ma was born on the 5th of December 1967 in Hebei province, China. He obtained a 5 year Bachelor’s Degree from Tsinghua University in China in 1990 in the area of Polymer Materials and Chemical Engineering. In addition, he worked at the Research Institute of Beijing Yanshan Petrochemical Corporation from 1990 to 1997. Further, he joined at the Department of Chemistry, University of Surrey (UK) in 2000. Since November 2000, he has been studying as a PhD student in the Polymer Technology Group (SKT) under the supervision of Dr U.S. Agarwal at the Eindhoven University of Technology, the Netherlands.